INFORMATION TO USERS

This manuscript has been reproduced from the microfilm master. UMI films the text directly from the original or copy submitted. Thus, some thesis and dissertation copies are in typewriter face, while others may be from any type of computer printer.

The quality of this reproduction is dependent upon the quality of the copy submitted. Broken or indistinct print, colored or poor quality illustrations and photographs, print bleedthrough, substandard margins, and improper alignment can adversely affect reproduction.

In the unlikely event that the author did not send UMI a complete manuscript and there are missing pages, these will be noted. Also, if unauthorized copyright material had to be removed, a note will indicate the deletion.

Oversize materials (e.g., maps, drawings, charts) are reproduced by sectioning the original, beginning at the upper left-hand corner and continuing from left to right in equal sections with small overlaps. Each original is also photographed in one exposure and is included in reduced form at the back of the book.

Photographs included in the original manuscript have been reproduced xerographically in this copy. Higher quality 6" x 9" black and white photographic prints are available for any photographs or illustrations appearing in this copy for an additional charge. Contact UMI directly to order.

UMI

A Bell & Howell Information Company
300 North Zeeb Road, Ann Arbor MI 48106-1346 USA
313/761-4700 800/521-0600

An Equilibrium Model for Helicity Injector Operation

by

Adam Kent Martin

A dissertation submitted in partial fulfillment
of the requirements for the degree of

Doctor of Philosophy

University of Washington

1997

Approved by Thomas R Jarboe

Program Authorized
to Offer Degree Physics

Date 21 March 1997

University of Washington

Abstract

An Equilibrium Model for Helicity Injector Operation

by Adam Kent Martin

Chairman of the Supervisory Committee:

Professor Thomas Jarboe
Department of Aeronautics and Astronautics

The Helicity Injected Tokamak (HIT) experiment is a low aspect ratio (A=1.5) tokamak formed and sustained by helicity injection. A critical issue facing its operation is the efficiency of the helicity injector. In order to study this, an equilibrium model of the injector has been developed which assumes that the open field-lines in the injector and the edge region are in force-free equilibrium with a uniform resistivity (η). This resistivity may include a dynamic as well as a classical component. This model yields good agreement with measurements of edge poloidal magnetic field and injector current, with as few as one fitting parameter. This model has been extended to shots with significant amounts of closed flux. The calculated equilibria are found to be consistent with measurements of edge electron temperature using a triple Langmuir probe. The equilibria are also found to be consistent with helicity conservation to within the accuracy of the measurements.

Table of Contents

List of Figures

Acknowledgements

I would like to thank professor Thomas Jarboe for fostering an exciting research environment, where I have been able to learn a great deal about plasmas. His many useful suggestions concerning my research, and insights into plasma physics have been invaluable.

I would like to thank professor Brian Nelson for his extensive help with my research and for making computers do things they ordinarily wouldn't do. I am also grateful to professor Alan Hoffman and professor Uri Shumlak for many useful discussions.

I am indebted to professor Tadao Uyama, professor Masayoshi Nagata and Dr. Richard Kenny of the Himeji Institute of Technology, for their help with my research during my stay there.

I am deeply indebted to our technical staff. Dan Lotz designed and built much of the experiment. John Rogers kept everything working and was a great help with vacuum systems. Dennis Peterson fabricated many vital components for the experiment and taught me what I know about machining. I have an abiding respect for their work; they are all superb engineers. And it was a great pleasure to work with them.

I would like to thank the other students who worked on the HIT experiment: Chad Painter, Leslie McCullough, Liyong Zhou, J.P. Xie, and especially Dave Orvis for many useful discussions and for the use of his poloidal probe data (and his stereo). I am also grateful to Mike Bohnet, Oggie Jones, and Dr. Jim Galambos for many useful discussions. Many undergraduates have contributed to the HIT experiment and I am grateful for their help: especially deserving of thanks are Noah Bettin, Jeff Friesen, Alan Miller, Bon

Sihavong, and Claudia Rubio.

I would like to thank professors Marshall Baker, Vladimir Chaloupka, and Tom Mattick, from whom I learned a great deal about Electrodynamics, Quantum Mechanics, and Lasers respectively. I would also like to thank professors Robert Holzworth and Oscar Vilches for their help and encouragement, and professor Wick Haxton for serving on my committee.

I would like to thank the friends I have made while in graduate school: Benedicte Bonomi who shares my love of music and hiking, and who has been a constant friend; Julie Drzewiecki for her irreverence and kindness; Richard West who rekindled my interest in space travel; and especially Diane Markoff for her kindness and encouragement - she has always been the best of friends in the worst of times. I could not forget to also thank Maria Silkey, who brought great joy to my life.

It goes without saying that I owe a great deal to my family. I would like to thank Carla and Warren Hashagen and Evy and Clark Martin, and their daughters (my nieces): Theodotia Hashagen, Melanie Martin, Cynthia Martin and Bridget Martin, for their encouragement and support through these years.

Foremost of all, I wish to thank my parents, William T. Martin and Mary Ellen Martin for their unhesitating support and encouragement for all my endeavors. I owe them more than I can say; they have been the best parents anyone could hope for.

1. Introduction

1.1 Motivation: Magnetic Confinement Fusion and the Tokamak

The effort to extract useful energy from controlled fusion has spawned numerous reactor concepts. Broadly, they fall into two categories: Inertial confinement and Magnetic confinement. The experiment described in this report belongs to the latter category.

In magnetic confinement fusion, the fuel is insulated from the material walls of the reactor vessel by a magnetic cage and heated to the point of ignition, i.e. of a self-sustaining reaction. Several kinds of devices have been built toward this end: the stellarator, the tokamak, the field reversed configuration (FRC), the spheromak, and the reversed field pinch (RFP). The tokamak is the most developed of these concepts, and is now the object of an extensive international research effort.

The tokamak is a toroidal device, both in the shape of the plasma, and in the shape of the enclosing vessel (fig 1.1). A toroidal current, I_p, driven in the plasma makes a poloidal magnetic field, B_p, which confines the plasma radially. A strong, externally produced toroidal field, B_t, stabilizes the plasma against kink instabilities. The effect of these fields, necessary for the confinement and stability of the plasma, is to make the torus expand. To counter this, a vertical field, B_v, is applied, which interacts with the plasma current to hold the torus in place.

The toroidal and vertical fields can easily be generated by external power supplies. Typically, the plasma current is induced by a transformer coil placed at the geometric axis of the torus with the plasma itself serving as the secondary. As the core of the transformer will eventually saturate, a plasma current driven in this way is limited to a finite duration. For the tokamak to be viable as a steady-state reactor, a means of driving the plasma current in

steady state is needed. Among the methods proposed of accomplishing this are current drive by neutral beam injection[1], electromagnetic waves[2], and by helicity injection[3].

Neutral beam injection current drive was first demonstrated on the DITE tokamak[4]. Tokamak current drive using lower-hybrid waves has been demonstrated on JT-60[5]; electron cyclotron waves have been used to drive current in DIII-D[6]. All of these methods rely on driving a high-energy tail in the electron distribution, and although efficient at low temperatures, do not scale favorably to reactor conditions[7]. Helicity injection offers a means of steady-state current drive that drives the bulk electron population rather than the tail, leading to relatively high efficiencies.

The experiment described in this report, the Helicity Injected Tokamak, is a tokamak formed and sustained solely by coaxial helicity injection current drive[3]. What follows is an investigation of the coaxial helicity injector.

In this chapter the background of the HIT experiment will be described. Section 1.2 is a discussion of the Taylor minimum energy principle. The efficiency of helicity injection is discussed in section 1.3. Different approaches to helicity injection current drive are briefly mentioned in section 1.4, and two experiments of particular relevance to the HIT experiment, the CTX spheromak and the SPHEX rodomak, are briefly described in sections 1.5 and 1.6 respectively. Finally, in section 1.7, the place of the HIT experiment in Tokamak research is discussed.

1.2 Helicity and the Taylor Minimum Energy Principle

Helicity, K, has been proposed as an important invariant in the description of plasmas[8], and is defined by:

$$K = \iiint \vec{A} \cdot \vec{B} dV$$

where **A** is the vector potential. It is a conserved on time scales short compared with the resistive decay time.

Helicity measures the linkage of flux with flux. This may be seen heuristically by rewriting the integral above in a different form for the case of two linked, non-interpenetrating flux tubes:

$$K = \iint \vec{A} \cdot d\vec{l} \; \vec{B} \cdot d\vec{a} = 2\Phi_1\Phi_2$$

where *d***l** is the differential arc-length parallel to **B**, and *d***a** is a differential area vector parallel to **B**. The integral is carried out along both flux-loops resulting in the factor of two. In a tokamak, where the poloidal and toroidal fluxes inter-penetrate, the factor is less than two and depends on the plasma current profile, but is still bilinear in the poloidal and toroidal fluxes. It is therefore bilinear in the toroidal field coil
current, I_{TF}, and the plasma current, I_p:

$$K \propto \alpha I_{TF} I_p$$

where α is a constant of proportionality that depends only on the plasma current profile and the aspect ratio. For fixed toroidal field, anything that adds to or maintains the tokamak helicity adds to or maintains its toroidal current.

This quantity, helicity, has been shown by Woltjer and by Taylor to be useful in

explaining the relaxation of a magnetized plasma to its final equilibrium state.[8,9] In the presence of resistivity, the system's magnetic energy will decay subject to the constraint that the total helicity of the system, K_o, is conserved. This constraint is sufficient to determine the final state of the system even though the details of its turbulent evolution are unknown. The minimization of the magnetic energy subject to conservation of helicity, leads to the following relation[8],

$$\nabla \times \vec{B} = \lambda \vec{B}$$

where λ is a global constant with the unit of reciprocal length. This relation determines the magnetic structure of the plasma. Since, by Ampere's law,

$$\nabla \times \vec{B} = \mu_o \vec{J} = \lambda \vec{B}$$

the current and magnetic field are proportional and aligned. From this equation, a general relation for λ can be derived:

$$\mu_o \vec{J} \cdot d\vec{A} = \lambda \vec{B} \cdot d\vec{A}$$

which may be rewritten as:

$$\lambda = \frac{\mu_o I}{\Phi}$$

where I is a current, and Φ is a flux. For the application of this principle, the system must be surrounded by a helicity barrier - a close fitting conducting wall which defines the

boundary conditions.

If a voltage is applied along open field lines that penetrate the helicity barrier, helicity may be injected. The rate of helicity injection is given by[10],

$$\dot{K}_{inj} = 2\int \vec{E}_{vac}\cdot\vec{B}_{vac}dV = 2V_{inj}\psi_{inj}$$

where ψ_{inj} is the injected flux, and V_{inj} is the voltage applied across that flux. This suggests the following helicity balance equation:

$$\frac{dK}{dt} = -\frac{K}{\tau_K} + 2V_{inj}\psi_{inj}$$

where K is the total helicity of the object and τ_K is the helicity decay time. This equation states that helicity is only destroyed by resistive decay and that there are no anomalous losses in the transfer of helicity from source to destination.

An alternate formula for λ may be obtained by dotting the electric field, **E**, into the equation relating **J** and **B**, $\mu_o\mathbf{J} = \lambda\mathbf{B}$:

$$\mu_o\int \vec{E}\cdot\vec{J}dV = \lambda\int \vec{E}\cdot\vec{B}dV$$

which, using the formula for the time rate of change of helicity, becomes:

$$\lambda = \frac{2\mu_o\dot{W}}{\dot{K}}$$

1.3 Efficiency of Helicity Injection

The efficiency of helicity injection has been shown for spheromaks to be just the ratio of the λ for the spheromak to the λ of the injector, $\epsilon = \lambda_{sph}/\lambda_{inj}$.[11] The efficiency of helicity injection in tokamaks may be derived if one assumes helicity balance.

Using the helicity balance equation for the tokamak:

$$\frac{dK_{tok}}{dt} = -\frac{K_{tok}}{\tau_K} + 2V_{inj}\Psi_{inj}$$

and rewriting this equation, using the relations derived above for λ, the definition of the injected helicity, and an expression for the toroidal flux given by: $\Phi = \gamma I_{TF}$, where γ is a constant dependent only on the aspect ratio and elongation, the following power balance equation is obtained:

$$\frac{dW}{dt} = \frac{\lambda_{tok}}{\lambda_{inj}} I_{inj} V_{inj} - \frac{\alpha}{2\gamma\tau_K} I_p^2$$

In the absence of any injected power, i.e. if the first term is zero, the tokamak energy decays at the rate, $(\alpha/2\gamma\tau_K)I_p^2$, which implies that the factor $(\alpha/2\gamma\tau_K)$ is the resistance of the tokamak. This power balance equation states that the rate of change of energy in the tokamak is equal to the power dissipated by the plasma current less the injected power multiplied by a factor, $\epsilon = \lambda_{tok}/\lambda_{inj}$, which is interpreted as the efficiency of helicity injection.

1.4 Helicity Injection Current Drive

The validity of the Taylor minimum energy principle has been demonstrated for

RFP's[12] and spheromaks[13], and it is of interest to see if this is the case for tokamaks as well.

Several methods have been proposed for toroidal current drive by helicity injection in tokamaks. These include DC helicity injection by electron beams[14], spheromak injection[15], and coaxial helicity injection[3].

The use of electron beams has been demonstrated only in low power devices, with very modest toroidal currents and non-axisymmetric geometries[14].

Current drive by spheromak injection has been demonstrated on a tokamak[16]. Again, this method is not axially symmetric and is further handicapped by low efficiencies, typically $\leq 5\%$. This is a consequence of the fact that the efficiency is given by:

$$\epsilon = \frac{\lambda_{tot}}{\lambda_{inj}} \sim \frac{a}{2qR} \sim \frac{1}{2}\frac{1}{3}\frac{1}{3} = \frac{1}{18}$$

where a and R are respectively the tokamak minor and major radii, and q is the safety factor.

Coaxial Helicity Injection current drive (CHI), the method employed by the HIT experiment, is axisymmetric and promises high efficiency.

1.5 Results of the CTX Spheromak Experiment

The spheromak is a compact toroid that has both toroidal and poloidal field[17]. They may be formed in a variety of ways. In CTX, they were formed with a magnetized coaxial plasma source similar to a Marshall gun. The source consists of two nested annular electrodes, the inner-most of which contains a poloidal field coil. A voltage is applied across the electrodes and current is drawn along the poloidal field lines. The resulting $\mathbf{J}\times\mathbf{B}$ force pushes the plasma and poloidal magnetic field out of the injector and into the flux conserver.

As the plasma injector maintains a voltage across the bias flux, it is also injecting helicity. If helicity is conserved, one would expect to find a toroidal as well as a poloidal field in the flux conserver region, even though initially there is only a poloidal field. This is in fact found to be true.

A detailed helicity balance on CTX was performed[11], using different injector voltages and bias fluxes, and it was found that the helicity was conserved to within the experimental error. The prediction of the Taylor minimum energy principle, that the hollow current profile of the driven spheromak relaxes to a flat current profile, was supported by the CTX data.[18]

The design of the HIT helicity injector is derived from that used on CTX, consequently their operation is similar, however with significant differences. The operation of the CTX plasma source, as it pertains to the HIT experiment, will be discussed in chapter 4.

1.6 Results of the SPHEX 'Rodomak' Experiment

SPHEX is a spheromak that uses CHI, similar to CTX. To test the effect of a pre-existing toroidal field on the device, a conducting rod was placed down the axis of the machine[19]. A modest current in this rod (60 kA) produced a toroidal field in both the injector and the confinement region. It was found that the addition of a toroidal field improved the operation of the plasma source, resulting in a higher impedance, and a lower current necessary to eject the plasma from the injector. In its operation as a 'Rodomak', SPHEX exhibited a 20 Khz global n=1 mode, just as it did when operated as a spheromak, but with greater amplitude.

1.7 The Helicity Injected Tokamak (HIT) Experiment

The goal of the HIT experiment is to investigate Coaxial Helicity Injection Current drive as a means of driving a steady-state toroidal current in a tokamak and to determine what effects this method has on tokamak confinement.

The HIT experiment has a low aspect ratio (A=1.7) and falls into the category of the spherical tokamak[3]. Theoretical work suggests favorable properties for spherical tokamaks[20], such as high plasma β; however the state of this theory is not highly developed, and more work needs to be done. The Small Tight Aspect Ratio Experiment (START) at Culham laboratory has made tokamaks with aspect ratios of 1.3, which exhibit stable equilibria, robustness to internal disruptions, and high temperatures[21], indicating at the very least that such objects are interesting. In addition to current drive experiments, HIT is well disposed to study the physics of such low aspect ratio tokamaks.

The organization of this dissertation is as follows: Chapter 2 describes the HIT experiment. In chapter 3, the diagnostics used in this study are described. Chapter 4 presents previous work in this area and the resistive equilibrium model, which is the subject of this dissertation. Chapter 5 presents the results of the model and the supporting data.

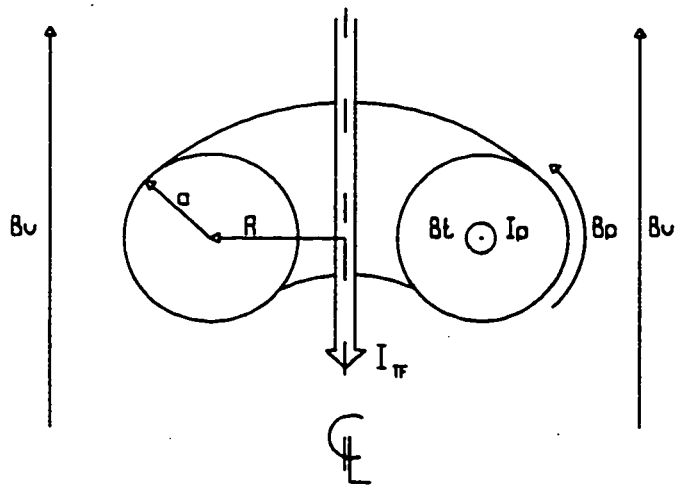

Figure 1.1: Basic geometry of the tokamak

2. Construction of the HIT Experiment

2.1 Flux Conserver and Vacuum Vessel

On the HIT experiment, a copper flux conserver is used instead of a vertical field coil to maintain the tokamak equilibrium. The flux conserver has the advantage over vertical field coils of being less expensive. It also stabilizes fast MHD instabilities.

The flux conserver on the HIT experiment consists of five main parts (see fig. 2.1): a helicity injector electrode, an absorber electrode, and two approximately hemispherical shells, all made of OFHC copper; and a central column, made of copper.

The center electrode is a 2.1 m long pipe concentric with the axis of the device, with an o.d. of 219 mm and a 12.7 mm thick wall. It was originally armored with a 0.25 mm thick coating of tungsten, which was deposited by plasma spraying. The tungsten coating on the center conductor was subsequently increased to 1.25 mm. The outer flux conserver consists of two 12.7 mm thick shells. The shells were rolled into approximately hemispherical shapes. Both shells have copper flanges welded on their perimeters. The shells are joined to each other with 64 stainless-steel bolts. These bolts are housed in 50 mm long copper bushings which electrically connect the two shells while holding them apart for diagnostic access in the midplane. The other end of the shells are bolted to the injector and absorber electrodes. The interior of the shells are sprayed with a 0.25 mm thick tungsten coating. All bolts used in the vacuum chamber are silver-plated to prevent them from galling.

The helicity injector consists of a cylindrical copper electrode, 12.7 mm thick, and hard soldered to the stainless-steel injector assembly. Gas is admitted into the injector through two small holes in the outer electrode, which are connected to a gas puff valve[22]. Gas can also be puffed in along the center column under the insulator. The interior surface of the

injector is sprayed with a 0.25 mm thick tungsten coating.

The thick conducting walls of the injector serve to freeze in the bias magnetic field over the time scales of a discharge. The two electrodes are separated by a toroidally symmetric, high-purity alumina insulator. The flux absorber at the other end of the device is similar in design to the helicity source, except that the alumina insulator extends further into the chamber to help prevent shorting of the injector voltage at this end.

The vacuum tank for the HIT experiment is a cylinder made of 9.5 mm thick stainless-steel and is 1.02 m long and 1.22 m in diameter. The tank has been modified with a variety of ports at midplane. The tank is capped with 32 mm thick stainless-steel end-plates which are sealed with viton o-rings. The injector and absorber assemblies are attached to these end-plates. The vacuum vessel and endplates were electro-polished for vacuum cleanliness.

2.2 Vacuum System

A schematic of the vacuum system is shown below (fig. 2.2). Rough pumping is performed by a Leybold D-60A trivac rotary-vane pump (displacement of 17 l/s), in series with a Leybold WSU 250 air-cooled Roots pump (displacement of 80 l/s). The Roots pump maintains a high pumping speed in the 1 Torr to 1 mTorr range, and is especially valuable for high steady-state throughput during glow-discharge cleaning. The vacuum chamber is always roughed out through an LN cooled trap, to prevent back-streaming of oil vapor from the rough pumps. The cold trap is always valved off on both sides for removal and cleaning when rough pumping is completed.

High vacuum is attained with an Airco-Temescal turbo-molecular pump (TMP), with a rated pumping speed of 450 l/s for N_2. The connection from the pump to the tank is

through a 254 mm diameter elbow, with a conductance of approximately 4000 l/s at 2 Mtorr (a typical pressure for glow-discharge cleaning) and 3200 l/s in the molecular regime. In neither case does the elbow present a significant flow restriction, and the overall pumping speed is limited only by the pumping speed of the TMP.

The plumbing in the roughline and foreline is constructed from 4 inch diameter schedule K copper water pipe, which is inexpensive and easy to work with. The rough line is made in sections, allowing it to be removed during modification of the experiment. The pipe sections are joined with o-ring static face seals on brass flanges. The brass flanges are joined to the copper pipe with a high-vacuum silver solder; the copper pipe and fittings are joined together with ordinary soft plumbing solder. The roughline and foreline were thoroughly cleaned after soldering with trichloroethane, hot water, and finally ethanol. Before being used on the vacuum chamber, the rough line was pumped out for an extended period of time, to remove any remaining volatiles. Only 300-series stainless-steel fittings are used in the high vacuum region.

The operation of the vacuum system is protected by a simple and robust controller which uses relay logic. This controller interlocks the valves and pumps to prevent the most expensive accidents. Both the turbo-molecular pump and the roots pump are interlocked to shut them off in the event of a temperature excursion. The controller also serves to centralize all the vacuum gauges, pump controls, and valve controls for ease of operation.

Great attention is paid to maintaining the system in as clean a state as possible. The seals used were either all metal conflat seals or viton o-rings. All o-rings are greased with sparingly-applied Apiezon high-vacuum grease. Rough vacuum components are cleaned with ethanol immediately prior to installation; high-vacuum components are cleaned first with

ethanol, then with freon. When letting the vessel up to atmospheric pressure, dry nitrogen is used to prevent water condensation inside. The dry nitrogen is scrubbed of hydrocarbon contaminants by passing it through an LN-cooled Zeolite trap.

A quadrupole residual gas analyzer (Dycor, model MA100M, made by Ametek) is used for helium leak checking and for monitoring vacuum purity. The Dycor MA100M RGA has a range of from 1 to 100 amu's and an electron multiplier for high sensitivity.

Hydrogen glow discharge cleaning and Titanium gettering are used for impurity control and wall conditioning.

Within a few days of pumping out, the base pressure typically drops to as 2.0×10^{-7} Torr and after Titanium gettering typically reaches 1.0×10^{-8} Torr. At such times the RGA shows the dominant vacuum impurity to be water.

2.3 Magnetic Field Coils and Power Supplies

2.3.1 Toroidal Field Coil and Associated Power Supply

The toroidal field (TF) coil (fig. 2.3) is maximally rated at 1 MA-turns, for a maximum toroidal B field of 1.8 Tesla at the inboard wall (outer surface of the center column)[23]. The coil is made of 250MCM type THHN cable wound through a long, hexagonal, honeycomb-like housing made from PVC pipes. The PVC pipes are used for added electrical insulation and to prevent the cables from shifting inside the center column due to magnetic forces. The cable is wound into 34 turns, one to a pipe. The coil is completed by six 1/4" brass straps that run along the faces of the hexagon. These serve to symmetrize the current distribution, and so minimize field errors. The cable is cut into six sections to permit ease of winding (friction would prevent the winding of one section into 34 turns). The

six sections are connected to the brass connectors by clamps on either end of the strap, making for a total of 40 turns. At either end of the PVC matrix, the cables are supported by phenolic clamps The return path of the coil on the outside of the vessel is through ten aluminum tubes, fixed to the device with aluminum plates. The tubes serve to hold the cable returns rigid against the considerable magnetic force exerted on them. Each individual cable return is wound through a PVC pipe, four to a return bundle. Each bundle of PVC pipe is wrapped in a sheet of mylar for further insulation.

In those regions where the coil is not constrained by supporting walls, between the PVC matrix and the return tubes, the coil is wound in the shape they would assume in the presence of the magnetic field. This minimizes the amount that the cable moves when the coil is energized, reducing fatigue and work-hardening. To hold the cables in place during winding and to prevent their deformation through wear, the cables are held in this shape by plywood frames which are supported on an aluminum frame attached to the endplates.

The Toroidal Field coil is described in greater detail in a Master's Thesis by D. J. Orvis[23].

The TF coil's power supply is a bank of 24 550μF, 11 kV high energy density capacitors with a total energy storage capacity of 800 kJ (fig 2.4). The capacitors are wired in parallel, and discharged through a D-size ignitron triggered by a Krytron pulser. Four high-voltage diode stacks from the LLNL 2XII-B flat-top modules are connected in parallel with the capacitors and the load (TF coil) and serve as a passive crowbar. The TF bank has a quarter cycle rise time of 7.5 ms, and the TF coil has an L/R time of 47 ms. The TF bank is protected by fuses, and has three independent energy dump systems: carbon resistors, water resistors, and in the last resort, pneumatic switches that directly short the capacitors. The

latter are also engaged during maintenance on the bank.

2.3.2 Bias Coils, Vertical Field Coils and Associated Power Supplies

The Bias field in the injector region, which is necessary for helicity injection, is produced by two solenoidal coils that fit over the outside of the injector assembly.

The inner coil (called the positive bias coil) consists of three concentric coils wound on an aluminum spool with # 12 wire. The mean diameters and number of turns of the three coils are respectively; 0.35 m and 1094 turns, 0.40 m and 918 turns, and 0.45 m and 931 turns. The outside of the coil is protected with an aluminum sheet and the coil and spool are insulated from the vacuum vessel (ground).

The positive bias coil is powered by a DC power supply, that full-wave-rectifies each phase of a three-phase 20 amp AC line. The coil itself inductively filters the power supply output. Each phase powers one of the three coils, which may be switched in or out of the bias coil circuit independently. The first phase is controlled by a Variac which allows for a continuous variation from 0 to 72,630 Ampere-turns.

The outer bias coil (called the negative bias coil) consists of 800 turns of # 12 magnet wire wound on an aluminum reinforced plywood spool with a mean diameter of 0.528 m. It is powered by a Rapid Model PSTA 2065415 400 V, 65 A, D.C. power supply.

There are two vertical field coils (VF coils) which fit over the end flanges of the vacuum vessel. They consist of 400 turns of # 12 magnet wire wound on a plywood spool with mean diameters of 1.38 m. The VF coils are powered by a Sorensen model DCR300-35A D.C. power supply.

For some of the data to be analyzed from the HIT experiment, the negative bias coil and VF coils were not present.

2.3.3 Helicity Injector Power Supplies

The other requirement for helicity injection, apart from the bias magnetic field, is that there a voltage be applied across the injector electrodes. This is provided by three capacitor banks, a pre-ionization (PI) bank, a formation bank, and a sustainment bank.

The PI bank (a schematic is shown in fig. 2.5) ionizes the gas. It consists of a single 100 μF capacitor and an A-size ignitron switch triggered by a Krytron pulser. The bank is rated at 10 Kv, though typically operated at 7 Kv, and has a quarter cycle rise time of about 15 μs. The PI bank is connected on the opposite side of the experiment as the other two banks; the inductance of the center column helps to reduce the current from ringing at the injector end.

The formation bank (fig. 2.6) provides the current to push the bias flux out into the confinement region. It has a capacitance of 3.3 Mf and is switched by an A size ignitron, triggered by a Krytron pulser. The current limit of the ignitron imposes a 2 Kv charge-voltage limit on the bank. It is designed to be critically damped, so that its output voltage does not reverse, and itself prevents the PI bank from ringing the helicity injector through zero. This insures that $\mathbf{E}\times\mathbf{B}$ is always pointing out of the injector and towards the absorber. The formation bank has subsequently been modified to include a pulse-forming network to broaden and flatten its output pulse, and a discharge resistor to prevent it being charged by the sustainment bank.

The sustainment bank (fig. 2.7) is modified from a 2XII-B flat-top module (obtained from LLNL). It consists of 40 trays of 24 electrolytic capacitors (1500 μF, 450 V) and a series inductance of 2 μH, arranged into ten rows of four trays each. Each row is charged with two rows positive (+450 V) and two rows negative (-450 V), for a total of 0.36 F at 900

V. Each tray is triggered by an SCR; the rows may be fired independently at times set by delay generators. In typical operation, the rows are fired sequentially to make a long, relatively flat current pulse.

2.4 Control and Timing System

The shot cycle is controlled by a programmable logic controller (GE Fanuc 90-30). The controller opens and closes dumps as necessary, activates charging supplies, energizes the bias coils, and triggers the digital delay generators (Data Design Corp. DG11 modules) which control the sequence in which the banks are fired. An optical pulse, carried by fiber optic cables, triggers the Krytron pulsers (or in the case of the sustainment bank, the SCR's) of the capacitor banks. This prevents pre-firing due to electrical cross-talk.

2.5 Data Acquisition System (DAS)

The DAS on the HIT experiment (as well as on proto-HIT) uses the CAMAC standard. It is controlled by a VAXstation 3200, which is interfaced with a Kinetic Systems 2060 serial highway driver, capable of controlling up to 63 CAMAC crates. The VAXstation 3200 runs the MIT Model Data System (MDS), a data acquisition software package. A variety of data acquisition modules and associated equipment are available, including LeCroy models 6810, 8210, and 2256 digitizers and 8100 differential amplifiers. Over 100 channels of digitizers are available.

Data analysis is performed using the Interactive Data Language (IDL) running on a DEC 3000/400 AXP with a RISC processor.

A set of active integrators with high gain and long integration times (on the order of

one second) were developed for the HIT experiment. They are packaged in CAMAC compatible modules and their gain settings are read and stored along with the data by MDS.

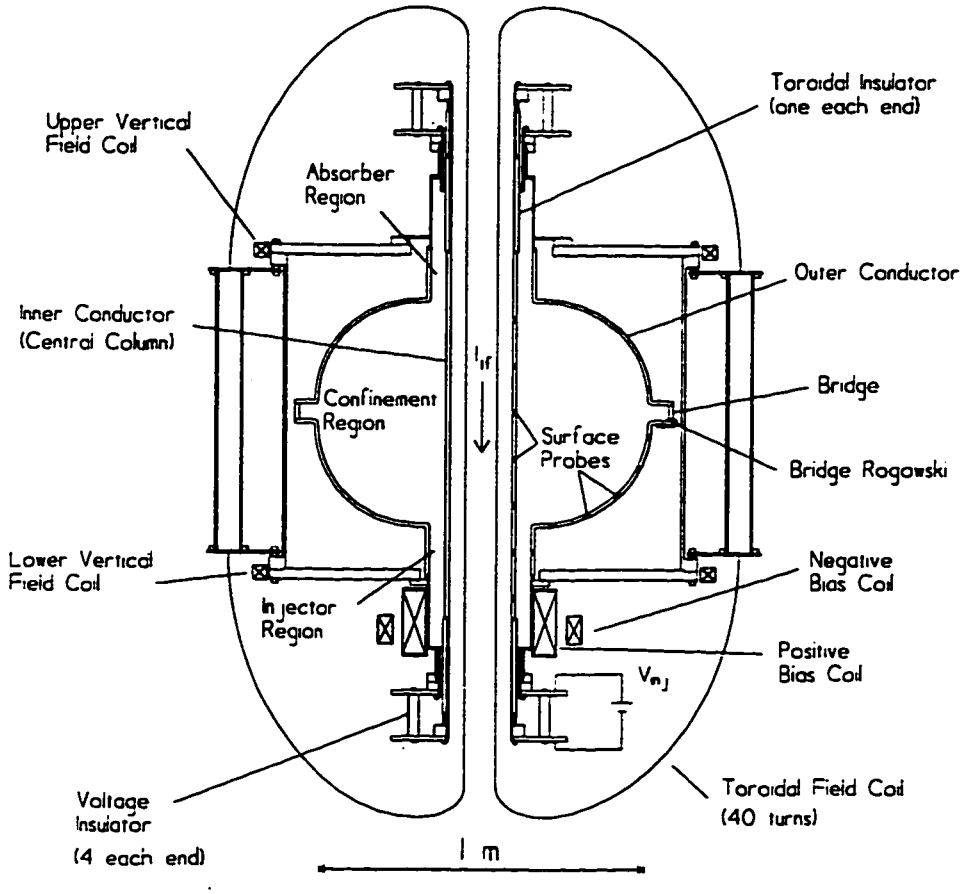

Figure 2.1: The Helicity Injected Tokamak (HIT) Experiment

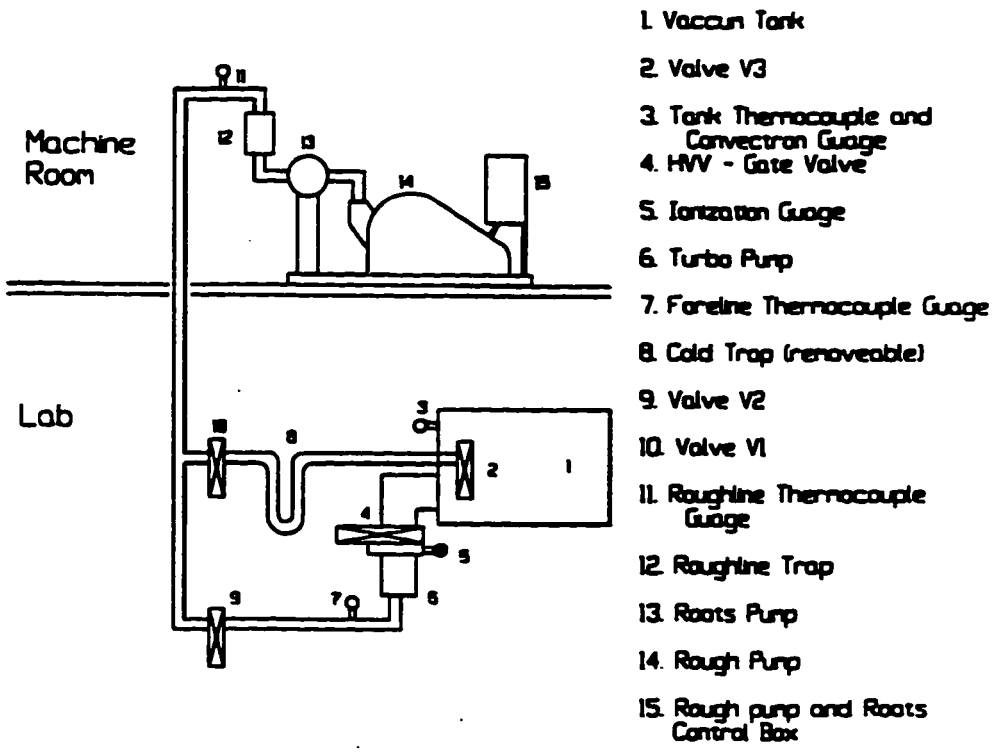

Figure 2.2: Schematic of the Vacuum System on the HIT experiment

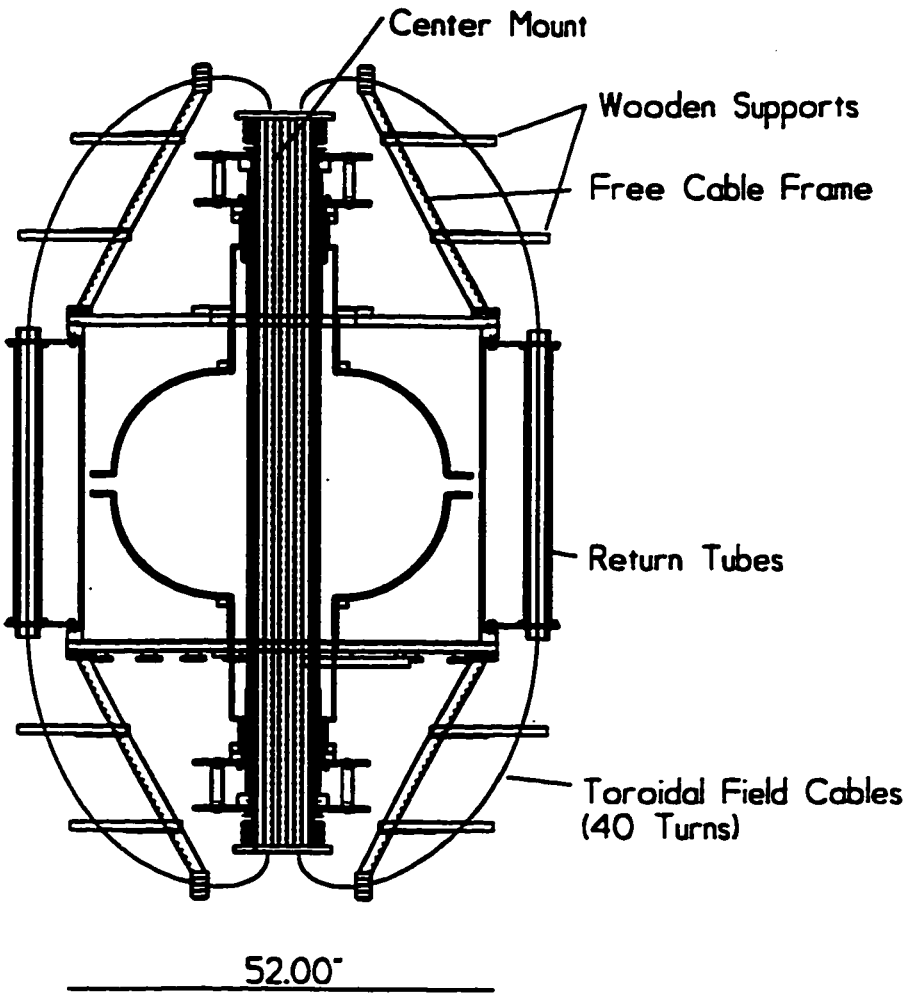

Figure 2.3: Major components of the TF coil

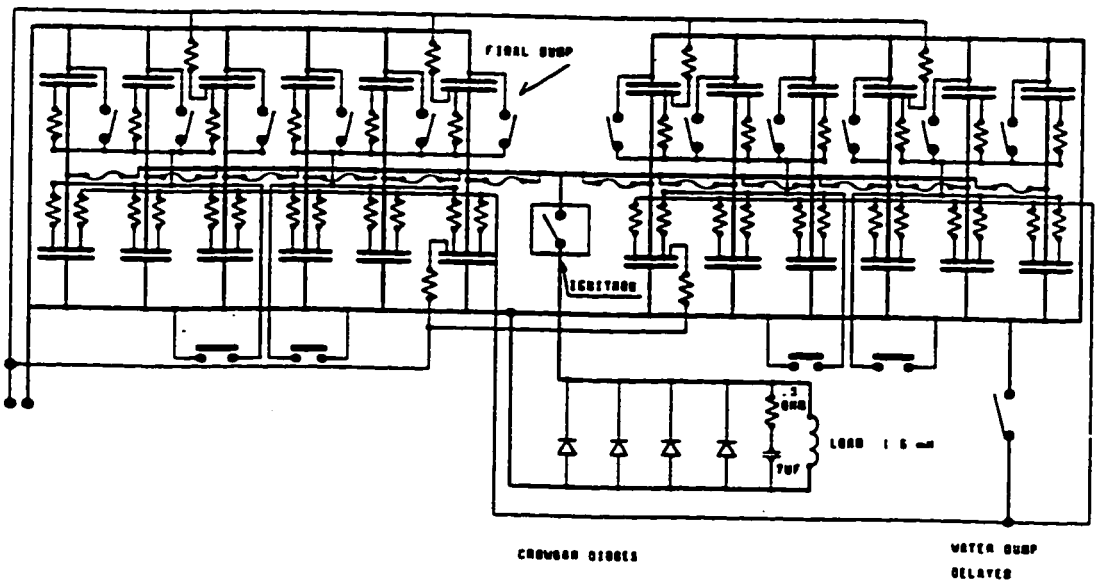

Figure 2.4: Schematic of the TF Bank

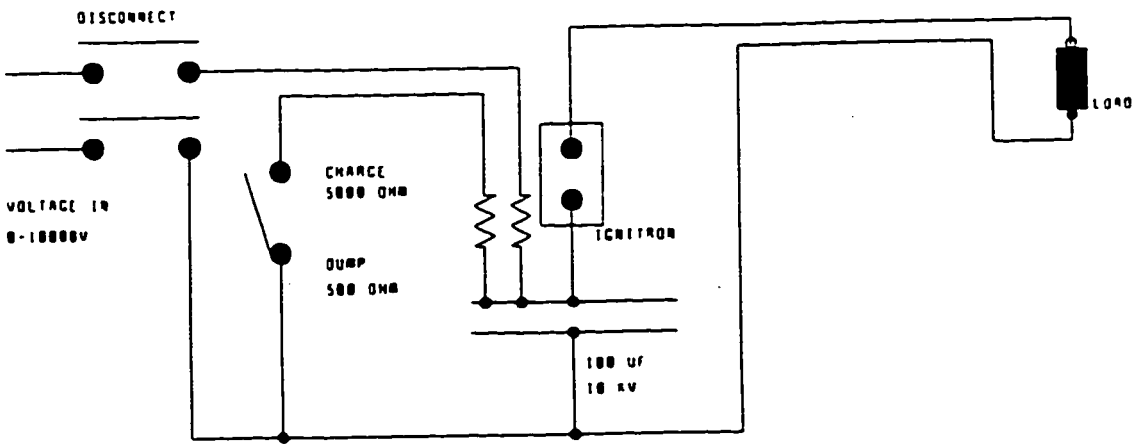

Figure 2.5: Schematic of the pre-ionization bank

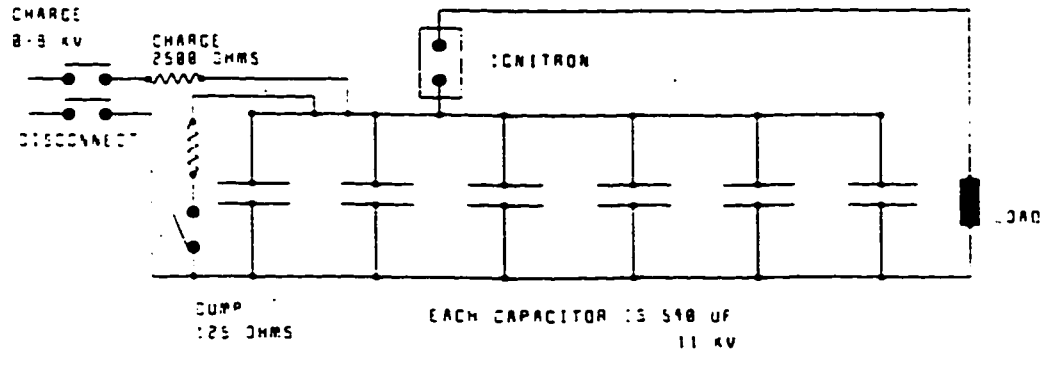

Figure 2.6: Schematic of the formation bank

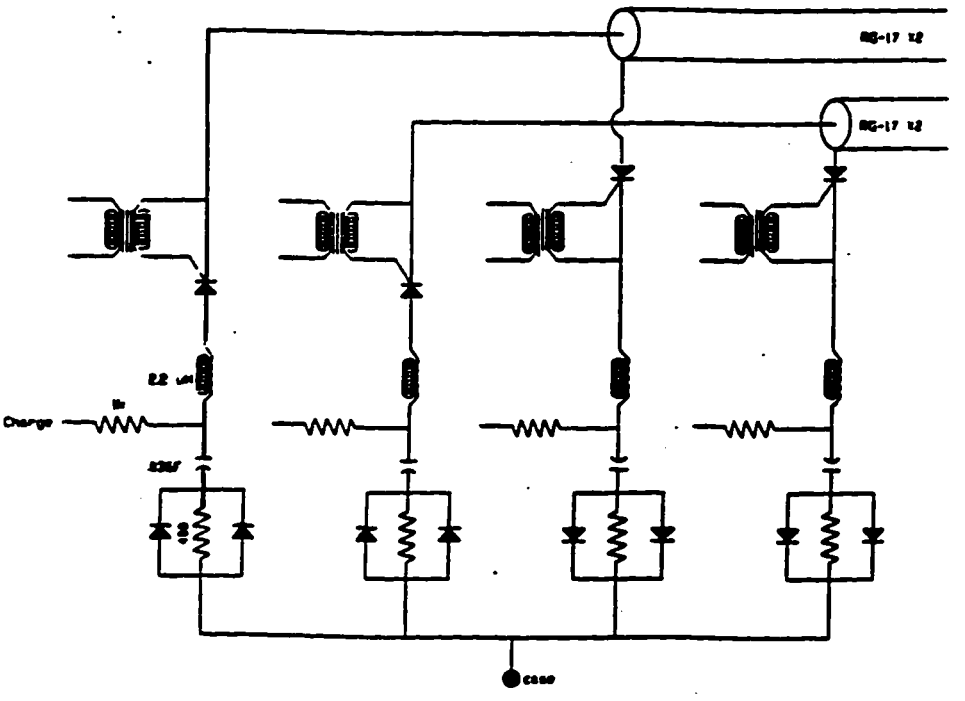

Figure 2.7: Schematic of the sustainment bank

3. Diagnostics on HIT

3.1 Introduction to Chapter 3

The HIT experiment has a variety of diagnostics, including: voltage probes, surface magnetic field probes, rogowski loops to measure current in the flux conserver, and flux loops to measure poloidal flux at the wall; the magnetic diagnostics are shown in fig. 3.1. There is also a 184.6 μm FIR heterodyne interferometry system, a ruby laser Thomson scattering diagnostic, two 0.2 m VUV monochrometers, and a triple Langmuir probe.

For the purposes of this work, the primary diagnostics used are the voltage probes, the surface magnetic field probes, and the triple Langmuir probe; these will be described in detail in this chapter.

3.2 Voltage Probes

Voltage probes are placed on both the injector and the absorber ends of the experiment. These consist of voltage dividers (divide by 100) attached to the electrodes. The dividers are contained in a metal box, grounded at the experimental grounding plane. The divided voltage-probe signals are carried by twisted pair cables to the input of a LeCroy 8100 differential amplifier.

3.3 Surface Magnetic Field Probe Array

The surface magnetic field probes were designed and built by D. J. Orvis and are described in detail elsewhere[24]. Here they will be described in brief.

The copper flux conserver of the HIT experiment has 36 magnetic-field probe triplets built into its surface. There are 18 probe locations at each of two toroidal positions; 7 on the

inner conductor, and 11 on the outer shell. Of these, three probes are in the injector region; 2 on the inner conductor, one on the outer injector electrode.

The probes are made from #32 magnet wire wound on forms machined from KLF teflon. The poloidal probes are placed closest to the surface to maximize their sensitivity.

Each of the probe triplets on the outer flux conserver are contained in a metal sheath which serves as a vacuum wall. The KLF forms are glued inside of an inconel can, that has a stainless steel Swagelok connector welded on to it. The twisted-pair probe-leads leave the probe through 3/16" stainless steel tubing connected to the probe sheath by the Swagelok connector. Inconel is used as it is resistive, and because of its robustness to plasma wall loading. The probes are mounted onto the flux conserver with stainless steel clamps.

The probe triplets on the inner flux conserver are cemented into their holes with silicone rubber cement. The holes are plugged with 0.5 mm thick inconel plates that are sealed with a 5% silver-95% tin solder. Since the central electrode is raised to several kilovolts during a discharge, the probes mounted on it are connected to digitizers in a floating rack, with isolated power. The floating rack is optically connected to the data acquisition system.

As the probes are surrounded by copper and the inconel of the probe sheaths, the magnetic field measured by the probe is not the same as that applied at the surface of the flux conserver. The Fourier components of the field diffuse into the copper at different rates, giving the probes a non-uniform frequency response. This is compensated for in the following way: A magnetic field is applied, and measured by both the surface probe and by a reference probe just above the surface. By taking the Fourier transform of both and dividing that of the reference probe by that of the surface probe, a complex frequency response function is

obtained. Magnetic field data is Fourier transformed, multiplied by the response function for that probe, and then inverse Fourier transformed, yielding the field at the surface of the probe.

In the case of the poloidal probes on the central electrode, the calibration was done by placing a single-turn solenoid around the central electrode before the experiment was assembled. The pre-ionization, formation, and sustainment banks, as well as an additional fast bank were in turn fired into the coil to produce the calibration fields. The shell probes were calibrated using the toroidal field.

The response functions obtained with each of the four banks individually are used to construct a single response function that is valid for the whole frequency range excited by the banks.

3.4 Langmuir Triple Probe

A triple langmuir probe was installed at the midplane to measure the electron temperature in the plasma edge; a diagram of the probe is shown in figure 3.2. The triple probe consists of one probe used as a floating probe and two used in a double probe configuration. The floating probe has a high impedance to ground and measures the floating voltage, V_f. The two remaining probes are connected in series, so that no net current is drawn from the plasma, and are biased above and below the floating probe. These two voltages are called V_- and V_+ respectively. The two probes, forming the double probe pair, also float. The three probes measure the voltage and current at three points on the I-V characteristic, and from this the electron temperature may be measured[25].

The probes are graphite rods held in a ceramic cylinder at the end of a stainless steel pipe, which serves as an electrostatic shield. The pipe is housed within a stainless steel

bellows assembly, mounted on the vacuum vessel, which allows the probe to be pulled out beyond the getter blind. The graphite rods are inserted in split hypodermic tubing which is soldered to teflon clad wires, which in turn are connected to insulated BNC feedthroughs on a conflat flange. This flange is connected to the stainless steel pipe with a swagelok connector and held off of the bellows by a ceramic insulator, which electrically isolates it from the tank. A hollow graphite cylinder is threaded on to the pipe to armor the probe against the plasma. The interior of the probe assembly and especially the solder joints were thoroughly cleaned with Freon before the probe was installed on the experiment. The tips are 1.2 mm in diameter and extend 4 mm beyond the end of the graphite armor.

The three signals from the probe are measured with differential voltage dividers, housed in a metal enclosure that is electrically connected to the machine ground at the data acquisition rack. The enclosure also contains an electrolytic capacitor which is used to bias the double probe. There are four output signals from the divider box, which when processed, yield V_f, V_-, V_+, and I_{probe}, the current in the double probe.

The belief time of the probe is calculated using a 1-D heat transport model which includes sheath effects[26]:

$$\tau_{belief} = \frac{\pi \rho \kappa C T^2_{boil}}{P^2}$$

where:

$$P = \frac{n_i}{\sqrt{2\pi m_i}} (kT_e)^{\frac{3}{2}} \left[\frac{1}{2} \ln\left(\frac{m_i}{m_e}\right) + 4 \right]$$

is the power per unit area deposited on the surface of the probe; and ρ, κ, C, and T_{boil} are respectively the density, heat conductivity, heat capacity, and boiling temperature of the probe material. Using conservative material constants for graphite, and assuming a number density of $n = 1 \times 10^{20}$ m_{-3}, the belief time is calculated to be 1.85 s for $T_e = 20$ eV and 9 ms for $T_e = 100$ eV. As discharges typically last about 6 to 10 ms, the probe's measurements should not be compromised during the course of the shot.

The current measured by the floating probe is by definition 0:

$$I(V_f) = 0 = I_{is} - I_{es} \exp\left[-\frac{(V_p - V_f)}{T_e} \right]$$

where I_{is} and I_{es} are the ion and electron saturation currents respectively, V_p is the plasma potential, and T_e is the electron temperature in eV. This equation yields a relation for V_p in terms of V_f:

$$V_p = V_f + \frac{T_e}{2} \ln\left(\frac{m_i}{m_e}\right)$$

The current from the probe biased at V_- is given by:

$$I(V_-) = I_{is} - I_{es}\exp\left[-\frac{(V_p - V_-)}{T_e}\right]$$

The current in the probe biased at V_+ is equal and opposite, and therefore given by:

$$I(V_+) = I_{es}\exp\left[-\frac{(V_p - V_+)}{T_e}\right] - I_{is}$$

Equating these two currents, and using the relation for V_p, gives an equation which may be solved numerically for T_e:

$$2e^{V_f/T_e} = e^{V_-/T_e} + e^{V_+/T_e}$$

3.5 The EFIT Equilibrium Fitting Code

EFIT, an equilibrium solver developed at GA Technologies, Inc.[27] has been adapted to compute the equilibrium of the HIT experiment. It solves the Grad-Shafranov equation in arbitrary geometries, using a Green's Function technique. The solution is obtained by Picard iterations, which approximately conserve the external magnetic measurements.

The equilibrium is fitted to global parameters of the plasma, such as the plasma current I_p, injector current, I_{inj}, and the paramagnetism $\Delta\Phi_t$. It is also fitted to local measurements of density, temperature, magnetic field, and flux. The free functions, $FF'(\chi)$ and $P(\chi)$, are modeled as polynomials in χ, a normalized stream function defined by:

$$\chi = \frac{\psi_0 - \psi}{\psi_0 - \psi_{sep}}$$

where ψ_0 and ψ_{sep} are ψ at the magnetic axis and separatrix respectively.

The fitting is interleaved with the equilibrium iterations which rapidly converges to an equilibrium with minimum fitting error. The EFIT code has been adapted to run on both the VAXstation 4000 and the DEC 3000/400 AXP.

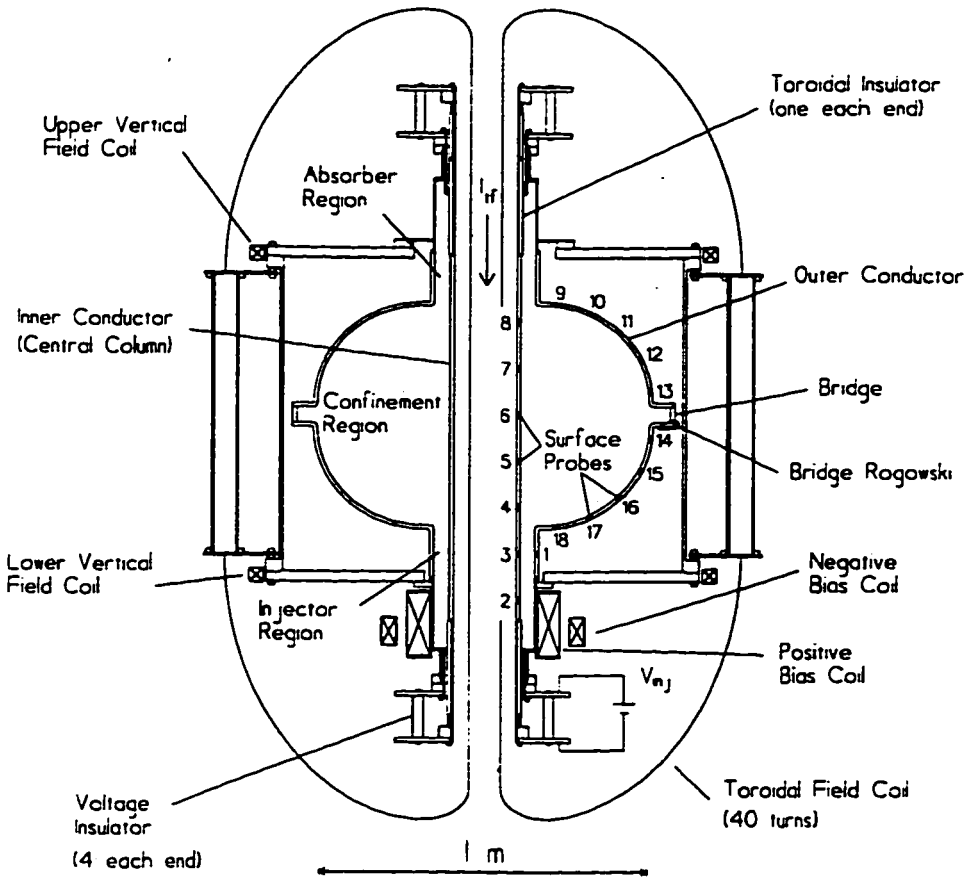

Figure 3.1: Magnetic diagnostics on the HIT experiment

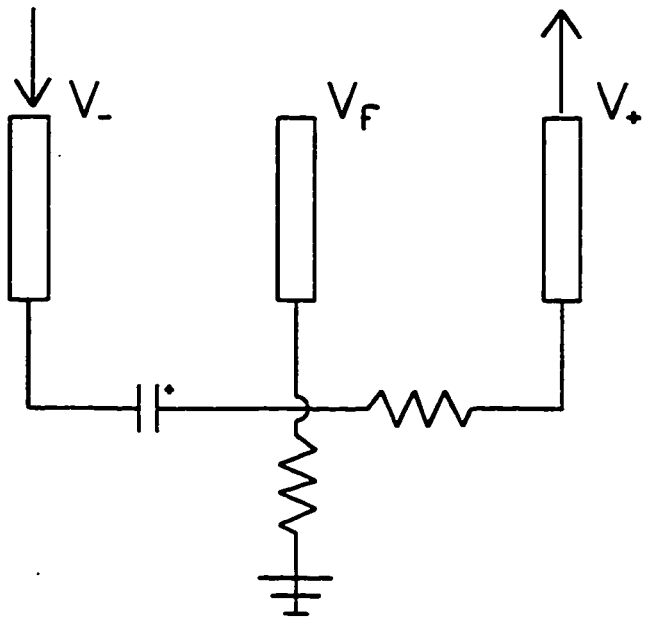

Figure 3.2: Diagram of the Langmuir triple probe

4. Resistive Open Field-Line Model for the HIT Helicity Injector and Edge Region

4.1 Overview of Chapter 4

This chapter introduces a model for the operation of the helicity injector, which is the subject of this dissertation; it is organized as follows: Sections 4.2 and 4.3 reviews previous work on this subject from the CTX spheromak experiment and the HIT tokamak experiment. Section 4.4 describes the assumptions of the resistive open field-line model and justifies them. Section 4.5 presents the model and section 4.6 describes its implementation.

4.2 Injector Operation on the CTX Experiment

An ideal MHD model of flux flow was used to predict the efficiency and impedance of the coaxial magnetized injector of the CTX experiment[28]. The injector was modeled as a magnetic channel with a sharp boundary between the axial flux frozen in the wall and the toroidal flux entrained in the plasma flow. A gun parameter was defined as follows:

$$\Lambda \equiv \frac{V_{gun}}{I_{gun}^{\,2}} \frac{4\pi^2 M}{e\mu_0^{\,2}}$$

where V_g and I_g are the measured gun voltage and current respectively and M is the ion mass. This was compared to the quantity $\Xi F(\lambda_g, r_e)$, where $\Xi \equiv (M/e)I_g/(dm/dt)$ is the Hall parameter and $F(\lambda_g, r_e)$ is a function derived from the ideal MHD model, with λ_g the λ of the gun and r_e the radius of the spheromak entrance region. A fit between these two quantities was obtained, using two parameters, the $\lambda_{threshold}$ of the injector and the Hall parameter Ξ. Although the best-fit $\lambda_{threshold}$ could be compared with independent measurements, Ξ was not

measured.

The voltage and current measurements were also found to obey a simple empirical law (ibid.):

$$V_g = \eta_{eff}\left(\frac{I_g - \psi_g \lambda_{threshold}}{\mu_0 r_c}\right)$$

where the gun voltage is linearly proportional to the excess current above the helicity injection threshold; η_{eff} is an empirically determined effective resistivity. This data is reproduced in figure 4.1. This suggests that the saturated plasma dynamic impedance can best be modelled with a simple resistivity in the inter-electrode volume.

4.3 Injector Operation on the HIT experiment: Initial Work

A simple model was used to predict the equilibrium operation of the HIT helicity injector on the proto-HIT experiment[29]. The amount of injector current necessary to stretch the bias flux out of the injector (called the stretch current, I_s), was sought as a function of the injector geometry and the applied bias flux and TF coil current.

The electrode was treated as two coaxial cylinders of infinite axial extent; this approximates a transition region between the injector, where flux penetrates the wall, and the confinement region. The magnetic fields for a Taylor state are solved subject to the boundary conditions, $B_\theta(a) = \mu_0 I_{TF}/2\pi a$, $B_\theta(b) = \mu_0 I_{TF}/2\pi b$, and $B_z(r_0) = 0$, where a and b are the inner and outer radii of the electrode respectively, r_0 is the reversal point of the field, and I_{TF} is the current in the toroidal field coil. Using the relation, $\lambda = \mu_0 I_s/\psi_{inj}$, I_{TF} may be solved in terms of I_s and λ:

$$I_{TF} = \frac{I_{ss}}{\left[AJ_1(\lambda r_0) + CY_1(\lambda r_0)\right]\frac{r_0}{a} - 1}$$

where:

$$A = \left[Y_1(\lambda b) - (a/b)Y_1(\lambda a)\right] / D$$

$$C = \left[(a/b)J_1(\lambda a) - J_1(\lambda b)\right] / D$$

and:

$$D = J_1(\lambda a)Y_1(\lambda b) - J_1(\lambda b)Y_1(\lambda a)$$

A comparison of this model to the data is shown in fig. 4.2.

A simpler expression may be derived using planar geometry, assuming that the electrode spacing, d = b - a, is small compared to the mean radius and that $I_{TF} \gg I_{ss}$:

$$I_{ss} = \frac{8\psi_{inj}^2}{\mu_0^2 d^2 I_{TF}}$$

This formula approaches the one shown above asymptotically as I_{TF} increases, although it diverges as $I_{TF} \to 0$. The non-transcendental form of this expression explicitly shows the dependence of the stretch current on the injector flux, electrode spacing and I_{TF}.

4.4 Underlying Assumptions of the Resistive Open Field-Line Model

Equilibrium solutions for the HIT experiment obtained from EFIT typically show that only about half of the 4.9 mWb of applied bias flux is pulled out of the injector and that only 20% of the injector current flows on these diverted field lines[30]. The remaining injector current flows on the short open flux that stays in the injector region, where the field lines are shortest. This suggests that the field line length is important, however EFIT assumes an approximately constant **J** in the injector region, independent of field-line length.

We propose a simple resistive model for the operation of the injector which assumes: (a) a force free ($\nabla\times\mathbf{B} = \lambda(\psi)\mathbf{B}$) equilibrium, (b) a simple resistive Ohm's law $\mathbf{E} = \eta\mathbf{J}$ and (c) a region-wise uniform resistivity.

The assumption of a simple equilibrium Ohm's law, $\mathbf{E} = \eta\mathbf{J}$ (assumption b) is justified as follows: In the full Ohm's law, the electric field, **E**, is balanced by four terms: the plasma dynamic term, the Hall term, the electron pressure term, and the resistive term. The electron pressure term is small along open field lines, or where the electron temperature is reasonable uniform, as should be the case on the open field lines. The Hall term is identically zero for a force-free plasma, as $\mathbf{J}\times\mathbf{B} = 0$. In equilibrium there is no plasma flow, eliminating the plasma dynamic term ($\mathbf{v}\times\mathbf{B} = 0$). Even if there is plasma flow, it is unlikely to be a purely dynamic process; if the transit time of flow through the injector is comparable to the resistive diffusion time, there will be significant slippage of plasma with respect to magnetic flux. In the HIT experiment, with a background toroidal field of the order of 1 Tesla, an electrode spacing of 50 mm, and typical injector voltages of 750 v, the $\mathbf{E}\times\mathbf{B}$ flow velocity is less than or of the order of 15,000 m/s, giving a transit time for plasma flow through the injector of 20 μs. The diffusion time for an injector plasma with T_e of 5 eV to 20 eV is in the range of

10 μs to 40 μs.

Even in the CTX experiment, which exhibited the highly dynamic behavior characteristic of spheromak injectors, the impedance was best modeled by a simple resistivity, in which was lumped both the classical Spitzer resistivity as well as the dynamic impedance due to magnetic activity. This works and has the virtue of simplicity. The HIT helicity injector is more quiescent than that of a spheromak, so this approach should be at least as successful as it was in CTX. We therefore assume that the injector impedance can be modeled by a simple resistivity, which includes both the Spitzer resistivity as well as a dynamic component due to magnetic activity.

The assumption of a uniform resistivity (assumption c) is justified for the following reasons:

1.) In low temperature, radiation-dominated plasmas, the resistivity tends to be uniform because Z_{eff} increases with increasing temperature, off-setting the explicit temperature dependence[17].

2.) On an open field line, heated ohmically and cooled by parallel thermal conduction, the average resistivity along the field line depends only on the applied voltage, independent of field line length. This is because the resulting temperature profile is self-similar, and has a peak temperature that is independent of the field line length.

3.) A uniform resistivity is a simple assumption.

The resistivity is uniform by region in the sense that it sometimes proves necessary to use a different resistivity for the injector and confinement regions. This is expected given the vastly different character of the field lines in the two regions; the field lines in the injector region are a few meters long, while the field lines in the confinement region are tens to

hundreds of meters long (fig 4.3). Consequently the heat transport and plasma dynamic mechanisms in these two regions may be quite different.

4.5 The Resistive Open Field-Line Model

The equilibrium in the open field-line region is calculated by solving the force-free Grad-Shafranov equation:

$$R\frac{\partial}{\partial R}\left(\frac{1}{R}\frac{\partial \psi}{\partial R}\right) + \frac{\partial^2 \psi}{\partial Z^2} + \lambda(\psi)\left(\int_0^{\psi}\lambda(u)du + \frac{\mu_0}{2\pi}I_{TF}\right) = 0$$

where ψ is the poloidal flux function and I_{TF} is the current flowing in the toroidal field coil. This form of the Grad-Shafranov equation where the source term is cast in terms of $\lambda(\psi)$ is adapted from one used for spheromaks[31]. The parameter $\lambda(\psi)$ is defined by:

$$\lambda(\psi) = \frac{\mu_0}{2\pi}\frac{dI}{d\psi} = \frac{dF}{d\psi}$$

where $F(\psi) = RB_\phi$ is the poloidal current function familiar from standard treatments of the Grad-Shafranov equation[32].

The resistive model for $\lambda(\psi)$ is derived by considering the general force free state:

$$\nabla \times \vec{B} = \lambda(\psi)\,\vec{B} = \mu_0 \vec{J}$$

Integrating this expression along an open field line, and using $\mathbf{J} = \mathbf{E} / \eta$, yields:

$$\lambda(\psi) \int \vec{B} \cdot d\vec{l} = \frac{\mu_0}{\eta} \int \vec{E} \cdot d\vec{l}$$

which may be rewritten:

$$\lambda(\psi) = \frac{\frac{\mu_0}{\eta} V_{inj}}{\int \vec{B} \cdot d\vec{l}}$$

where $V_{inj} = \int \mathbf{E} \cdot d\mathbf{l}$ is the voltage applied across the injector electrodes.

4.6 Implementation of the Model

4.6.1 General Method

The equilibrium is calculated using ROLEQS2 (Resistive Open-Line Equilibrium Solver), a simple Grad-Shafranov solver written by the author, that uses a simultaneous over-relaxation method (SOR) adapted from "Numerical Recipes"[33]. The source code for ROLEQS2 is given in Appendix C. Interleaved with every equilibrium iteration, $\lambda(\psi)$ on the open field-lines is calculated from the $\psi(R,Z)$ of the previous iteration. This is done by launching a field line at every value of ψ along the center column. The field-line is traced out using a fourth-order Runge-Kutta solver[34], and the value of $\int \mathbf{B} \cdot d\mathbf{l}$ is evaluated. Using the line integral and assuming a value for η, $\lambda(\psi)$ is calculated. In general, two resistivities are used; η_1 for the case $\psi > \psi_{sep}$ and η_2 for the case $\psi < \psi_{sep}$. This allows for different conditions on the two types of open field-lines; the short lines in the injector region and the long lines in the confinement region. The parameterization of $\lambda(\psi)$ on the closed flux is discussed in section 4.6.3.

The calculation continues until the poloidal flux $\psi(R,Z)$ converges to a solution. The convergence criterion is that the total error, defined by:

$$R \equiv \sum_{ij} |\psi_{ij}^{n+1} - \psi_{ij}^{n}|^2$$

decreases to some fraction of the initial error, $R < \epsilon R_{initial}$, where typically $\epsilon = 0.001$. The function $\lambda(\psi)$ is checked after the fact to ensure that it too has converged. The measured values of injector voltage and toroidal field coil current are used in this calculation.

4.6.2 Equilibria with no Closed Flux

There are a number of shots from early in the operating history of HIT which have low plasma currents and little or no closed flux. This was due to the magnetic geometry of the bias flux that was used. Initially a single bias coil was used, producing a dipole field (fig. 4.3.a), which was oppositely directed to the poloidal field of any closed flux that may have formed. This had the effect of disconnecting the tokamak from the injector and attaching it to the wall, where it quickly decayed, significantly degrading the plasma's performance. A second bias coil was subsequently added, which produces a quadrupole bias field, eliminating this problem (fig 4.3.b).

For these early shots there is an extensive set of B-poloidal measurements both in the injector and in the confinement region. We have used these shots initially in developing this model for the following two reasons:

1.) The magnetic fields produced by closed flux shortens the field line length and consequently decreases the resistance on these field lines and changes the $\lambda(\psi)$ profile. Since knowledge of the closed flux profile is needed to properly include this effect, it is more

straightforward to only look at cases with no closed flux; this allows a direct comparison of theory and experiment.

2.) Three magnetic field probes were available in the injector region, which allows a stringent test of the applicability of this model. Two of the probes were removed after these early shots, coincident with the addition of the quadrupole bias coil set.

In calculating the equilibria for these early shots, it was assumed that there was no closed flux. This was imposed as a constraint on the solution by requiring that $\psi \leq \psi_{sep}$ for $Z \geq Z_{sep}$. Both ψ_{sep} and Z_{sep} are determined from the equilibrium ("sep" refers to separatrix). For the early shots, with little or no closed flux, the re-entrant field-lines due to the dipole bias field begin and end on the flux conserving shell, an equipotential surface. Since no current can be driven on these field lines, they were taken out of the calculation by treating this region as part of the flux conserving shell. Consequently the probes in this region, numbered 14 to 18, will not be compared to the calculation. For these early shots, no flux loops were available to measure the flux soaked into the walls, so ψ at the boundary was assumed to be the vacuum ψ.

The two resistivities are adjusted to obtain a good fit between the measured and calculated injector current and surface poloidal magnetic fields. The overall measure of the fit between the measured and calculated magnetic fields, χ^2, is calculated according to:

$$\chi^2 = \sum_{n=1}^{N} \left(\frac{B_p^{meas} - B_p^{calc}}{\sigma_B} \right)^2$$

where σ_B is the uncertainty in the poloidal magnetic field and is taken to be 0.01 Tesla. This work is described in ref. 35.

4.6.3 Equilibria with Closed Flux

Extending this model to more interesting conditions requires the inclusion of closed flux in the problem, for the reasons discussed in the previous section. For shots where closed flux was present, $\lambda(\psi)$ on the closed field-lines was defined by:

$$\lambda(\psi) = \lambda_{edge}\left[1 + \alpha\frac{\psi - \psi_{sep}}{\psi_0 - \psi_{sep}}\right]$$

where ψ_0 is the value of ψ at the magnetic axis. This paramaterization of $\lambda(\psi)$ uses two independent parameters; λ_{edge}, the value of λ at the separatrix, and α, a shape parameter. In addition, a linear pressure profile is assumed:

$$P(\psi) = P_0\frac{\psi - \psi_{sep}}{\psi_0 - \psi_{sep}}$$

where P_0 is the plasma pressure at the magnetic axis.

For these closed flux shots, the poloidal flux loops were available. Measurements from the flux loops were spline-fit on to the grid points corresponding to the flux conserver.

Altogether there are five fitting parameters that determine the equilibrium: the two edge resistivities, η_1 and η_2; three parameters for the closed flux, λ_{edge}, α, and P_0. These parameters are varied to obtain a good fit to I_p, I_{inj}, and B_{pol} as measured by the quantity χ^2 defined by:

$$\chi^2 = \frac{1}{N_{total}} \left[\sum_{n=Inj,Plas} \frac{(I_n^{meas} - I_n^{calc})^2}{\sigma_n^2} + \sum_{n=1}^{N_{mod}} \frac{(B_n^{meas} - B_n^{calc})^2}{\sigma_n^2} \right]$$

Some fraction of the injector current flows through the outer flux conserver wall and appears as bridge current. It is as yet unclear whether this current is due to shorting at the absorber, field-aligned current entering the wall on soaked-in flux, or current diffusion across the diverted flux. For now, it is assumed that this current flows at the absorber, and its value is subtracted from the injector current for these calculations.

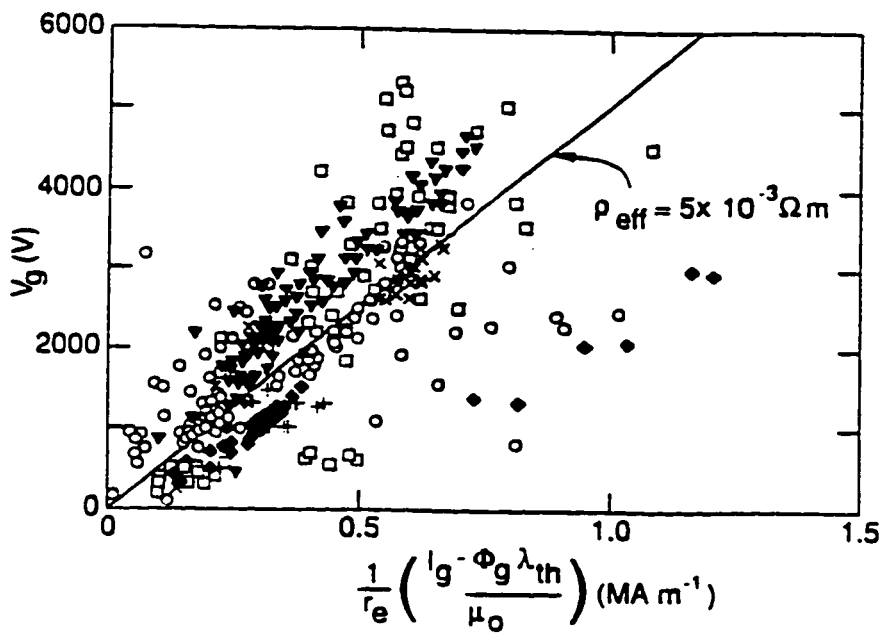

Figure 4.1: CTX gun voltage vs. current above the helicity injection threshold (Reproduced from Barnes et. al., Reference 28).

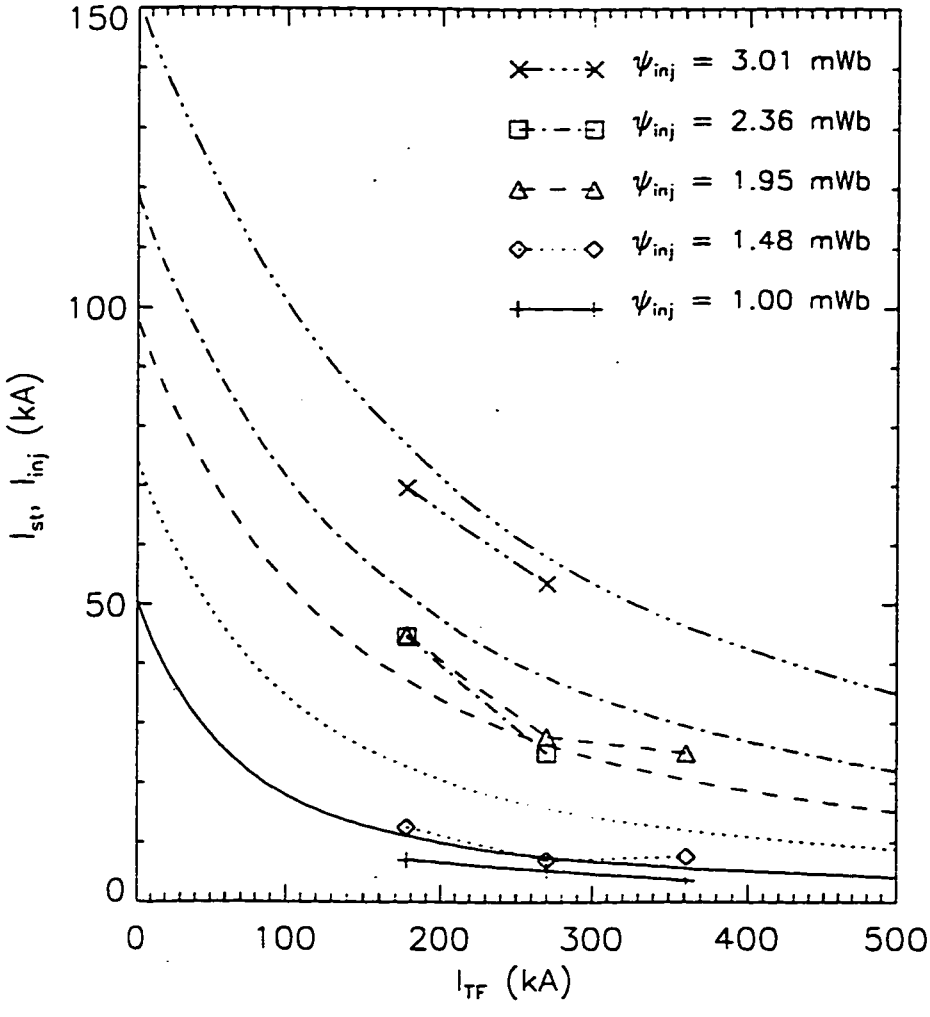

Figure 4.2: Current Required to stretch bias flux, I_{st} versus toroidal field current, I_{TF}. Points are measured values of I_{inj} and curves are model calculations of I_{st}.

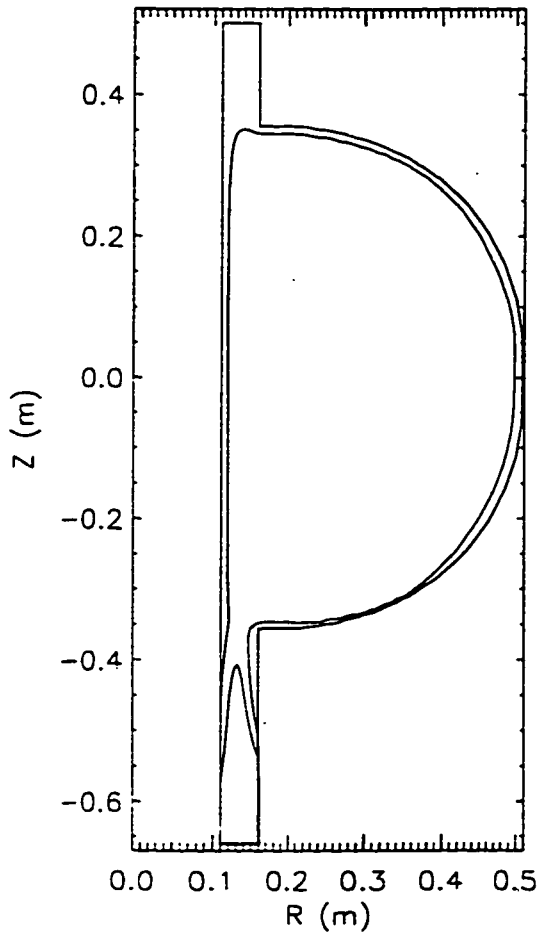

Figure 4.3: Representative long and short field-lines

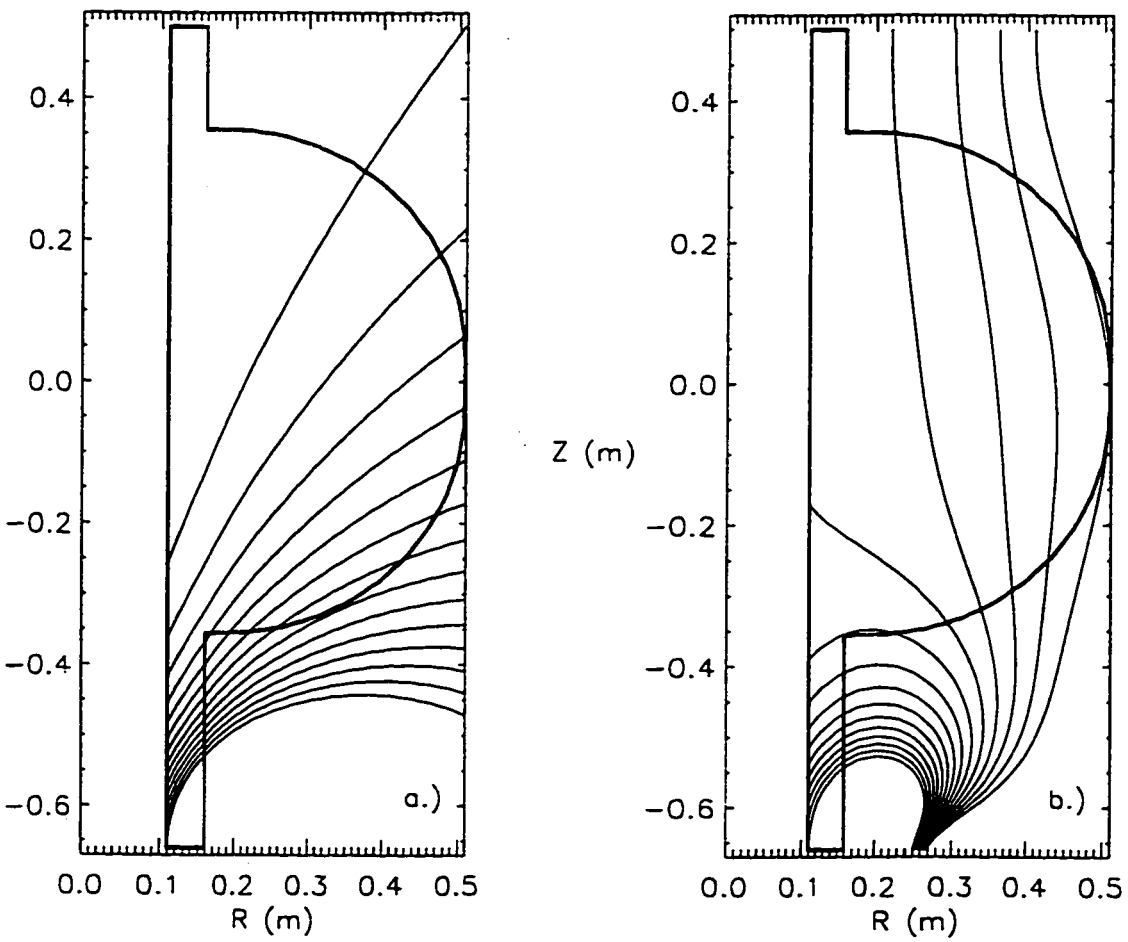

Figure 4.4: Contours of vacuum poloidal flux; a.) dipole field b.) quadrupole field

5. Results of the Resistive Open Field-line Model

5.1 Results

5.1.1 Equilibria with no Closed Flux

Figure 5.1. shows plots of I_{inj} and V_{inj} vs. time for a shot using only the positive bias coil (dipole bias field) and which has little or no closed flux. The flux contours calculated using this model at two times during this shot (dashed vertical lines in figure 5.1) are shown in figure 5.2. Figure 5.3.a shows a comparison of the measured and calculated surface poloidal magnetic fields at time $t_. = 0.5$ ms. One uniform resistivity is used for this calculation; $\eta = 8.0 \times 10^{-5}$ Ω-m. Figure 5.3.b shows the comparison of measured and calculated fields at time $t = 1.0$ ms. In this case two resistivities are used; $\eta_1 = 1.62 \times 10^{-4}$ Ω-m in the injector and $\eta_2 = 4.5 \times 10^{-5}$ Ω-m in the confinement region. The fits for a variety of other shots and times are included in appendix A. Figure 5.4 shows plots of the fitting parameters, η_1 and η_2 for a series of times during this same shot.

5.1.2 Equilibria with Closed Flux

Figure 5.5. shows plots of I_{inj}, I_p, and V_{inj} vs. time for a high performance shot (Shot 6737). The electron temperature at the magnetic axis, from Thomson scattering, was measured to be $T_e = 77$ eV at this time. This was used to calculate the pressure, P_0, for use in the equilibrium calculation. The calculated flux contours for this shot are shown in figure 5.6; a comparison of the measured and calculated surface poloidal magnetic fields is shown in figure 5.7. The two edge resistivities used are $\eta_1 = 2.0 \times 10^{-5}$ Ω-m in the injector and $\eta_2 = 2.2 \times 10^{-5}$ Ω-m in the confinement region.

Figure 5.8 shows plots of I_{inj}, V_{inj} and I_{plasma} vs. time for a shot where data from the langmuir probe was available (Shot 9552). Figures 5.9 and 5.10 show the calculated flux

contours and the measured and calculated surface poloidal magnetic fields respectively. The two edge resistivities used are $\eta_1 = 1.5 \times 10^{-5}$ Ω-m in the injector and $\eta_2 = 3.0 \times 10^{-5}$ Ω-m in the confinement region.

The equilibria calculated for shots with the langmuir probe do not fit the B probe data as well as those without it, especially those probes on the outer shell below the midplane. This may be a probe effect: the probe tips were not baked before use and they may have released impurities into the plasma. The increase in plasma resistivity due to these impurities can cause current to flow across field lines, which violates the force-free assumption implicit in the model.

Additional fits for closed flux equilibria are included in Appendix B.

5.1.3 Edge Temperature Measurements

A number of shots were taken when the langmuir probe was available for measurement of the edge electron temperature at the midplane. It often occurred that a large current pulse was measured by the probe, at which time the floating voltage, V_f would drop below the negative bias voltage, V_-. It is believed that at these times the probe was no longer measuring a well defined characteristic, which makes it impossible to infer T_e.

The voltage traces from the langmuir probe for shot 9552 are shown in figure 5.11; figure 5.12 shows the resultant T_e vs. time. The electron temperature is measured to be approximately 20 eV during the first 4 ms of the shot, then climbs to values in excess of 100 eV coincident with the peak in I_p.

5.2 Discussion

5.2.1 Equilibria with no Closed Flux

The resistive open-field-line model agrees well with the data, with as few as one fitting parameter. In the first case (fig. 5.3.a), $\eta = 8.0 \times 10^{-5}$ Ω-m, corresponding to a T_e of about 5 eV, assuming $Z_{eff} = 3$, and parallel Spitzer resistivity. This temperature is in rough agreement with previous estimates of T_e in cold, radiation dominated plasmas in the Proto-HIT experiment[29]. For these early shots, as with all the proto-HIT data, there was a dipole bias field and no glow-discharge cleaning or Titanium gettering was used for impurity control.

In the second case at t = 1.0 ms (fig. 5.3.b), $\eta_1 = 1.62 \times 10^{-4}$ Ω-m in the injector region and $\eta_2 = 4.5 \times 10^{-5}$ Ω-m in the confinement region, corresponding to electron temperatures of 3.5 eV and 8 eV respectively.

As seen in figure 5.4, the resistivity in the injector region is typically larger than that in the confinement region, with η_1 reaching values as high as 0.8 mΩ-m. At those times when η_1 becomes much larger than η_2, I_{inj} is relatively low - of the order of 1 or 2 kA, and it is possible that the injector becomes gas starved at these times, which would lead to an increase in resistivity. However, this may also be evidence that the impedance has a dynamic component. Relaxation activity, which is expected for a lambda that is peaked in the injector, can cause a back-EMF which manifests itself as an effective resistivity, as was discussed in section 4.4.

Using the resistivities in figure 5.4 and assuming $2 \leq Z_{eff} \leq 4$ the inferred electron temperature in the injector region lies in the range $1 \text{ eV} \leq T_e \leq 6 \text{ eV}$; that in the confinement region in the range $3 \text{ eV} \leq T_e \leq 11 \text{ eV}$. If those times when I_{inj} is low are omitted the inferred temperatures in the injector and confinement regions are $3 \text{ eV} \leq T_e \leq$

6 eV and 6 eV $\leq T_e \leq$ 11 eV respectively.

5.2.1 Equilibria with Closed Flux

The equilibrium calculation yields good agreement with measurements for shot 6737, a high performance shot (fig. 5.7), with an essentially uniform resistivity of ~ 2.0x10-5 Ω-m. This corresponds to an electron temperature of T_e = 12 - 19 eV assuming a Z_{eff} of 2 to 4. These high performance shots made use of a quadrupole bias field and in addition, both glow-discharge cleaning and Titanium gettering were used for impurity control. The lambda profile is quite hollow, actually decreasing to zero at the magnetic axis. The amount of diverted flux for this equilibrium is 3 mWb out of the applied bias flux of 5.1 mWb; there is 12.8 mWb of closed flux.

For shot 9552, the resistivities used were $\eta_1 = 1.5 \times 10^{-5}$ Ω-m and $\eta_2 = 3.0 \times 10^{-5}$ Ω-m, corresponding to electron temperatures of 14 eV $\leq T_e \leq$ 23 eV in the injector and 9 eV $\leq T_e \leq$ 14 eV in the confinement region, assuming Z_{eff} ranges between 2 and 4. At this time (4.85 ms) T_e = 43 eV from the langmuir probe. The measurements of T_e using the langmuir probe correspond to resistivities which are consistently less than those required by the equilibrium. The excess resistivity over the Spitzer value may be due to magnetic activity. The diverted flux is 3.28 mWb out of an applied flux of 4.7 mWb and the closed flux is 9.4 mWb. The profile is hollow, and a finite pressure was used in calculating the equilibrium. The fit to the data is not as good as in the previous shot discussed, particularly on the outer shell below midplane, possibly because of the effect of the langmuir probe. The tips of the probe were not baked prior to use, which could have added impurities to the plasma during the shot. The resistivity due to these impurities would result in current reaching the wall across the field lines, violating the assumption of field aligned current

implicit in the model.

5.2.3 Helicity Balance Considerations

If there are no anomalous helicity losses, an effective resistivity for helicity balance (η_K) may be defined. This assumes that the electron temperature is uniform throughout the whole plasma volume. The helicity conservation equation is in this case:

$$2V_{inj}\psi_{inj} = \eta_K \int \vec{J}\cdot\vec{B}dV$$

The rate of helicity injection $K_{inj} = 2V_{inj}\psi_{inj}$, together with the volume integral $\int \mathbf{J}\cdot\mathbf{B}dV$, evaluated from the calculated equilibrium, gives η_K. For the high performance shot discussed above (shot 6737), $\eta_K = 9.8 \times 10^{-6}$ Ω-m. For a shot where Langmuir probe data was available (shot 9552), $\eta_K = 1.0 \times 10^{-5}$ Ω-m at time t = 4.85 ms; this corresponds to an electron temperature of 19 eV $\leq T_e \leq$ 30 eV assuming $2 \leq Z_{eff} \leq 4$. At this same time T_e at the edge is measured to be 43 eV with the Langmuir probe. A measured T_e greater than that calculated from η_K is consistent with the picture of a dynamic impedance on the open field lines driving current on the closed field lines through a coupling mechanism that conserves helicity.

5.3 Suggested Future Work

The HIT-II experiment should prove a useful vehicle for further research in this area. The equilibrium flux control system will allow a variety of edge flux arrangements to be investigated as to their current drive efficiencies. HIT-II has a full complement of edge B poloidal probes in the injector region. In addition, it will be possible to place a langmuir

probe in the injector region as well as the confinement region, allowing T_e to be measured in both places. A Bremsstrahlung diagnostic for the measurement of Z_{eff} will also be available. Together, these three measurements will allow a more stringent test of the resistive open field-line model. Measurement of the injector voltage at a faster digitization rate, that can resolve the voltage spikes, will allow the relation between the edge resistivity and the voltage fluctuations to be investigated.

Incorporation of this model into EFIT, which uses a constrained optimization technique, will make the model more efficient in its operation, in addition to allowing EFIT to more correctly treat the edge region.

5.4 Summary

An equilibrium model for helicity injector operation has been developed that treats the open field lines as being in a force-free equilibrium determined by the field-line length, the applied injector voltage and an effective resistivity. This resistivity may include a dynamic component in addition to the purely resistive Spitzer part. The equilibria calculated using this model agree with measurements of B_{pol} and I_{inj} and I_p, with as few as one fitting parameter. Equilibria with purely open flux as well as those with both open and closed flux have been calculated and found to agree with experiment.

These calculations are consistent with electron temperature, as measured with a langmuir probe, in that the purely Spitzer resistivity due to T_e is always less than the resistivity required by the equilibrium. The excess resistivity above the Spitzer value may be due to magnetic activity, especially in the cases where closed flux is formed. Further, when helicity balance is used to calculate the resistivity, the corresponding T_e is within the accuracy

of the Langmuir probe measurement.

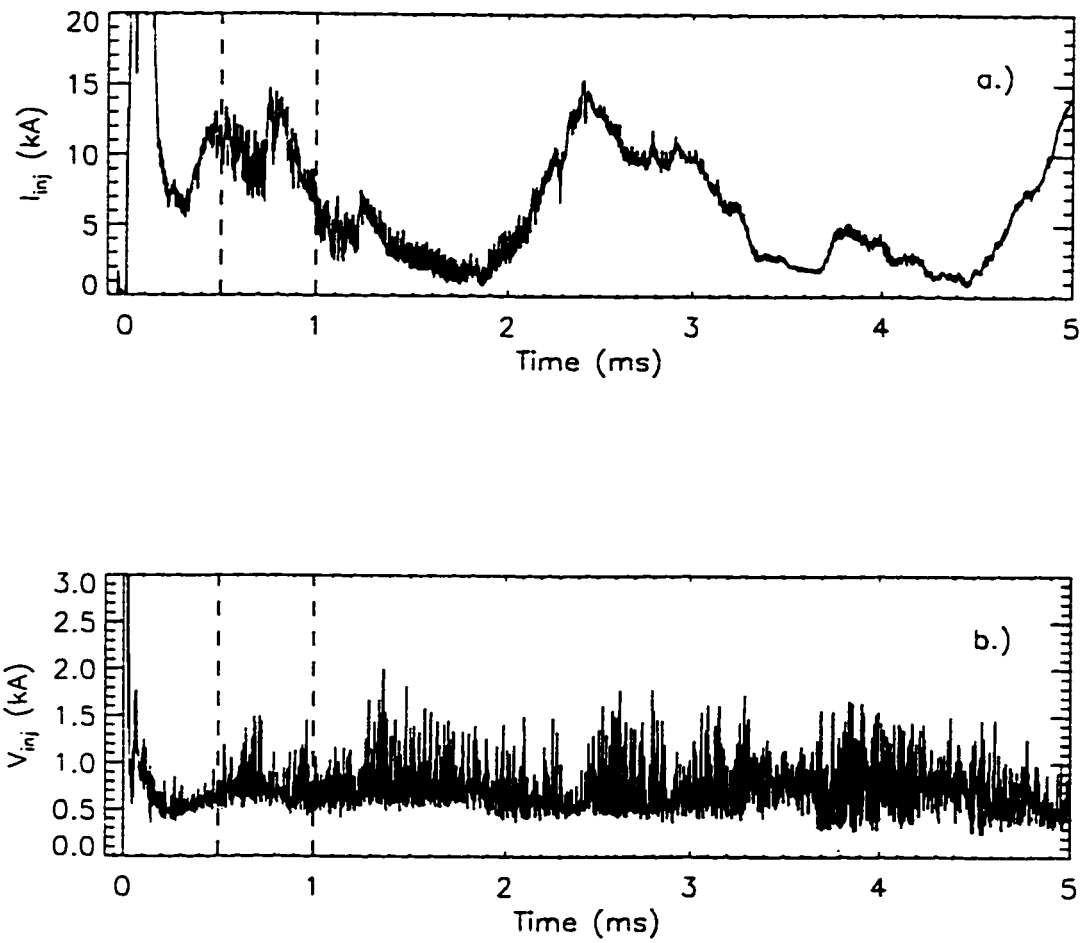

Figure 5.1: Current and voltage waveforms for a shot (3371) with a dipole bias field and no closed flux; a.) I_{inj} vs. time b.) V_{inj} vs time. Dashed lines at t = 0.5 ms and t = 1.0 ms indicate two times where equilibria are calculated.

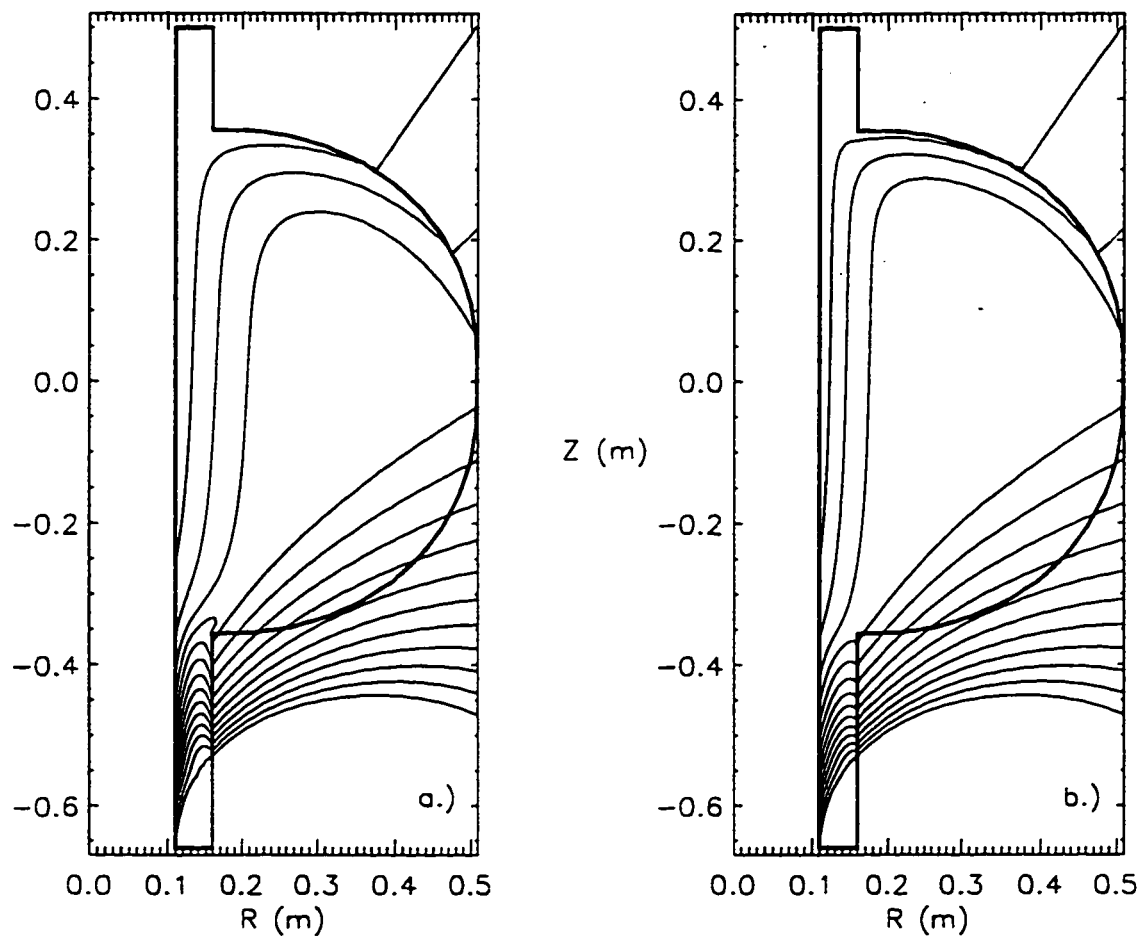

Figure 5.2: Flux contours for a shot (3371) with no closed flux; a.) t = 0.5 ms b.) t = 1.0 ms

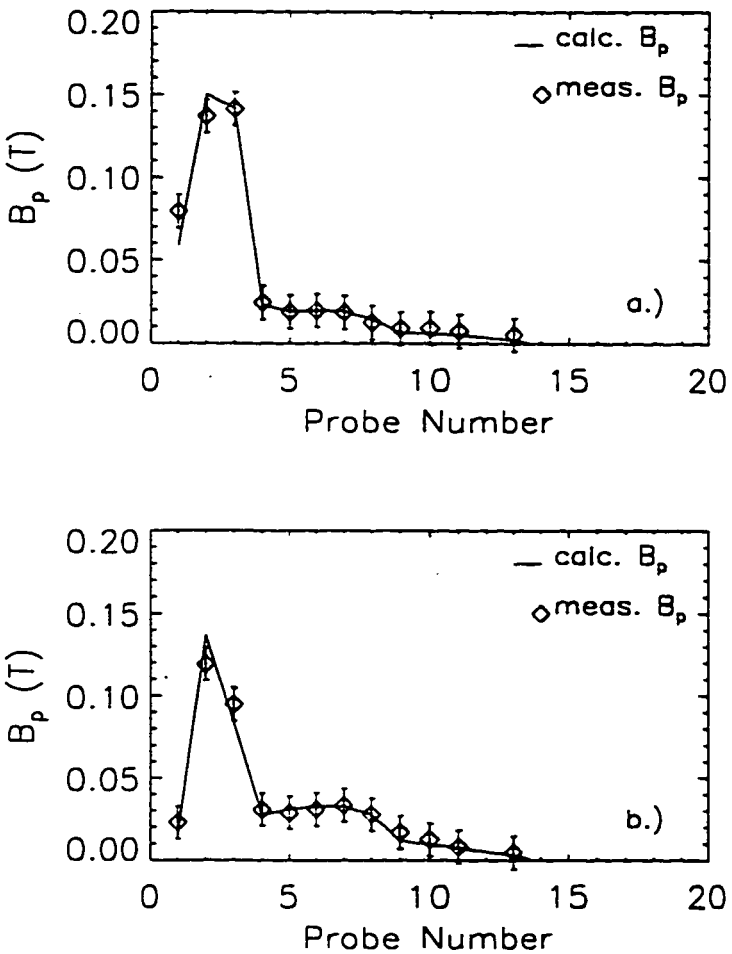

Figure 5.3: Comparison of measured and calculated B poloidal fields for a shot (3371) with no closed flux; a.) t = 0.5 ms, measured I_{inj} = 10.9 kA, calculated I_{inj} = 11.3 kA, χ^2 = 0.54; b.) t = 1.0 ms, measured I_{inj} = 6.7 kA, calculated I_{inj} = 6.7 kA, χ^2 = 0.46.

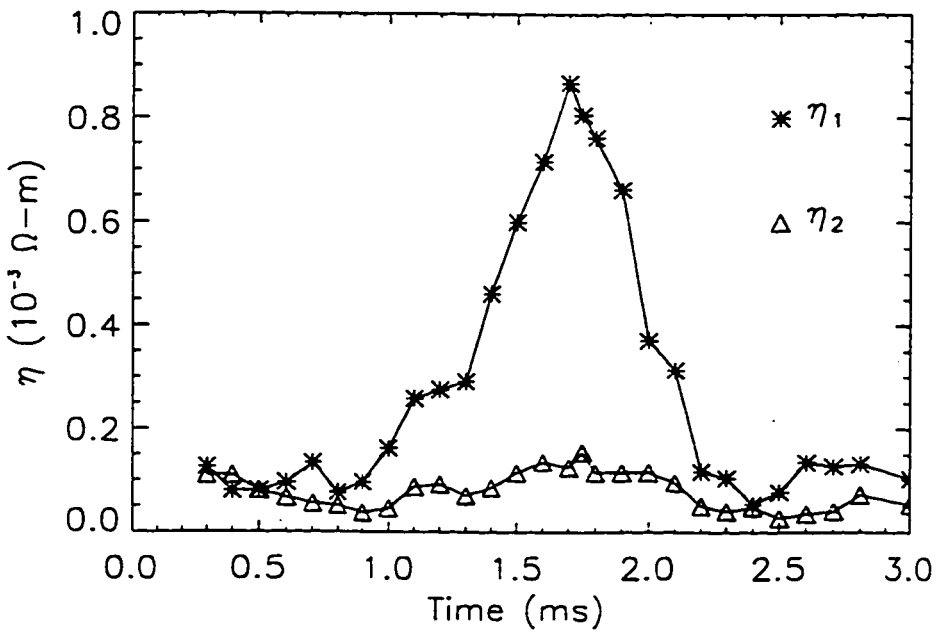

Figure 5.4: Fitting parameters, η_1 and η_2 vs. time for a shot (3371) with no closed flux

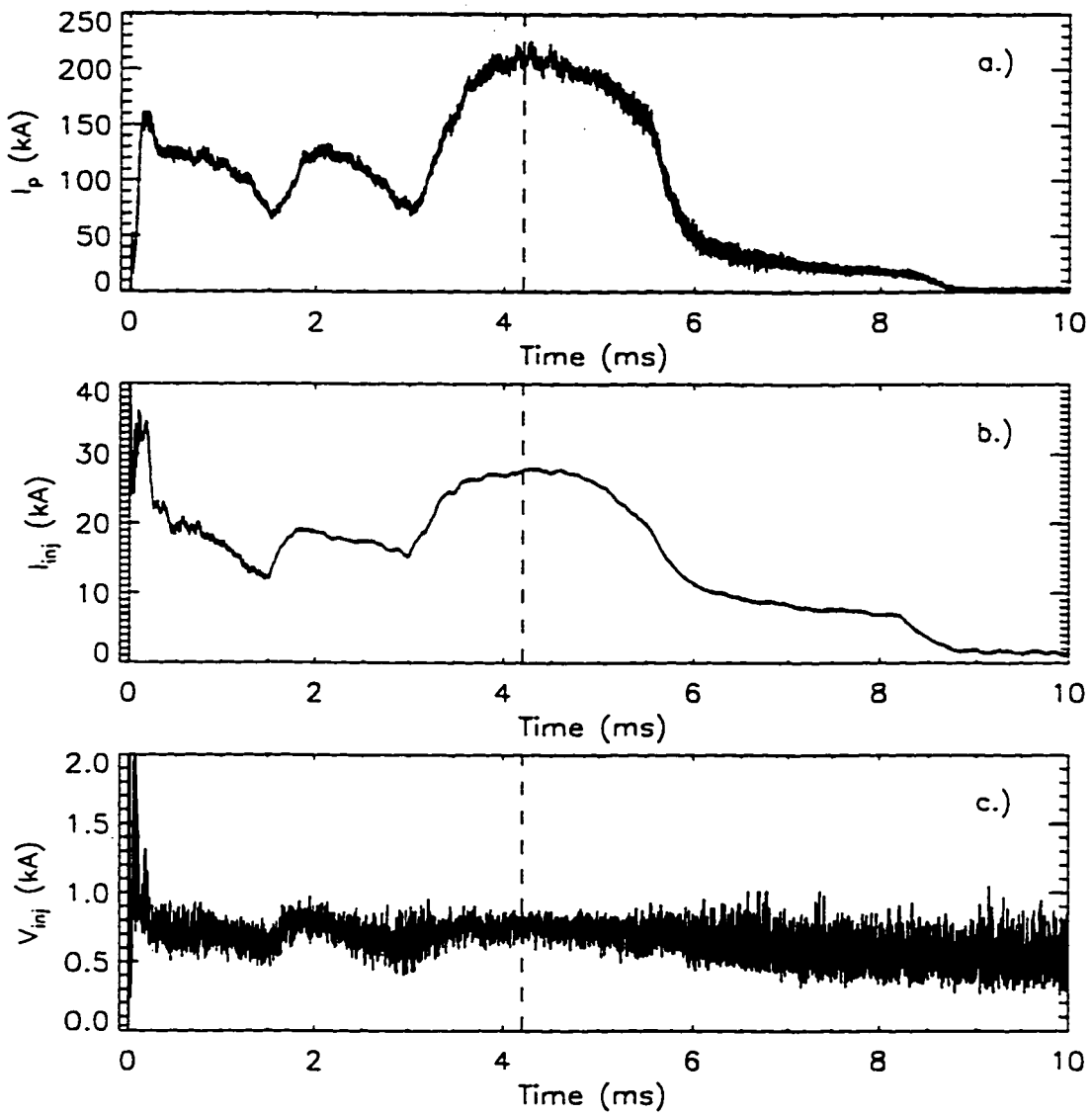

Figure 5.5: Current and voltage waveforms for a high performance shot (6737) with a quadrupole bias field; a.) I_{inj} vs. time b.) I_p vs. time c.) V_{inj} vs time. The dashed line at t = 4.2 ms indicates where the equilibrium is calculated.

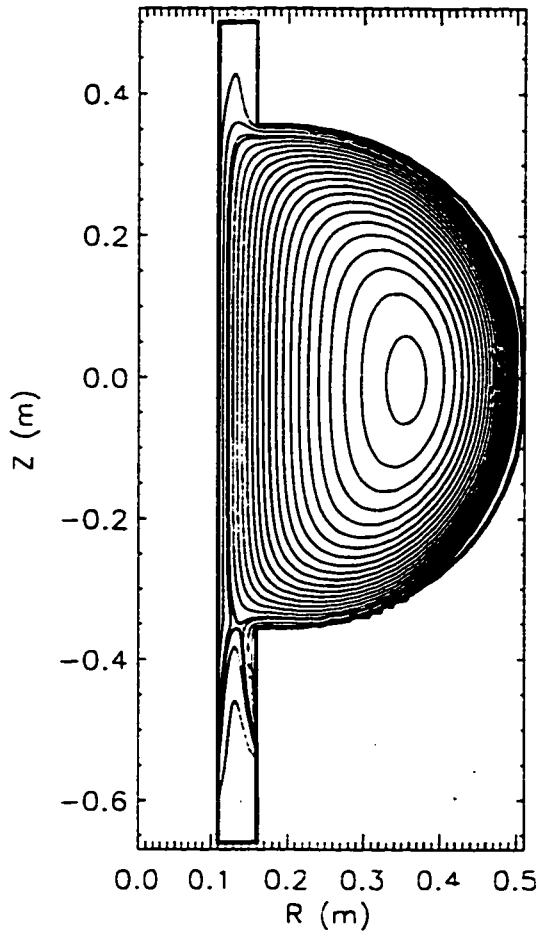

Figure 5.6: Flux contours for a high performance shot (6737) at t = 4.2 ms

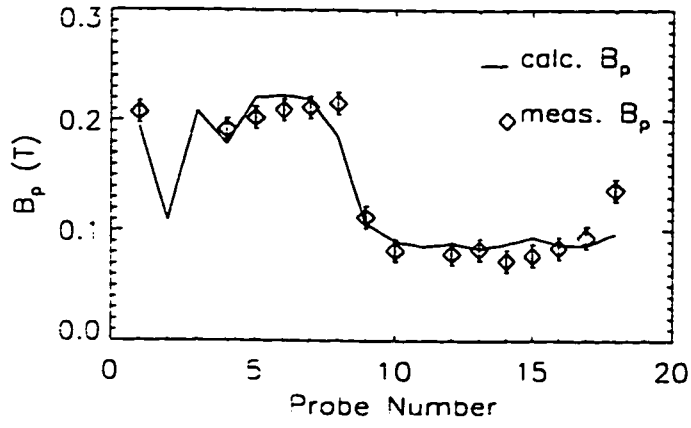

Figure 5.7: Comparison of measured and calculated B poloidal fields for shot 6737 at time t = 4.2 ms; measured I_{inj} = 20.2 kA, calculated I_{inj} = 20.9 kA, measured I_p = 206 kA, calculated I_p = 202 kA, χ^2 = 2.6

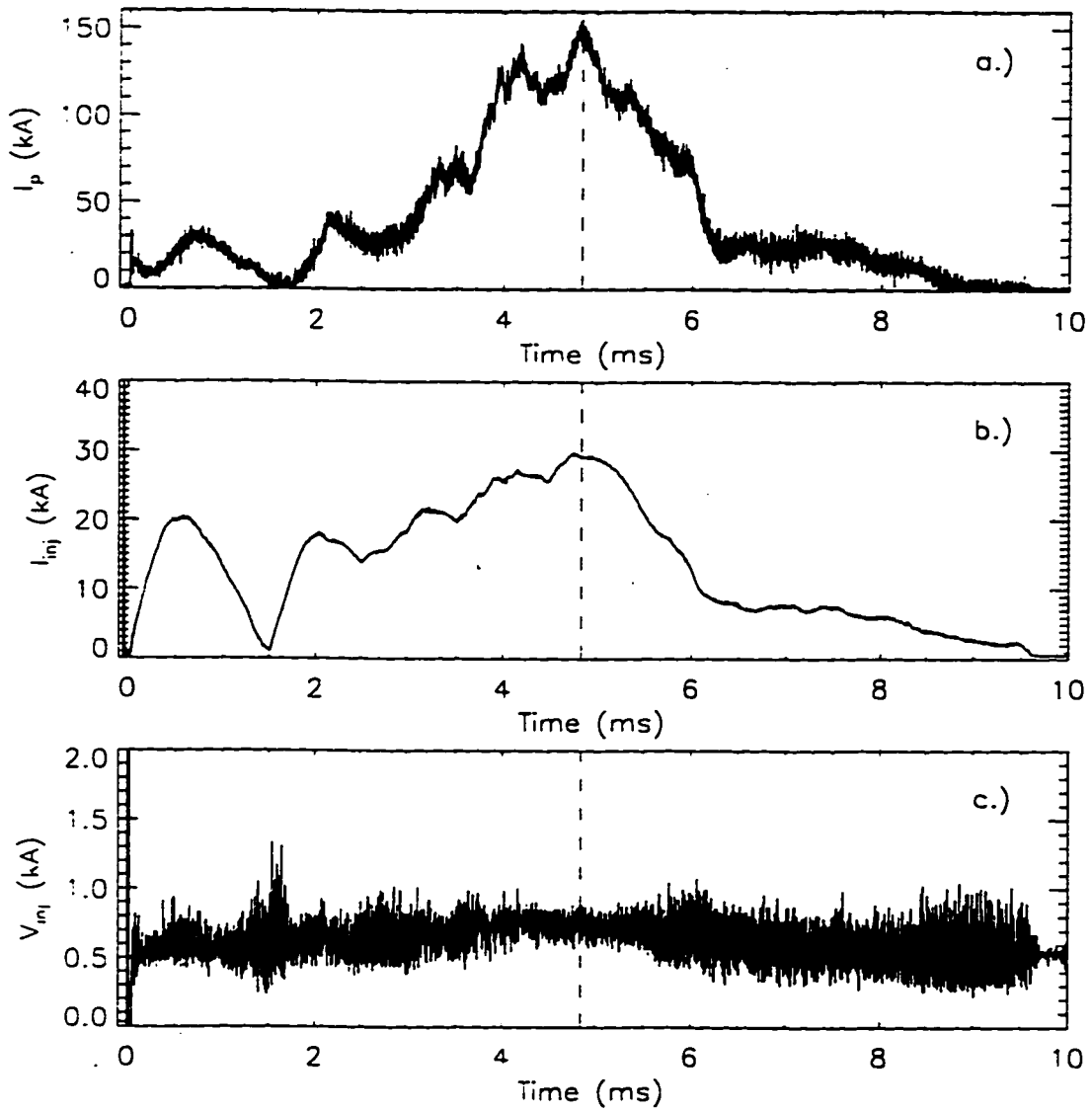

Figure 5.8: Current and voltage waveforms for a shot (9552) where the langmuir triple probe was available; a.) I_{inj} vs. time b.) I_p vs. time c.) V_{inj} vs time. The dashed line at t = 4.85 ms indicates where the equilibrium is calculated.

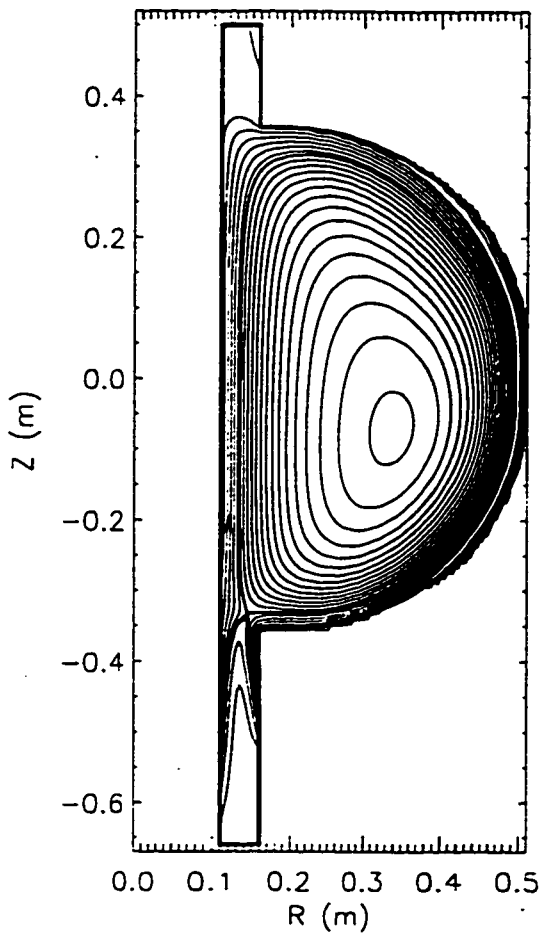

Figure 5.9: Flux contours for shot 9552 at t = 4.85 ms

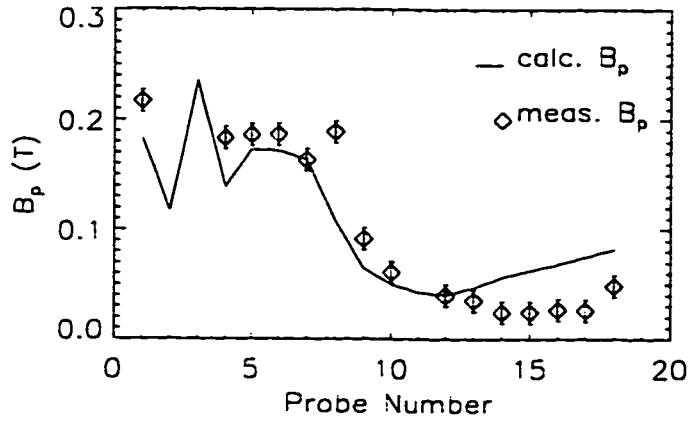

Figure 5.10: Comparison of measured and calculated B poloidal fields for shot 9552 at time t = 4.85 ms; measured I_{inj} = 11.2 kA, calculated I_{inj} = 15.7 kA, measured I_p = 147, calculated I_p = 150, χ^2 = 14.3

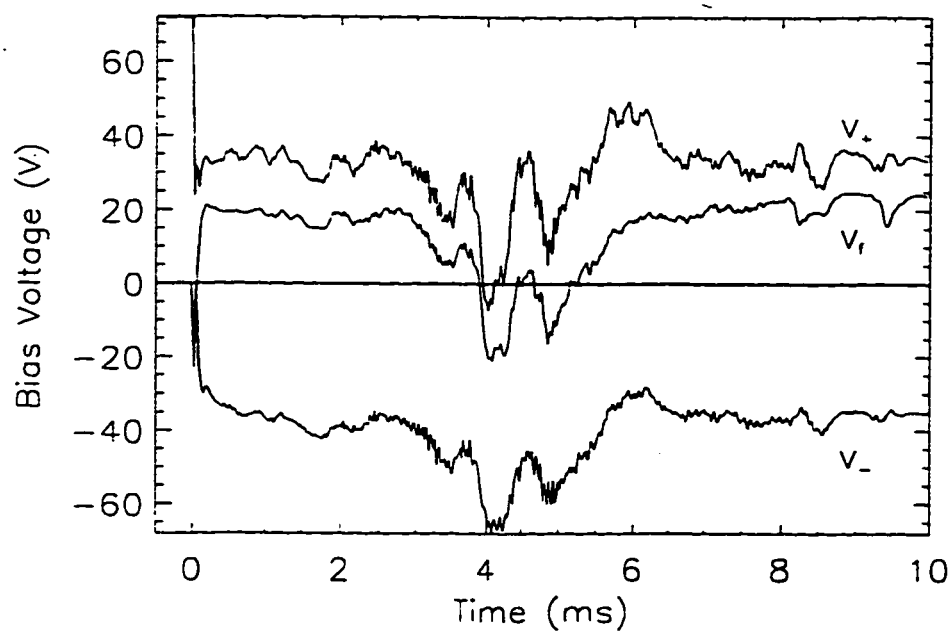

Figure 5.11: Voltage waveforms from Langmuir triple probe (shot 9552)

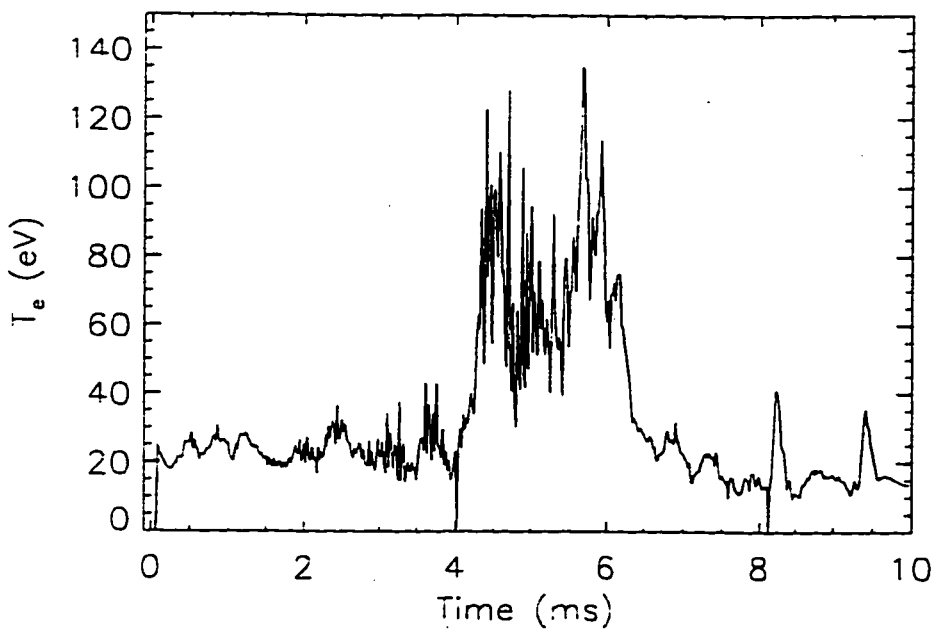

Figure 5.12: Electron Temperature measured by Langmuir triple probe (shot 9552)

List of References

1. T. Ohkawa, "New Methods of Driving Plasma Current in Fusion Devices", *Nuclear Fusion* **10**(2), 1970, pg. 185

2. D.J.H. Wort, "The Peristaltic Tokamak", *Plasma Physics* **13**(3), March 1971, pg. 258

3. T.R. Jarboe, "Formation and Sustainment of a Tokamak by Coaxial Helicity Injection", *Fusion Technology* **15**, Jan. 1989, pg. 7

4. W.H.M. Clark, J.G. Cordey, M. Cox, R.D. Gill, J. Hugill, J.W.M. Paul, and D.F.H. Start, "Measurements of the Beam-Driven Current in the DITE Tokamak", *Physical Review Letters* **45**(13), 29 Sept. 1980, pg. 1101

5. T. Imai, et al., "Lower Hybrid Current Drive and Higher Harmonic ICRF Heating Experiments on JT-60", *Plasma Physics and Controlled Nuclear Fusion Research, IAEA Conference Proceedings* **1**, 1991, pg. 645

6. T.C. Luce, et al., "Electron Cyclotron Heating and Current Drive Results from the DIII-D Tokamak", *Plasma Physics and Controlled Nuclear Fusion Research, IAEA Conference Proceedings* **1**, 1991, pg. 631

7. A.H. Boozer, "Power Requirements for Current Drive",*Physics of Fluids* **31**(3), March 1988, pg. 591

8. L. Woltjer, "A Theorem on Force-Free Magnetic Fields", *Proceedings of the National Academy of Sciences* **44**(6), April 1958, pg. 489

9. J.B. Taylor, "Relaxation of Toroidal Plasma and Generation of Reverse Magnetic Fields", *Physical Review Letters* **33**(19), Nov. 1974, pg. 1139

10. T.H. Jensen, M.S. Chu, "Current Drive and Helicity Injection", *Physics of Fluids* **27**(12), Dec. 1984, pg. 2881

11. C.W. Barnes, J.C. Fernandez, I. Henins, H.W. Hoida, T.R. Jarboe, S.O. Knox, G.J. Marklin, "Experimental Determination of the Conservation of Magnetic Energy from the Balance Between Source and Spheromak", *Physics of Fluids* **29**, Oct. 1986, pg. 3415

12. D. C. Robinson, R.E. King, " Factors Influencing the Period of Improved Stability in ZETA", *Plasma Physics and Controlled Nuclear Fusion, IAEA Conference Proceedings* **1**, 1969, pg. 263

13. W.C. Turner, G.C. Goldenbaum, E.H.A. Granneman, J.H. Hammer, C.W. Hartman, D.S. Prono, J. Taska, "Investigations of the Magnetic Structure and the Decay of a Plasma-Gun-Generated Compact Torus", *Physics of Fluids* **26**(7), July 1983, pg. 1965

14. M. Ono, G.J. Green, D. Darrow, C. Forest, H. Park, T.H. Stix, "Steady-State Tokamak Discharge via dc Helicity Injection", *Physical Review Letters* **59**(19), Nov. 1987, pg. 2165

15. C.W. Hartman, J.H. Hammer, "New Type of Collective Accelerator", *Physical Review Letters* **48**(14), 5 April 1982, pg. 929

16. M.R. Brown, P.M. Bellan, "Efficiency and Scaling of Current Drive and Refuelling by Spheromak Injection into a Tokamak", *Nuclear Fusion* **32**(7), 1992, pg. 1125

17. T.R. Jarboe, "Review of Spheromak Research", *Plasma Physics and Controlled Fusion*, **36**, 1994, pg. 945

18. S.O. Knox, C.W. Barnes, G.J. Marklin, T.R. Jarboe, I. Henins, H.W. Hoida, B.L. Wright, "Observations of Spheromak Equilibria Which Differ from the Minimum-Energy State and Have Internal Kink Distortions", *Physical Review Letters*, **56**(8), 24 Feb. 1986, pg. 842

19. P.K. Browning, G. Cunningham, S.J. Gee, K.J. Gibson, A. al-Karkhy, D.A. Kitson, R. Martin, M.G. Rusbridge, "Injection and Sustainment of Plasma in a Preexisting Toroidal Field Using a Coaxial Helicity Source", *Physical Review Letters* **68**(11), March 1992, pg. 1718

20. Y-K. M. Peng, D.J. Strickler, "Features of Spherical Torus Plasmas", *Nuclear Fusion* **26**(6), 1986, pg. 769

21. A. Sykes et. al., "First Results from the START Experiment", *Nuclear Fusion* **32**(4), 1992, pg. 694

22. C. Painter, "General Description and Operating Instructions for the Hydrogen Gas Injection System on the Helicity Injected Tokamak (HIT)", University of Washington, AERL internal report, 1992

23. D. Orvis, "Coil Design on the Helicity Injected Tokamak", Masters Thesis, University of Washington, 1992

24. D. Orvis, T.R. Jarboe, "Calibration of Magnetic Probes Mounted in a Copper Wall", *Review of Scientific Instruments* **66**(5), May 1995, pg. 3263

25. R. Hoyt, "Optimization of Applied Magnetic Nozzles for Coaxial Plasma Accelerators", Ph.D. Dissertation, University of Washington, 1994

26. D.E.T.F Ashby, *Journal of Nuclear Energy* C **5**(83), 1962

27. L.L. Lao, H. St. John, R.D. Stambaugh, A.G. Kellman, W. Pfeiffer, "Reconstruction of Current Profile Parameters and Plasma Shapes in

Tokamaks", *Nuclear Fusion* 25(11), 1985, pg. 1611

28. C.W. Barnes, T.R. Jarboe, G.J. Marklin, S.O. Knox, I. Henins, "The Impedance and Energy Efficiency of a Coaxial Magnetized Plasma Source used for Spheromak Formation and Sustainment", *Physics of Fluids B* 2(8), August 1990, pg. 1871

29. B.A. Nelson, T.R. Jarboe, A. Martin, C. Painter, "Tokamak Formation and Sustainment by Coaxial Helicity Injection Current Drive", *Nuclear Fusion* 34(8), 1994, pg. 1111

30. B.A. Nelson, T.R. Jarboe, D. Orvis, L. McCullough, J.P. Xie, C.X. Zhang, L. Zhou, "Formation and Sustainment of a 150 Ka Tokamak by Coaxial Helicity Injection", *Physical Review Letters*, 72(23), 6 June 1994, pg. 3666

31. D.A. Kitson, P.K. Browning, "Partially Relaxed Magnetic Field Equilibria in a Gun-Injected Spheromak", *Plasma Physics and Controlled Fusion* 32(14), 1990, pg. 1265

32. J.P. Freidberg, "Ideal Magnetohydrodynamics", *New York: Plenum*, 1987, pg. 110

33. W.H. Press, B.P. Flannery, S.A. Teukolsky, W.T. Vetterling, "Numerical Recipes (FORTRAN)", *Cambridge: Cambridge University Press*, 1986, pg. 655

34. D. Kahaner, C. Moler, S. Nash, "Numerical Methods and Software", *Prentice Hall*, 1989

35. A.K. Martin, T.R. Jarboe, "An Equilibrium Model for Helicity Injector Operation in the Helicity Injected Tokamak (HIT) Experiment", *Plasma Physics and Controlled Fusion* 38, 1996, pg. 1967

Appendix A. Open Flux Equilibrium Fits

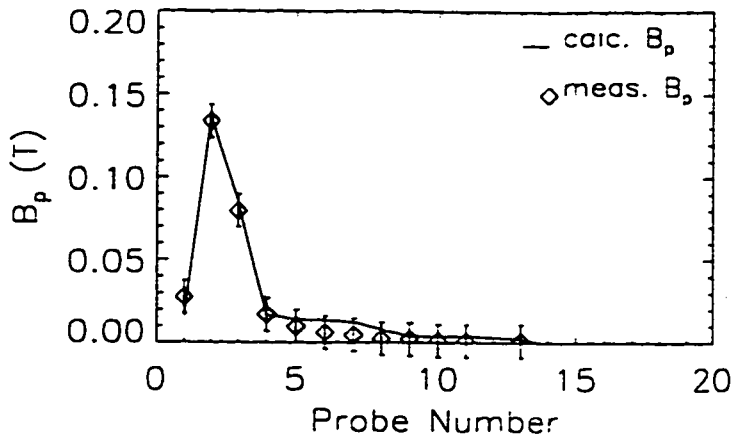

Figure A.1: Equilibrium fit for shot 3371 at t = 0.3 ms; η_1 = 1.26 x 10^{-4} Ω-m, η_2 = 1.1 x 10^{-4} Ω-m; measured I_{inj} = 6.5 kA, calculated I_{inj} = 6.5 kA; χ^2 = 0.30

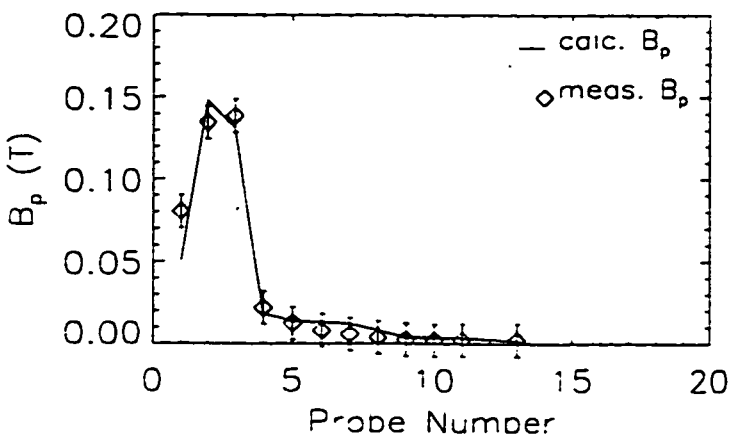

Figure A.2 : Equilibrium fit for shot 3371 at t = 0.4 ms; η_1 = 7.9 x 10^{-5} Ω-m, η_2 = 1.1 x 10^{-4} Ω-m; measured I_{inj} = 10.4 kA, calculated I_{inj} = 10.4 kA; χ^2 = 1.03

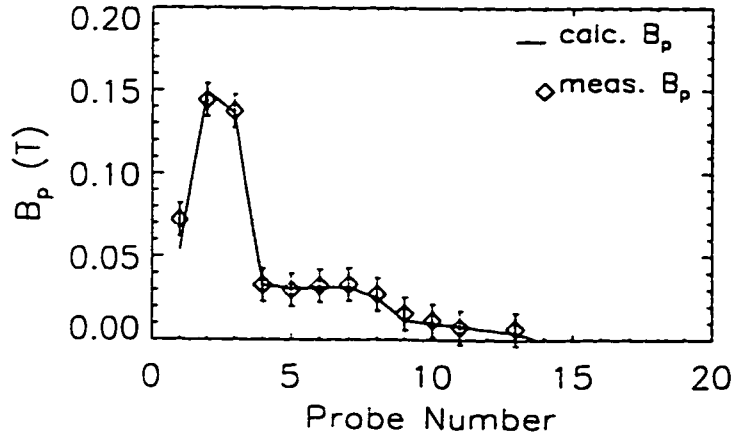

Figure A.3 : Equilibrium fit for shot 3371 at t = 0.6 ms; η_1 = 9.5 x 10^{-5} Ω-m, η_2 = 6.6 x 10^{-5} Ω-m; measured I_{inj} = 10.9 kA, calculated I_{inj} = 10.8 kA; χ^2 = 0.33

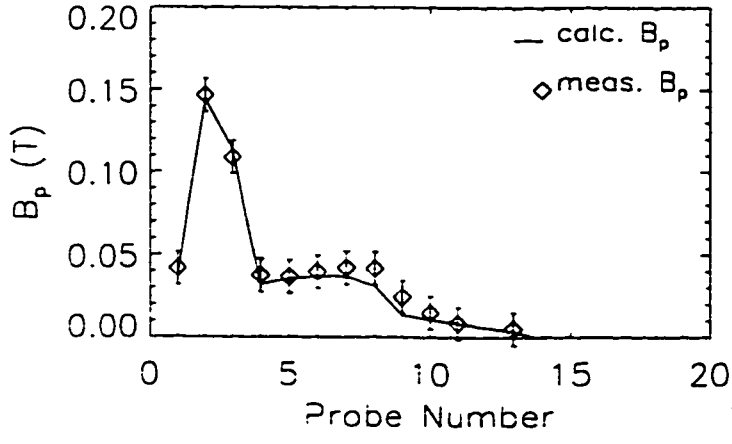

Figure A.4 : Equilibrium fit for shot 3371 at t = 0.7 ms; η_1 = 1.34 x 10^{-4} Ω-m, η_2 = 5.5 x 10^{-5} Ω-m; measured I_{inj} = 9.3 kA, calculated I_{inj} = 9.3 kA; χ^2 = 0.30

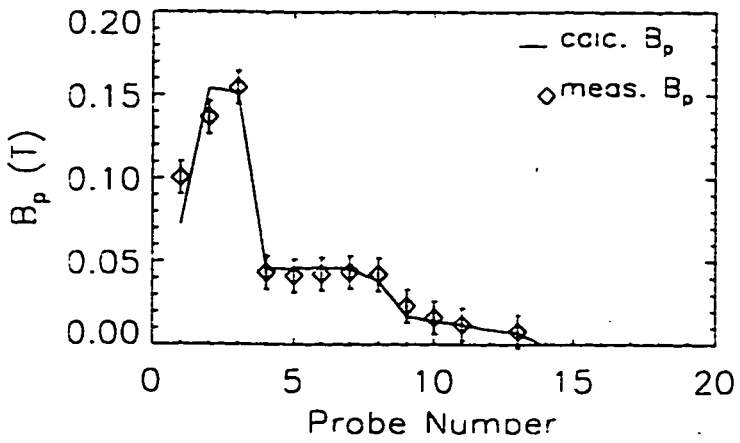

Figure A.5: Equilibrium fit for shot 3371 at t = 0.8 ms; η_1 = 7.6 x 10^{-5} Ω-m, η_2 = 5.1 x 10^{-5} Ω-m; measured I_{inj} = 12.7 kA, calculated I_{inj} = 12.6 kA; χ^2 = 1.03

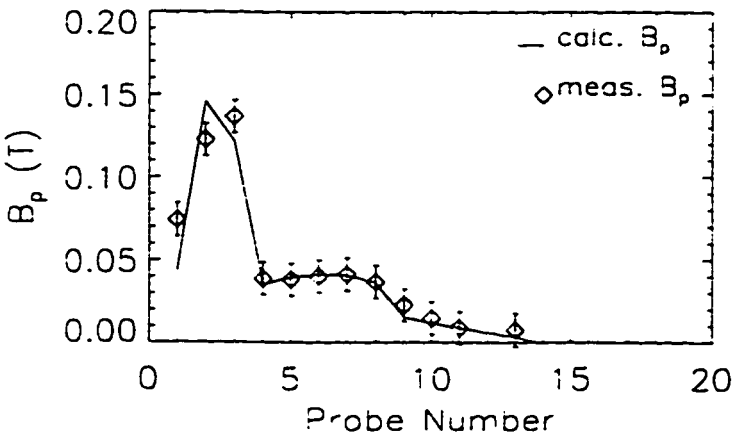

Figure A.6: Equilibrium fit for shot 3371 at t = 0.9 ms; η_1 = 9.6 x 10^{-5} Ω-m, η_2 = 3.7 x 10^{-5} Ω-m; measured I_{inj} = 10.1 kA, calculated I_{inj} = 10.1 kA; χ^2 = 1.51

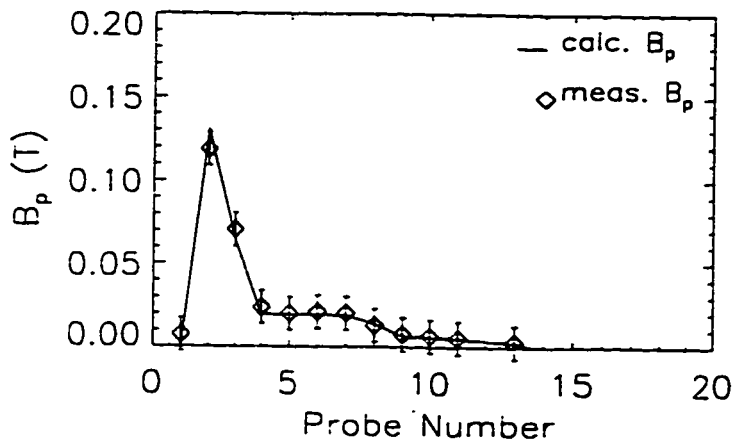

Figure A.7: Equilibrium fit for shot 3371 at t = 1.1 ms; η_1 = 2.59 x 10^{-4} Ω-m, η_2 = 8.7 x 10^{-5} Ω-m; measured I_{inj} = 4.6 kA, calculated I_{inj} = 4.6 kA; χ^2 = 0.21

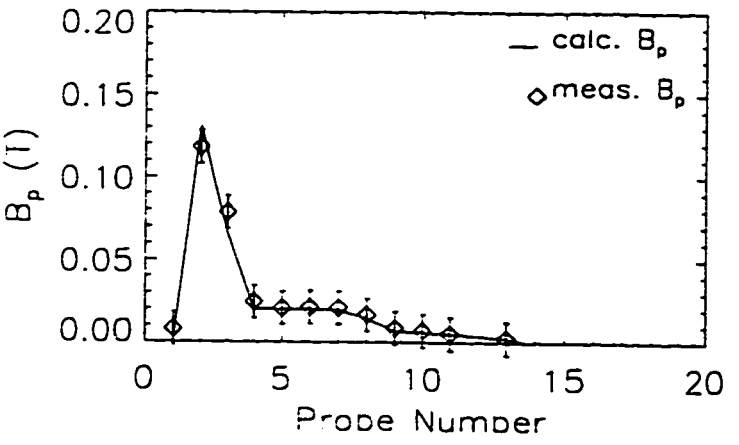

Figure A.8: Equilibrium fit for shot 3371 at t = 1.2 ms; η_1 = 2.76 x 10^{-4} Ω-m, η_2 = 9.2 x 10^{-5} Ω-m; measured I_{inj} = 4.7 kA, calculated I_{inj} = 4.7 kA; χ^2 = 0.35

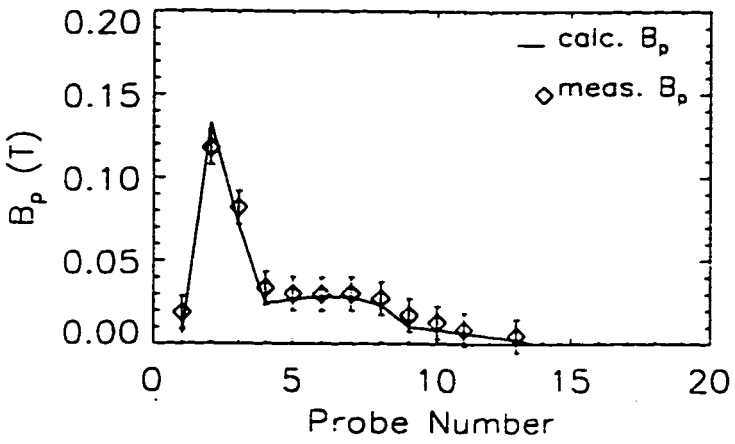

Figure A.9: Equilibrium fit for shot 3371 at t = 1.3 ms; η_1 = 2.92 x 10^{-4} Ω-m, η_2 = 7.0 x 10^{-5} Ω-m; measured I_{inj} = 5.4 kA, calculated I_{inj} = 5.4 kA; χ^2 = 0.60

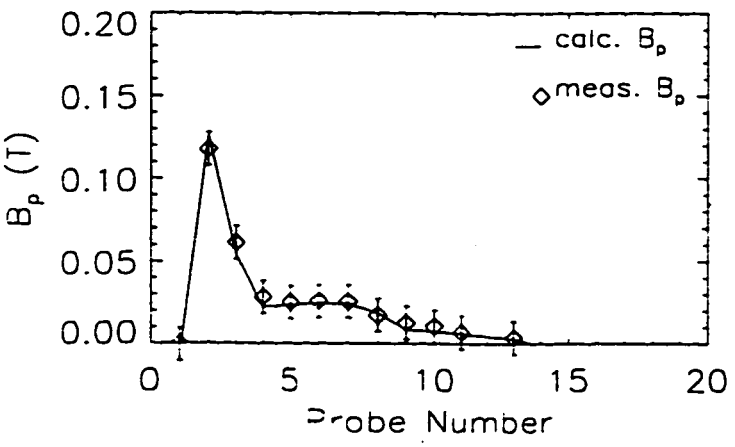

Figure A.10: Equilibrium fit for shot 3371 at t = 1.4 ms; η_1 = 4.62 x 10^{-4} Ω-m, η_2 = 8.5 x 10^{-5} Ω-m; measured I_{inj} = 3.3 kA, calculated I_{inj} = 3.3 kA; χ^2 = 0.22

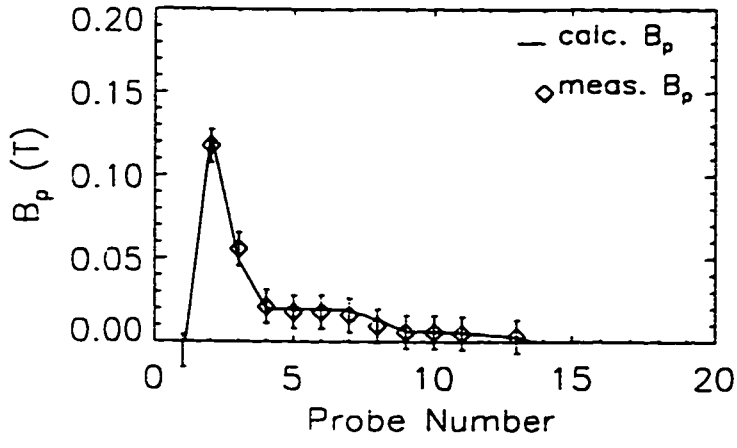

Figure A.11: Equilibrium fit for shot 3371 at t = 1.5 ms; η_1 = 6.0 x 10^{-4} Ω-m, η_2 = 1.15 x 10^{-4} Ω-m; measured I_{inj} = 2.6 kA, calculated I_{inj} = 2.6 kA; χ^2 = 0.14

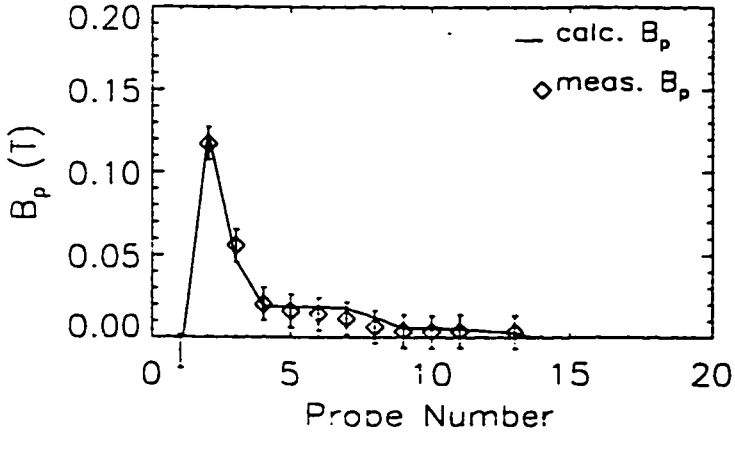

Figure A.12: Equilibrium fit for shot 3371 at t = 1.6 ms; η_1 = 7.16 x 10^{-4} Ω-m, η_2 = 1.35 x 10^{-4} Ω-m; measured I_{inj} = 2.3 kA, calculated I_{inj} = 2.3 kA; χ^2 = 0.21

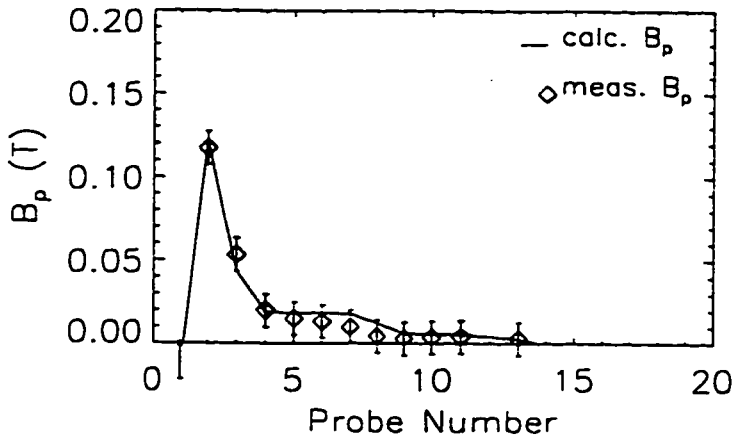

Figure A.13: Equilibrium fit for shot 3371 at t = 1.7 ms; η_1 = 8.68 x 10^{-4} Ω-m, η_2 = 1.25 x 10^{-4} Ω-m; measured I_{inj} = 1.8 kA, calculated I_{inj} = 1.9 kA; χ^2 = 0.26

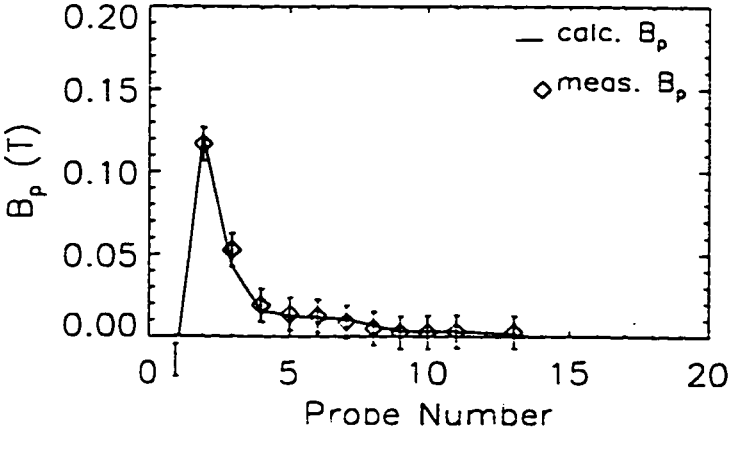

Figure A.14: Equilibrium fit for shot 3371 at t = 1.75 ms; η_1 = 8.06 x 10^{-4} Ω-m, η_2 = 1.55 x 10^{-4} Ω-m; measured I_{inj} = 1.7 kA, calculated I_{inj} = 1.7 kA; χ^2 = 0.11

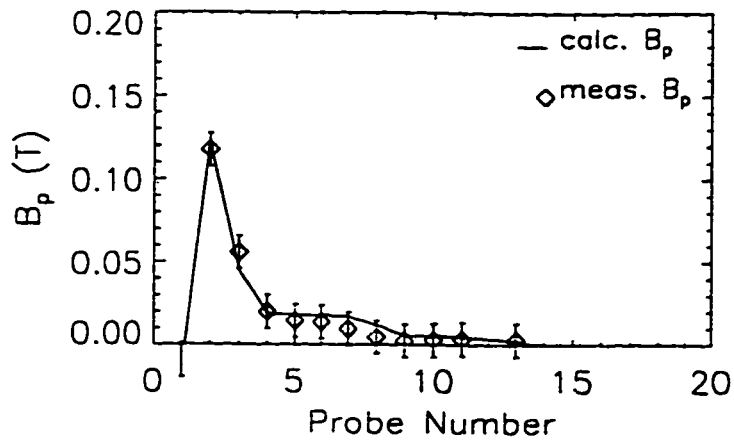

Figure A.15: Equilibrium fit for shot 3371 at t = 1.8 ms; η_1 = 7.62 x 10^{-4} Ω-m, η_2 = 1.15 x 10^{-4} Ω-m; measured I_{inj} = 2.0 kA, calculated I_{inj} = 2.1 kA; χ^2 = 0.27

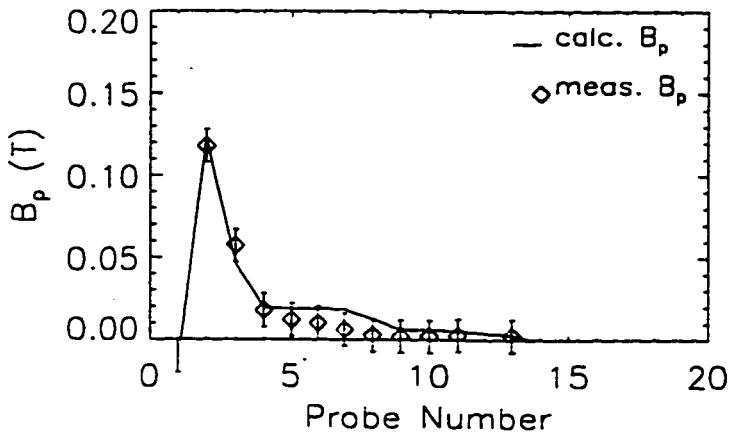

Figure A.16: Equilibrium fit for shot 3371 at t = 1.9 ms; η_1 = 6.62 x 10^{-4} Ω-m, η_2 = 1.15 x 10^{-4} Ω-m; measured I_{inj} = 2.2 kA, calculated I_{inj} = 2.3 kA; χ^2 = 0.48

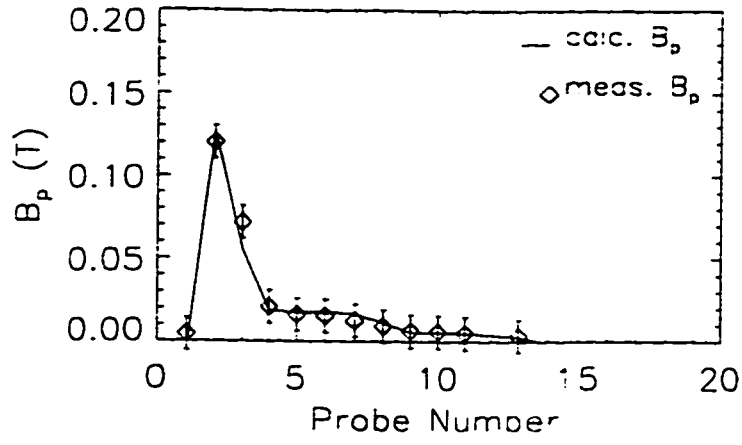

Figure A.17: Equilibrium fit for shot 3371 at t = 2.0 ms; η_1 = 3.71 x 10^{-4} Ω-m, η_2 = 1.15 x 10^{-4} Ω-m; measured I_{inj} = 3.5 kA, calculated I_{inj} = 3.5 kA; χ^2 = 0.39

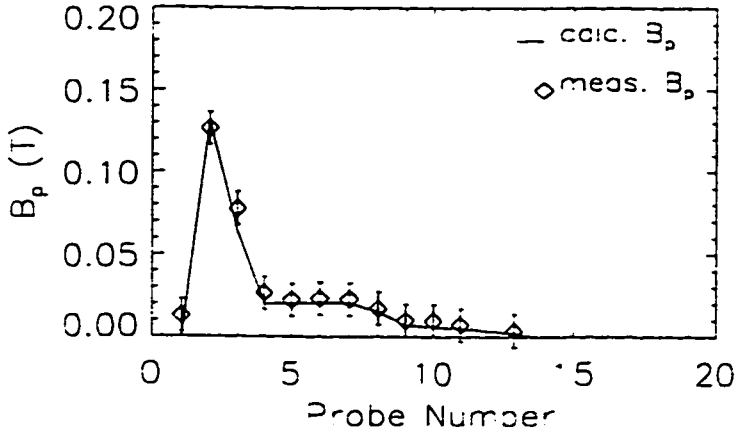

Figure A.18: Equilibrium fit for shot 3371 at t = 2.1 ms; η_1 = 3.14 x 10^{-4} Ω-m, η_2 = 9.5 x 10^{-5} Ω-m; measured I_{inj} = 4.6 kA, calculated I_{inj} = 4.6 kA; χ^2 = 0.39

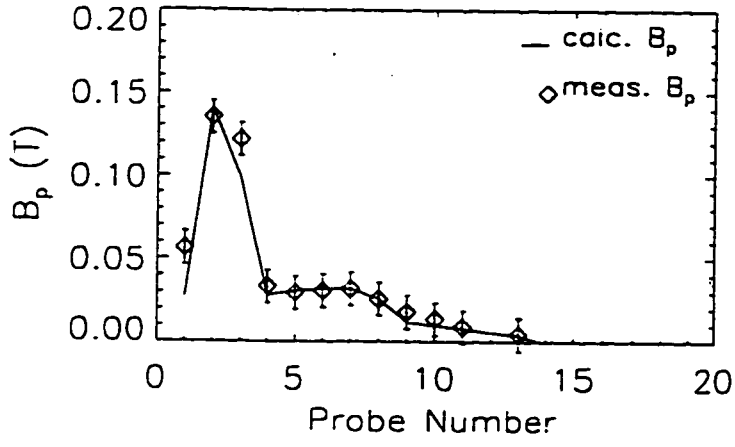

Figure A.19: Equilibrium fit for shot 3371 at t = 2.2 ms; η_1 = 1.17 x 10^{-4} Ω-m, η_2 = 5.0 x 10^{-5} Ω-m; measured I_{inj} = 8.2 kA, calculated I_{inj} = 8.3 kA; χ^2 = 1.28

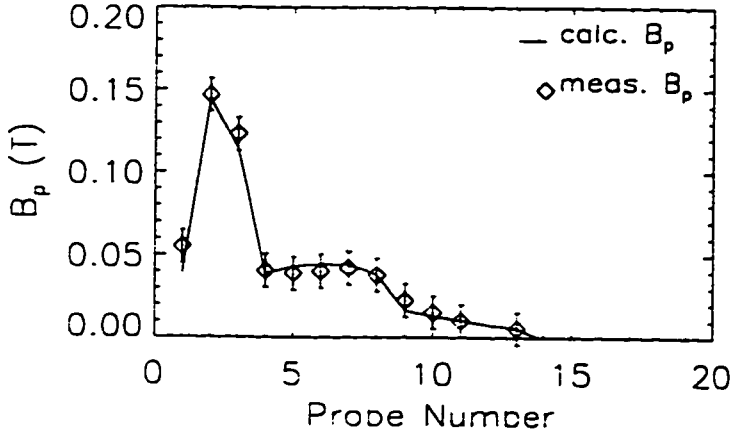

FIgure A.20: Equilibrium fit for shot 3371 at t = 2.3 ms; η_1 = 1.05 x 10^{-4} Ω-m, η_2 = 4.0 x 10^{-5} Ω-m; measured I_{inj} = 9.8 kA, calculated I_{inj} = 9.8 kA; χ^2 = 0.37

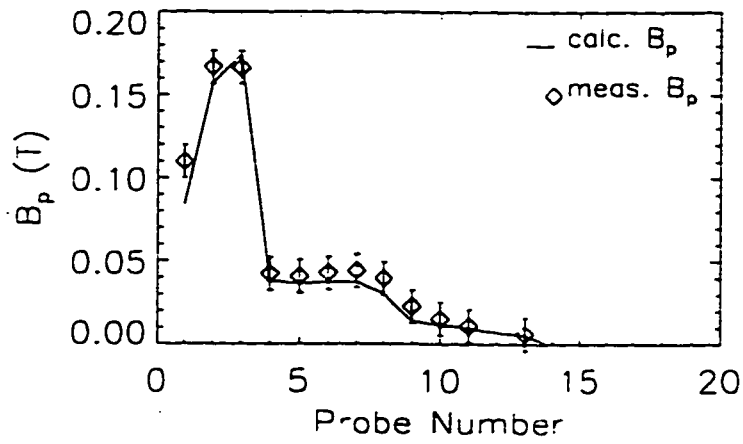

Figure A.21: Equilibrium fit for shot 3371 at t = 2.4 ms; η_1 = 5.3 x 10^{-5} Ω-m, η_2 = 4.8 x 10^{-5} Ω-m; measured I_{inj} = 14.1 kA, calculated I_{inj} = 14.3 kA; χ^2 = 0.93

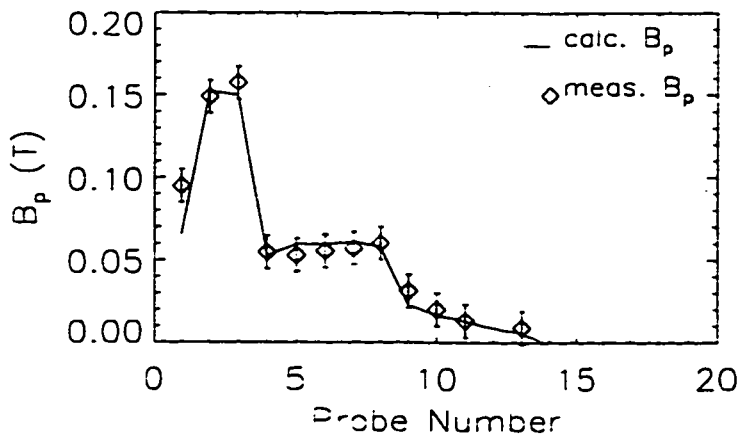

Figure A.22: Equilibrium fit for shot 3371 at t = 2.5 ms; η_1 = 7.7 x 10^{-5} Ω-m, η_2 = 2.7 x 10^{-5} Ω-m; measured I_{inj} = 13.1 kA, calculated I_{inj} = 13.2 kA; χ^2 = 0.95

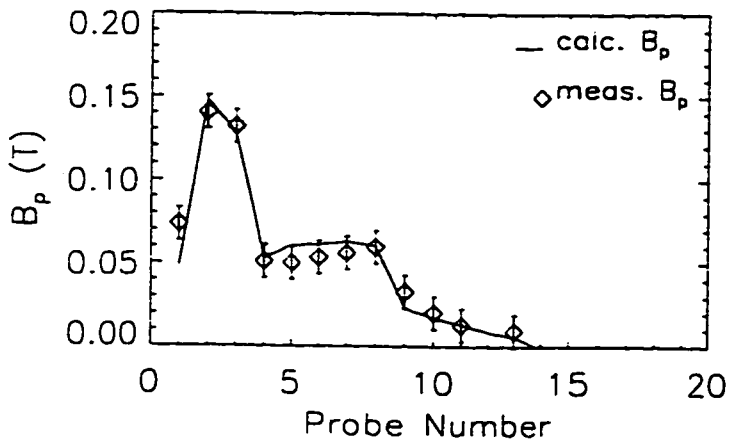

Figure A.23: Equilibrium fit for shot 3371 at t = 2.6 ms; η_1 = 1.35 x 10^{-4} Ω-m, η_2 = 3.5 x 10^{-5} Ω-m; measured I_{inj} = 11.2 kA, calculated I_{inj} = 11.5 kA; χ^2 = 0.88

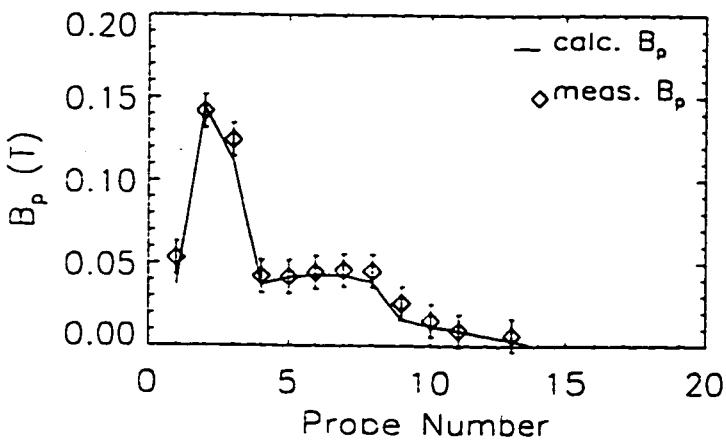

Figure A.24: Equilibrium fit for shot 3371 at t = 2.7 ms; η_1 = 1.27 x 10^{-4} Ω-m, η_2 = 4.0 x 10^{-5} Ω-m; measured I_{inj} = 9.7 kA, calculated I_{inj} = 9.7 kA; χ^2 = 0.53

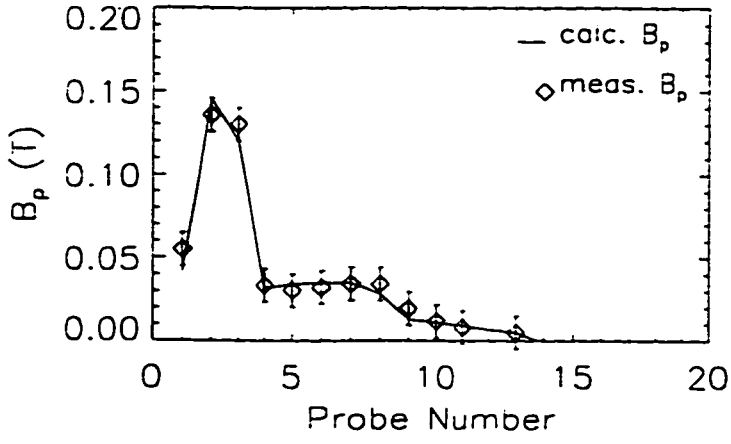

Figure A.25: Equilibrium fit for shot 3371 at t = 2.8 ms; η_1 = 1.32 x 10^{-4} Ω-m, η_2 = 7.2 x 10^{-5} Ω-m; measured I_{inj} = 10.1 kA, calculated I_{inj} = 10.1 kA; χ^2 = 0.39

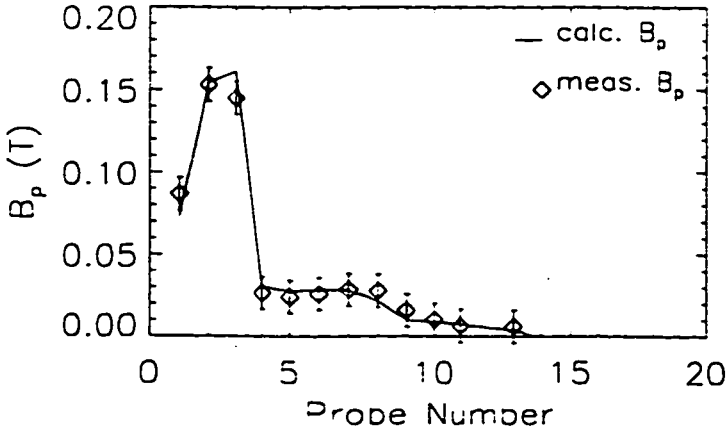

Figure A.26: Equilibrium fit for shot 3372 at t = 0.55 ms; η_1 = 9.3 x 10^{-5} Ω-m, η_2 = 9.4 x 10^{-5} Ω-m; measured I_{inj} = 12.6 kA, calculated I_{inj} = 12.7 kA; χ^2 = 0.46

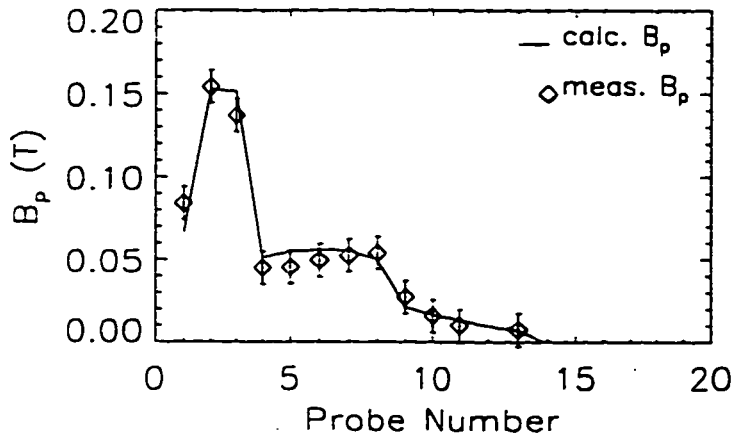

Figure A.27: Equilibrium fit for shot 3372 at t = 4.0 ms; η_1 = 7.8 x 10^{-5} Ω-m, η_2 = 3.8 x 10^{-5} Ω-m; measured I_{inj} = 13.3 kA, calculated I_{inj} = 13.3 kA; χ^2 = 0.64

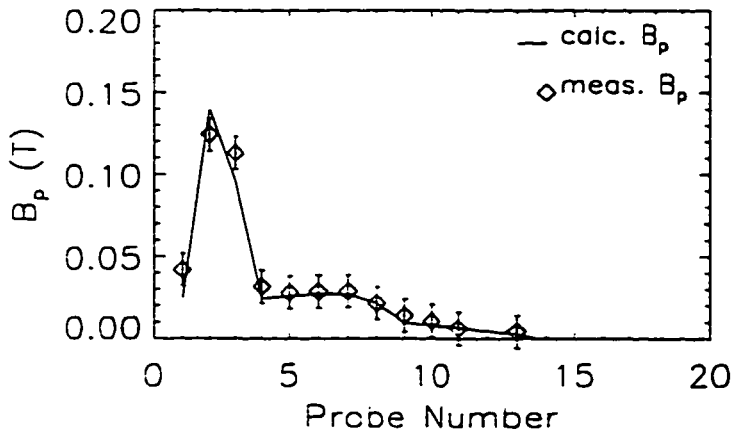

Figure A.28: Equilibrium fit for shot 3376 at t = 0.5 ms; η_1 = 1.56 x 10^{-4} Ω-m, η_2 = 6.8 x 10^{-5} Ω-m; measured I_{inj} = 7.7 kA, calculated I_{inj} = 7.7 kA; χ^2 = 0.78

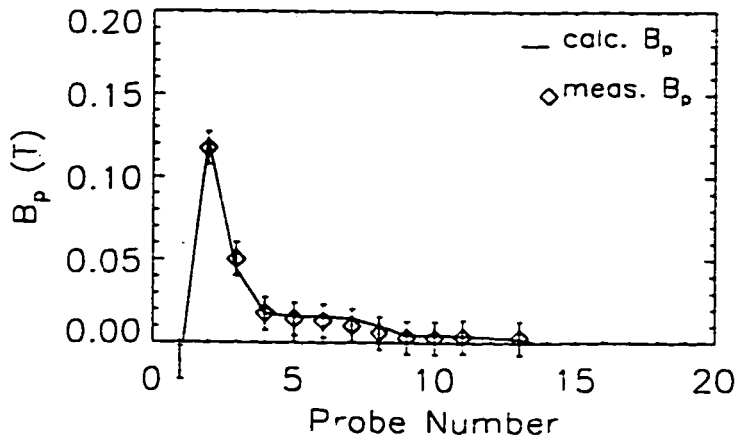

Figure A.29: Equilibrium fit for shot 3376 at t = 1.5 ms; η_1 = 9.68 x 10^{-4} Ω-m, η_2 = 1.60 x 10^{-4} Ω-m; measured I_{inj} = 2.0 kA, calculated I_{inj} = 1.9 kA; χ^2 = 0.10

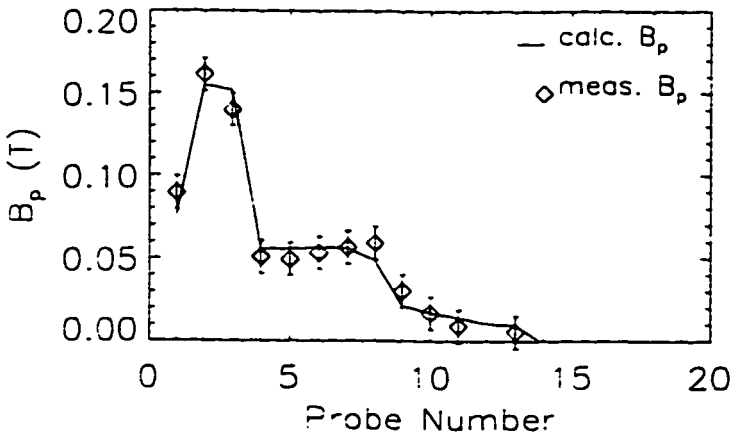

Figure A.30: Equilibrium fit for shot 3376 at t = 2.5 ms; η_1 = 8.5 x 10^{-5} Ω-m, η_2 = 5.0 x 10^{-5} Ω-m; measured I_{inj} = 13.6 kA, calculated I_{inj} = 13.5 kA; χ^2 = 0.56

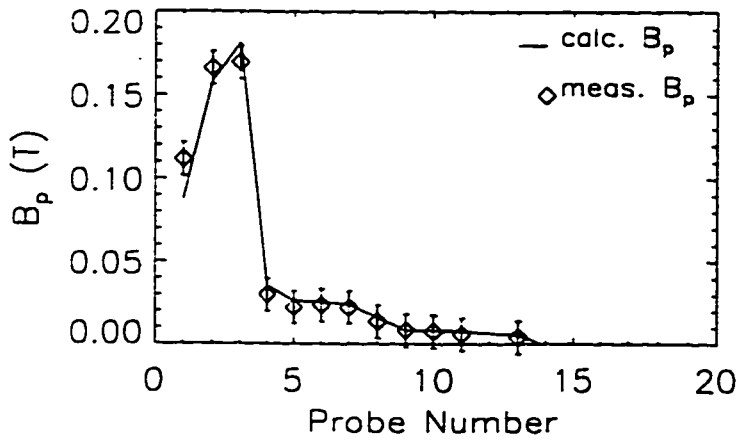

Figure A.31: Equilibrium fit for shot 3382 at t = 0.55 ms; η_1 = 6.2 x 10^{-5} Ω-m, η_2 = 1.1 x 10^{-4} Ω-m; measured I_{inj} = 13.7 kA, calculated I_{inj} = 13.9 kA; χ^2 = 0.71

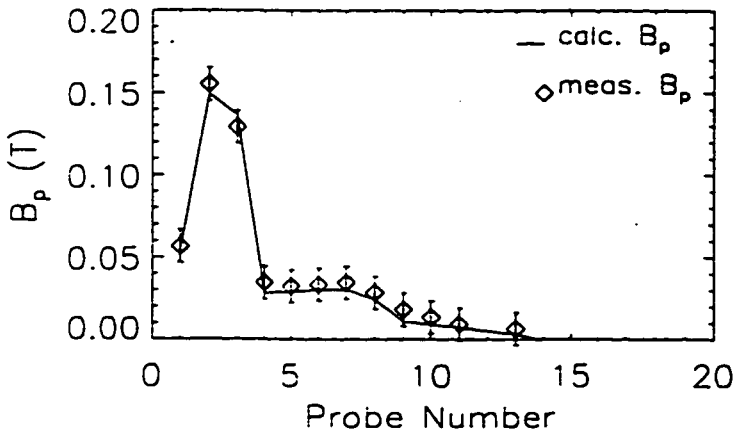

Figure A.32: Equilibrium fit for shot 3388 at t = 1.0 ms; η_1 = 8.3 x 10^{-5} Ω-m, η_2 = 5.5 x 10^{-5} Ω-m; measured I_{inj} = 11.1 kA, calculated I_{inj} = 11.0 kA; χ^2 = 0.23

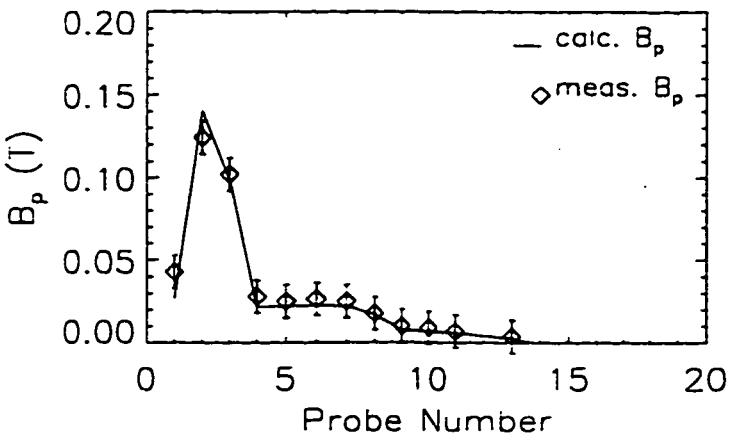

Figure A.33: Equilibrium fit for shot 3388 at t = 2.0 ms; η_1 = 1.15 x 10^{-4} Ω-m, η_2 = 6.3 x 10^{-5} Ω-m; measured I_{inj} = 8.0 kA, calculated I_{inj} = 8.1 kA; χ^2 = 0.52

Appendix B. Closed Flux Equilibrium Fits

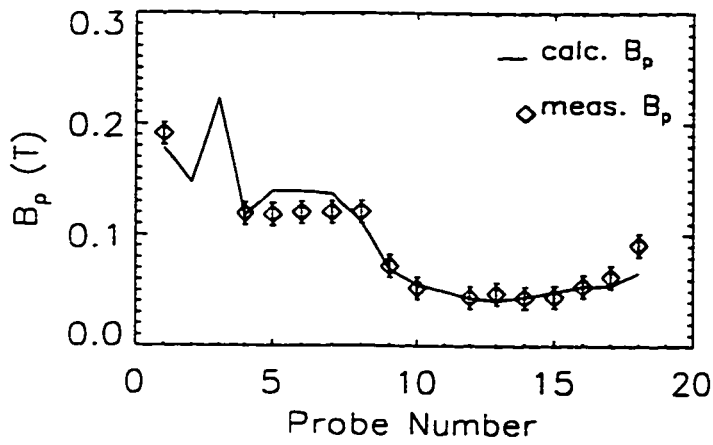

Figure B.1: Equilibrium fit for shot 6737 at t = 2.0 ms; η_1 = 2.0 x 10^{-5} Ω-m, η_2 = 3.8 x 10^{-5} Ω-m; measured I_{inj} = 20.2 kA, calculated I_{inj} = 15.9 kA; measured I_p = 123.3 kA, calculated I_p = 122.8 kA; χ^2 = 5.65; $\psi_{diverted}$ = 2.71 mWb, ψ_{closed} = 5.12 mWb

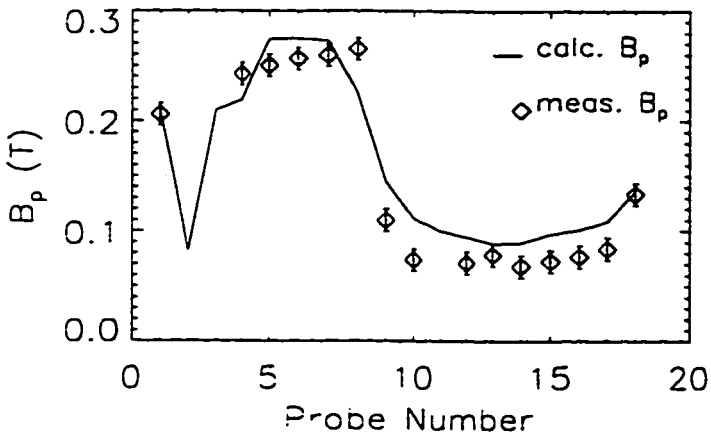

Figure B.2: Equilibrium fit for shot 6822 at t = 4.403 ms; η_1 = 3.0 x 10^{-5} Ω-m, η_2 = 4.8 x 10^{-5} Ω-m; measured I_{inj} = 20.6 kA, calculated I_{inj} = 21.9 kA; measured I_p = 227.6 kA, calculated I_p = 245.8 kA; χ^2 = 6.54; $\psi_{diverted}$ = 2.68 mWb, ψ_{closed} = 12.5 mWb

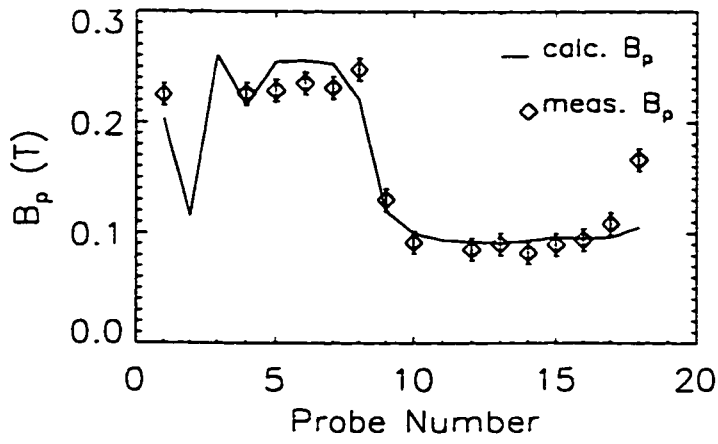

Figure B.3: Equilibrium fit for shot 7708 at t = 3.905 ms; η_1 = 1.5 x 10^{-5} Ω-m, η_2 = 2.2 x 10^{-5} Ω-m; measured I_{inj} = 23.3 kA, calculated I_{inj} = 25.0 kA; measured I_p = 234.1 kA, calculated I_p = 228.9 kA; χ^2 = 4.97; $\psi_{diverted}$ = 3.62 mWb, ψ_{closed} = 13.0 mWb

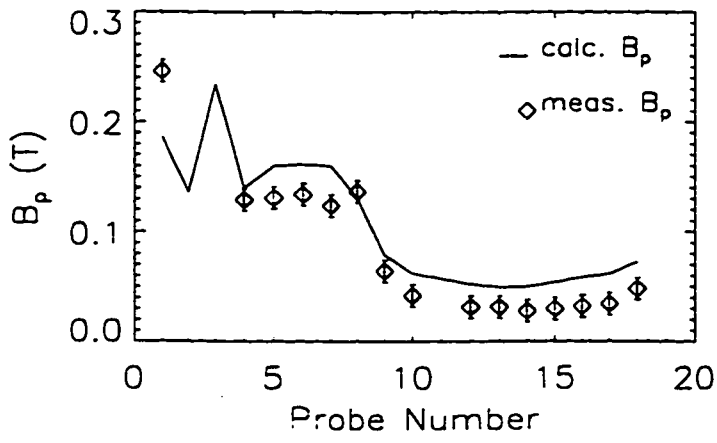

Figure B.4: Equilibrium fit for shot 9552 at t = 4.0 ms; η_1 = 9.0 x 10^{-6} Ω-m, η_2 = 4.0 x 10^{-5} Ω-m; measured I_{inj} = 16.9 kA, calculated I_{inj} = 15.0 kA; measured I_p = 112.3 kA, calculated I_p = 141.8 kA; χ^2 = 9.70; $\psi_{diverted}$ = 3.75 mWb, ψ_{closed} = 5.54 mWb

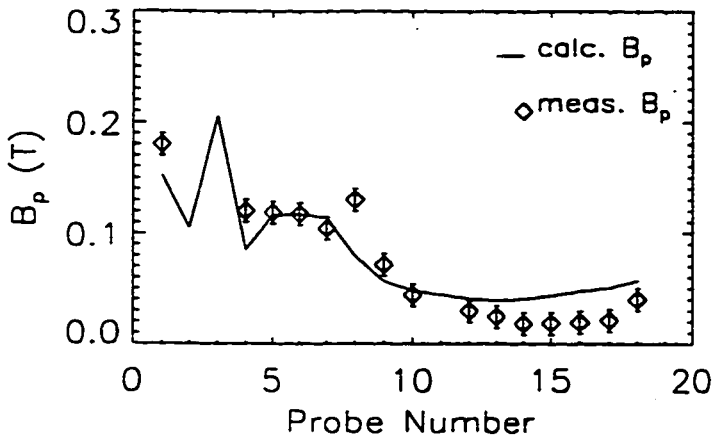

Figure B.5: Equilibrium fit for shot 9552 at t = 5.45 ms; η_1 = 3.0 x 10^{-5} Ω-m, η_2 = 6.0 x 10^{-5} Ω-m; measured I_{inj} = 7.2 kA, calculated I_{inj} = 14.9 kA; measured I_p = 100.2 kA, calculated I_p = 102.4 kA; χ^2 = 20.2; $\psi_{diverted}$ = 2.32 mWb, ψ_{closed} = 5.86 mWb

Appendix C. FORTRAN Source Code for ROLEQS2

C.1 Source code for roleqs2.for

```
      program roleqs2
c*************************************************************
c**
c**    ROLEQS2
c**
c**    MODULE: Main Program
c**
c**
c**    MODULES USED: grid.for
c**                  init.for
c**                  relax.for
c**                  lamcalc.for
c**                  bcalc.for
c**                  blength.for
c**                  interpol.for
c**                  output.for
c**
c**    RECORD OF MODIFICATION
c**        06/08/96.....first created
c**
c*************************************************************

c-- This program solves the force-free Grad-Shafranov equation
c-- for the HIT experiment using an SOR solver adapted from numerical
c-- recipes
c--
c-- Lambda on the open flux is defined by the model:
c--
c--       lambda(psi) = ( uo * V / eta ) / INT (B dot dl)
c--
c-- Lambda on the closed flux is defined by:
c--
c--       lambda(psi) = elam + alpha * ( psi - psisep )
c--
c-- The code is optimized - that is to say, it finds the "best"
c-- set of parameters that minimizes a total error chisqr
c-- This is done using the KMN routine UNCMIN.FOR, a Newton's-method
c-- based algorithm from the text book by Kahaner, Moler, and Nash (1988)
c--
c--                                Adam Martin, August 1996
c-------------------------------------------------------

c-- Define common blocks
```

```
      include 'roleqs2.inc'

c-- Dimension work space array needed by uncmin.for
      dimension work(119)

c-- Declare function call fcn.for to be external
      external fcn

c-- Read in data

      namelist/input/nshot,ntime,outfile,boundfile,vacfile,omega
     .              ,itermax,nlambda,iclose,iopti,expitf,expvinj
     .              ,expig,expib,expip,expp0,nprobe,expbp,nparam
     .              ,pvec0,sigig,sigib,sigip,sigbp,epso1,epso2,epsf
      read(5,input)

c-- Define constants
      ZERO = 0.0d0
      ONE = 1.0d0
      TWO = 2.0d0
      SIX = 6.0d0
      PI  = 3.14159265359d0
      perm0 = 1.256637e-6

c-- Define dimensions of solution region
      imax = 130
      jmax = 150
      r0 = 0.1095375
      r1 = 0.158959
      r2 = 0.508
      h1 = 0.3045
      h2 = 0.711
      h3 = 0.1445
      zb = h1
      zt = h1 + h2
      h  = h1 + h2 + h3

c-- Define vacuum F
      fvac = 2.0e-7 * expitf

c-- Begin

c-- Define grid

      call grid
```

```
c-- pvec0 is a vector containing the initial guesses for the
c-- fitting parameters. They are: eta1, eta2, elam, alpha,
c-- the two resistivities, the edge lambda in the closed flux
c-- and the slope parameter, alpha

      eta1   = 1.0e-6 * pvec0(1)
      eta2   = 1.0e-6 * pvec0(2)
      elam   = 0.1    * pvec0(3)
      alpha  = 0.02   * pvec0(4) - 1.0
      if (expp0 .gt. 0.0) then
       pres0  = expp0 * pvec0(5) / 20.0
      endif
      psicu  = 1.0e-5 * pvec0(6)
      psicm  = 1.0e-5 * pvec0(7)

      resfac1 = perm0 * expvinj / eta1
      resfac2 = perm0 * expvinj / eta2

c-- Define mesh coefficients, read in limiter location and
c-- locations of b-poloidal probes

      call init

c-- Load psiinit into psi
      do j=1,jmax
      do i=1,imax
        psi(i,j) = psiinit(i,j)
      enddo
      enddo

c-- Solve the equation
c-- if iopti = 1, the code is run in optimization mode
c-- if iopti = 0, an equilibrium is calculated using the
c--   initial paramaters contained in pvec0

      if (iopti .eq. 1) then

c-- Initialize the psi array by running relax to a tolerance
c-- epso1
       call relax(0,epso1,n)
       call chi2calc(chi2)

       do j=1,jmax
       do i=1,imax
         psiinit(i,j) = psi(i,j)
       enddo
```

```
      enddo

      print*,'n = ',n,'          chi2 = ',chi2

c-- Run optimization package UNCMIN.FOR from the KMN library
c-- Kahaner, Moler, and Nash, 1988

c-- First, initialize nopti
      nopti = 0

      call uncmin(nparam,pvec0,fcn,pvec,f,info,work,119)

c-- Print out resultant parameters
      print*,' '
      do k=1,nparam
        print*,'pvec(k) = ',pvec(k)
      enddo
      print*,' '

      eta1  = 1.0e-6  * pvec(1)
      eta2  = 1.0e-6  * pvec(2)
      elam  = 0.1     * pvec(3)
      alpha = 0.02    * pvec(4) - 1.0
      if (expp0 .gt. 0.0) then
       pres0 = expp0  * pvec(5) / 20.0
      endif
      psicu = 1.0e-5  * pvec(6)
      psicm = 1.0e-5  * pvec(7)

c-- run relax to desired precision

c-- Reinitialize psiinit
      call init

c-- Load psiinit into psi
      do j=1,jmax
      do i=1,imax
        psi(i,j) = psiinit(i,j)
      enddo
      enddo

      call relax(1,epsf,n)
      call chi2calc(chimin)

     else
```

```
c-- Run non-optimized equilibrium

      call relax(1,epsf,n)
      call chi2calc(chimin)

     endif

c-- Write Solution to an output file

     call output(n)

     end
```

C.2 Source code for grid.for

```
     subroutine grid
c**********************************************************************
c**
c**    ROLEQS2
c**
c**    MODULE: grid.for
c**
c**    SUBPROGRAM DESCRIPTION:
c**            Defines separate solution grid
c**
c**    RECORD OF MODIFICATION:
c**        18/10/95.....first created
c**
c**********************************************************************

     include 'roleqs2.inc'

c-- begin; Make grid, r and z

     dr = (r2 - r0) / real(imax-1)
     dz = h / real(jmax-1)

c-- define r(i)
     do i = 1,imax
       r(i) = r0 + dr*(i-1)
     enddo

c-- define z(j)
     do j = 1,jmax
       z(j) = dz*(j-1)
```

```
      enddo

c-- define dela (area element)
      dela = ( r(2) - r(1) ) * ( z(2) - z(1) )

      return
      end
```

C.3 Source code for init.for

```
      subroutine init
c*************************************************************************
c**
c**    ROLEQS2
c**
c**    MODULE: init.for
c**
c**    SUBPROGRAM DESCRIPTION:
c**            Define coefficients and source terms, initialize
c**            flux to the vacuum flux on the grid, read in
c**            boundary conditions
c**
c**    RECORD OF MODIFICATION:
c**        18/10/95.....first created
c**
c*************************************************************************

      include 'roleqs2.inc'

      dimension dum(300)
      dimension flc(150), fls(150)

c-- Read in vacuum flux data and boundary conditions
c-- from the file logical: vacfile
      open (unit=1,status='old',file=vacfile)
      read (1,100) ((psiv(i,j), i=1,imax), j=1,jmax)
      close (unit=1,status='keep')
  100 format (1x,e15.12)

c-- Read in limiter boundary for confinement grid
      open (unit=1,status='old',
     .      file='user$disk:[adam.sor.infiles]lim.dat')
      read (1,200) (rlim(j), j=1,jmax)
      close (unit=1,status='keep')
  200 format (1x,e15.12)
```

```
c-- Read in flux on limiter from the file logical: boundfile
      open (unit=1,status='old',file=boundfile)
      read (1,300) (dum(j),  j=1,2*jmax)
      close (unit=1,status='keep')
  300  format (1x,e15.12)
      do j=1,150
        jj = j + 150
        flc(j) = dum(j)
        fls(j) = dum(jj)
      enddo

c-- Read in probe locations from file probloc.dat
      open (unit=1,status='old',
     .      file='user$disk:[adam.sor.infiles]probloc.dat')
      read (1,400) (rprobe(k),  k=1,nprobe)
      read (1,400) (zprobe(k),  k=1,nprobe)
      read (1,400) (aprobe(k),  k=1,nprobe)
      read (1,400) (sprobe(k),  k=1,nprobe)
      close (unit=1,status='keep')
  400  format (1x,e15.12)

c-- Define psilg, the value of psi at the injector insulator,
c-- above which (in psi, that is) no current can flow
      psilg = flc(1)

c-- Define alam0
      alam0 = 2.e-7 * expig / psilg

c-- Define vacuum F
      fvac = 2.0e-7 * expitf

c-- Calculate mesh coefficients, set up ienable flag,
c-- and set up initialized flux, psiinit

      do jj=1,jmax
      j = jmax - jj + 1
      ibegin = 0
      do i=1,imax

        psiinit(i,j) = ZERO
c       psiinit(i,j) = psiv(i,j)

        a(i,j) = ONE/dr/dr - ONE/TWO/dr/r(i)
        b(i,j) = ONE/dr/dr + ONE/TWO/dr/r(i)
        c(i,j) = ONE/dz/dz
        d(i,j) = c(i,j)
```

```
      e(i,j) = - TWO/dr/dr - TWO/dz/dz
      ienable(i,j) = 1

c-- Test for vacuum region ouside of limiter
      if (r(i) .ge. rlim(j)) then
       ienable(i,j) = 0
      endif

c-- Test for "dead" region, below gun insulator
      if ( psiv(i,j) .ge. psilg) then
c      if ( psiv(i,j) .ge. psiv(1,1)) then
       ienable(i,j) = 0
       if (r(i) .le. r1) then
        psiinit(i,j) = psiv(i,j)
       endif
      endif

c-- Initialize psi on limiter to measured psi values

c-- center conductor:
      if (i .eq. 1) then
       psiinit(i,j) = flc(j)
      endif

c-- Outer shell:
      if ( (r(i-1) .lt. rlim(j)) .and.
     .     (r(i)   .ge. rlim(j)) ) then
       psiinit(i,j) = fls(j)
       ibegin = i
c       if (j .le. 20) then
c        psiinit(i,j) = psiv(i,j)
c        if (psiinit(i,j) .lt. fls(21)) psiinit(i,j) = fls(21)
c       endif
      endif

      if ( (j .lt. jmax) .and. (i .gt. ibegin) .and.
     .     (rlim(j) .ne. rlim(j+1)) ) then
       if ((r(i) .gt. rlim(j)) .and. (r(i) .lt. rlim(j+1))) then
        psiinit(i,j) = fls(j) + (fls(j+1) - fls(j)) *
     .                 (r(i) - rlim(j)) / (rlim(j+1) - rlim(j))
       endif
       if ((r(i) .lt. rlim(j)) .and. (r(i) .gt. rlim(j+1))) then
        psiinit(i,j) = fls(j+1) + (fls(j) - fls(j+1)) *
     .                 (r(i) - rlim(j+1)) / (rlim(j) - rlim(j+1))
       endif
      endif
```

```
c-- Top of limiter:
        if ( (j .eq. jmax) .and. (r(i) .le. rlim(j)) ) then
         psiinit(i,j) = flc(j) + ( fls(j) - flc(j) ) * ( r(i) -
     .                  r(1) ) / ( rlim(j) - r(1) )
        endif

      enddo
      enddo

c-- Find the last location along the center column where
c-- current can leave the electrode (zcon)
cakm+
       psicu = fls(150)
c       psicu = fls(132)
c       psic = ( fls(132) + fls(131) ) / TWO
cakm-

      i = 1
      j = 1
      jflag = 1
      do while ( jflag .eq. 1 )
       if (psiinit(i,j) .le. psicu) then
        jflag = 0
       else
        j = j + 1
       endif
       if (j .eq. jmax) jflag = 0
      enddo
      if (j .ge. 2) then
       j1 = j - 1
      else
       j1 = 1
      endif
      zcon = z(j1)
c      zcon = 10.0
cakm+
      print*,'psicu = ',psicu
      print*,'zcon = ',zcon-0.66
cakm-
      return
      end
```

C.4 Source code for relax.for

```
      subroutine relax(ifin,eps,n)
c*************************************************************************
c**
c**    ROLEQS2
c**
c**    MODULE: relax.for
c**
c**    SUBPROGRAM DESCRIPTION:
c**           Solves GS equation for a given lambda (psi)
c**         using the SOR (Simultaneous Over-Relaxation)
c**         method with Chebyshev acceleration. In every
c**           iteration, a solution is first obtained over
c**           the gun grid, then over the chamber grid, then
c**           a solution is obtained on the boundary between
c**           them. Lambda is recalculated every iteration
c**           based on the field-line lengths.
c**
c**    SUBROUTINES: lamcalc.for
c**                 magaxfind.for
c**               sourcefind.for
c**                 sepfind.for
c**
c**    RECORD OF MODIFICATION:
c**        18/10/95.....first created
c**
c*************************************************************************
      include 'roleqs2.inc'

c-- SOR in alternating checkerboard pattern
      do n = 1, itermax

       if (n .le. nlambda) then
c-- Find separatrix, psisep and zsep
        call sepfind
c-- Calculate lambda(psi) for the open flux
        call lamcalc(ifin,n)
       endif

c-- Find psi at magnetic axis
       if (iclose .eq. 1) then
        call magaxfind
       endif

c-- Solve the equation
```

```
      enorm = ZERO
c-- There are two different branches - if iclose = 1, the solution
c-- allows closed flux; if iclose = 0, it does'nt
      if (iclose .eq. 1) then
c-- Case where closed flux is allowed
       do j = 2, jmax-1
       do i = 2, imax-1
          if ( mod(i+j,2) .eq. mod(n,2) ) then
         if (ienable(i,j) .eq. 1) then
          if ( (psi(i,j) .lt. psisep) .or.
     .          (z(j) .lt. zsep) ) then
c-- Solve equation on open flux
           psip = psi(i,j)
           call sourcefind(psip,sorp,alamp)
           resid = a(i,j)*psi(i+1,j) + b(i,j)*psi(i-1,j) +
     .                c(i,j)*psi(i,j+1) + d(i,j)*psi(i,j-1) +
     .               e(i,j)*psi(i,j) + sorp
           psi(i,j) = psi(i,j) - omega * resid / e(i,j)
           err(i,j) = resid / e(i,j)
           if (psi(i,j) .gt. psilg) then
            psi(i,j) = psilg
            resid = ZERO
            err(i,j) = ZERO
           endif
          else
c-- Solve equation on closed flux
           ec(i,j) = fvac * elam * alpha / delpsi
     .                - TWO/dr/dr - TWO/dz/dz
           resid = a(i,j)*psi(i+1,j) + b(i,j)*psi(i-1,j) +
     .              c(i,j)*psi(i,j+1) + d(i,j)*psi(i,j-1) +
     .              ec(i,j)*psi(i,j) +
     .              fvac * elam * ( ONE - alpha * psisep / delpsi )
           if (expp0 .gt. 0.0) then
            resid = resid + perm0 * r(i) * r(i) * pres0 / delpsi
           endif
           psi(i,j) = psi(i,j) - omega * resid / ec(i,j)
           err(i,j) = resid / ec(i,j)
          endif
         else
          resid = ZERO
          psi(i,j) = psiinit(i,j)
          err(i,j) = ZERO
         endif
c-- New convergence criterion
         enorm = enorm + resid * resid
        endif
```

```
      end do            ! loop on j
      end do            ! loop on i
     else
c-- Case where no closed flux is allowed
      do j = 2, jmax-1
      do i = 2, imax-1
       if ( mod(i+j,2) .eq. mod(n,2) ) then
        if (ienable(i,j) .eq. 1) then
         if ( (psi(i,j) .lt. psisep) .or.
     .          (z(j) .lt. zsep) ) then
c-- Solve equation on open flux
          psip = psi(i,j)
          call sourcefind(psip,sorp,alamp)
          resid = a(i,j)*psi(i+1,j) + b(i,j)*psi(i-1,j) +
     .            c(i,j)*psi(i,j+1) + d(i,j)*psi(i,j-1) +
     .            e(i,j)*psi(i,j) + sorp
          psi(i,j) = psi(i,j) - omega * resid / e(i,j)
          err(i,j) = resid / e(i,j)
          if (psi(i,j) .gt. psilg) then
           psi(i,j) = psilg
           resid = ZERO
           err(i,j) = ZERO
          endif
         else
c-- Solution in no flux region
          resid = ZERO
          psi(i,j) = psisep
          err(i,j) = ZERO
         endif
        else
         resid = ZERO
         psi(i,j) = psiinit(i,j)
         err(i,j) = ZERO
        endif
        enorm = enorm + resid * resid
       endif
      end do          ! loop on j
      end do          ! loop on i

     endif

c-- terminate if error (difference between psi-new and psi-old
c-- falls below eps
      if (n .eq. 1) enormi = enorm
      erriter(n) = enorm/enormi
```

```
c-- If the code is being run in un-optimized mode, print out
c-- the error at every iteration
      if (iopti .eq. 0) then
       print*,'n = ',n,'          erriter(n) = ',erriter(n)
      endif

      if (enorm .lt. (eps*enormi)) return

     end do              ! SOR iteration on n

     return
     end
```

C.5 Source code for sepfind.for

```
     subroutine sepfind
c*************************************************************************
c**
c**    ROLEQS2
c**
c**    MODULE: sepfind.for
c**
c**    SUBPROGRAM DESCRIPTION:
c**           Finds the value of psi at the separatrix
c**
c**    RECORD OF MODIFICATION:
c**       12/07/95.....first created
c**
c*************************************************************************
     include 'roleqs2.inc'

     dimension seppos(80), rpos(80), zpos(80)

c-- Find separatrix

c-- Scan grid for possible separatrix locations
     psi1 = psi(1,1)
     psi2 = psi(1,2)
     rtemp1 = ZERO
     rtemp2 = ZERO
     jpos = 0
     do j=3,50
      psi3 = psi(1,j)
      i = 2
      do while ( ( ienable(i,j) .eq. 1 ) .and.
```

```
     .          ( r(i) .le. r1 ) )
           if ( psi(i,j) .gt. psi3 ) then
            psi3 = psi(i,j)
            rtemp3 = r(i)
           endif
           i = i + 1
          enddo
          if (iclose .eq. 1) then
           if ( ( psi2 .lt. psi1 ) .and.
     .          ( psi2 .lt. psi3 ) .and.
     .          ( z(j-1) .lt. (h1 + 0.1) ) ) then
c    .           ( z(j-1) .le. (h1 + 0.01) ) ) then
            jpos = jpos + 1
            seppos(jpos) = psi2
            rpos(jpos) = rtemp2
            zpos(jpos) = z(j-1)
           endif
          else
           if ( ( psi2 .lt. psi1 ) .and.
     .          ( psi2 .le. psi3 ) .and.
     .          ( z(j-1) .lt. (h1 + 0.1) ) ) then
            jpos = jpos + 1
            seppos(jpos) = psi2
            rpos(jpos) = rtemp2
            zpos(jpos) = z(j-1)
           endif
          endif
          psi1 = psi2
          psi2 = psi3
          rtemp1 = rtemp2
          rtemp2 = rtemp3
         enddo

c-- Choose among possible separatrices
         if (jpos .eq. 1) then
          psisep = seppos(1)
          rsep   = rpos(1)
          zsep   = zpos(1)
         endif
         if ( (jpos .eq. 0) .or. (jpos .eq. 1) ) goto 10
         psisep = seppos(1)
         rsep = rpos(1)
         zsep = zpos(1)
         do jjj=2,jpos
          if (seppos(jjj) .le. psisep) then
           psiseptemp = seppos(jjj)
```

```
       rseptemp   = rpos(jjj)
       zseptemp   = zpos(jjj)
      endif
     enddo
 10   continue
     if (psisep .eq. ZERO) psisep = 0.5*psilg
cakm+
     if (zseptemp .ge. (h1/TWO)) then
      psisep = psiseptemp
      rsep   = rseptemp
      zsep   = zseptemp
     endif
cakm-
     return
     end
```

C.6 Source code for lamcalc.for

```
     subroutine lamcalc(ifin,n)
c**********************************************************************
c**
c**    ROLEQS2
c**
c**    MODULE: lamcalc.for
c**
c**    SUBPROGRAM DESCRIPTION:
c**            Calculates lambda as a function of psi:
c**            lambda(psi) is calculated assuming that the
c**            voltage drop is purely resistive.  Using this
c**            model:
c**
c**             lambda(psi) = ( uo * V / eta ) / INT (B dot dl)
c**
c**            The integral is done over the field line at a
c**            particular value of psi.  The field line length
c**            is calculated using a crude Euler solver
c**
c**    SUBROUTINES: bcalc.for
c**                 blength.for
c**
c**    RECORD OF MODIFICATION:
c**        18/10/95.....first created
c**
c**********************************************************************
     include 'roleqs2.inc'
```

```
      if (n .le. 1) then
       goto 10
      else
       goto 20
      endif

c-- Begin iterations using linear lambda model
c-- Specify lambda as: lam = lam0*( 1. + sin(PI*(psi/psi0 - 1/2)) )
 10   continue
      do j=1,jmax
       alam(j) = abs( alam0*( ONE + sin( PI*( psi(1,j)/psilg
     .          - ONE/TWO ) ) ) )
       if (z(j) .ge. zcon) alam(j) = ZERO
      enddo
      goto 30

c-- Calculate lambda by doing field line integral

 20   continue

c-- First calculate B-poloidal on the grid
      call bcalc

c-- Calculate line integral of B dot ds and lamda
      i=1
      do j=1,jmax
       if (z(j) .ge. zcon) goto 25
       if (j .eq. jmax) goto 25
       rinit = r(i)
       zinit = z(j)
       brinit = br(i,j)
       bzinit = bz(i,j)
       btinit = bt(i,j)
       call blength(rinit,zinit,brinit,bzinit,btinit
     .           ,arclen,bdsint,torwnd)
 25    continue
       angle(j) = torwnd
       bint(j)  = bdsint
       arc(j)   = arclen
       if (bdsint .eq. ZERO) then
c        if (j .ge. 2) alam(j) = alam(j-1)
         alam(j) = ZERO
       else
        if ( psi(i,j) .ge. psisep) then
         alam(j) = resfac1 / abs(bdsint)
        else
```

```
        alam(j) = resfac2 / abs(bdsint)
       endif
cakm+
       if ( (j .eq. 1) .and. (alam(j) .gt. 20.0) ) alam(j) = 0.0
cakm-
      endif
      if (z(j) .ge. zcon) alam(j) = ZERO
     enddo

cakm+
c-- Correct psisep based on lambda profile
c-- Find the index number, jsep, corresponding to psisep
c     i = 1
c     j = 1
c     jsep = 3
c     jflag = 1
c     do while(jflag .eq. 1)
c       if ( ( arc(j+1) .gt. ( 2.0 * arc(j) ) ) .or.
c    .       ( arc(j+1) .gt. 499.0) ) then
c        jsep = j + 1
c        jflag = 0
c       else
c        j = j + 1
c       endif
c       if ( (j .eq. (jmax-2)) .or. (jsep .eq. (jmax-2) ) ) jflag = 0
c     enddo
c     psisep = psi(i,jsep)
cakm-

 30   continue

c-- Save lambda function for this iteration
     if (ifin .eq. 1) then
      do j = 1,jmax
       reclam(j,n) = alam(j)
      enddo
     endif

c-- Calculate source function by calculating: lambda * integral(lambda)
     temp = ZERO
     i = 1
     jj = jmax
c     temp = psi(i,jj) * alam(jj) / TWO
     source(jj) = alam(jj) * (temp + fvac)
     do j=2,jmax
      jj = jmax - j + 1
```

```
      temp = temp + ( alam(jj) + alam(jj+1) ) *
     .          ( psi(i,jj) - psi(i,jj+1) ) / TWO
      source(jj) = alam(jj) * (temp + fvac)
     enddo

     return
     end
```

C.7 Source code for bcalc.for

```
     subroutine bcalc
c*************************************************************************
c**
c**    ROLEQS2
c**
c**    MODULE: bcalc.for
c**
c**    SUBPROGRAM DESCRIPTION:
c**           Calculates Poloidal and Toroidal fields on the
c**           grid.
c**
c**    SUBROUTINES: sourcefind.for
c**
c**    RECORD OF MODIFICATION:
c**        18/10/95.....first created
c**
c*************************************************************************
     include 'roleqs2.inc'

c-- Calculate B-field on grid

     do j=1,jmax
     do i=1,imax

      if (ienable(i,j) .eq. 1) then

c-- Br
       if ((j .eq. 1) .or. (j .eq. jmax)) then
        if (j .eq. 1) then
         br(i,j) = -(psi(i,j+1) - psi(i,j))/r(i)/dz
        else
         br(i,j) = -(psi(i,j) - psi(i,j-1))/r(i)/dz
        endif
       else
        br(i,j) = -(psi(i,j+1) - psi(i,j-1))/TWO/r(i)/dz
```

```
        endif

c-- Bz
        if ((i .eq. 1) .or. (i .eq. imax)) then
         if (i .eq. 1) then
          bz(i,j) = (psi(i+1,j) - psi(i,j))/r(i)/dr
         else
          bz(i,j) = (psi(i,j) - psi(i-1,j))/r(i)/dr
         endif
        else
         bz(i,j) =  (psi(i+1,j) - psi(i-1,j))/TWO/r(i)/dr
        endif

c-- Bt
        psip = psi(i,j)
        if ( (z(j) .ge. zsep) .and. (psip .ge. psisep) ) then
         fac = fvac
        else
         call sourcefind(psip,sorp,alamp)
         if (alamp .eq. 0.0) then
          fac = fvac
         else
          fac = sorp/alamp
         endif
        endif
        bt(i,j) = fac/r(i)

       else

        br(i,j) = ZERO
        bt(i,j) = fvac / r(i)
        bz(i,j) = ZERO

       endif

      enddo
      enddo

      return
      end
```

C.8 Source code for blength.for

```
      subroutine blength(rinit,zinit,brinit,bzinit,btinit
     .                   ,arclen,bdsint,torwnd)
```

```
c**********************************************************************
c**
c**    ROLEQS2
c**
c**    MODULE: blength.for
c**
c**    SUBPROGRAM DESCRIPTION:
c**           Calculates arclength of a field line on a given
c**           flux surface and the line integral of B on this
c**           arc.  Also calculates the total toroidal angular
c**           excursion of the field line.
c**
c**    SUBROUTINES: interpol.for
c**
c**    RECORD OF MODIFICATION:
c**        18/10/95.....first created
c**
c**********************************************************************
      include 'roleqs2.inc'

      dimension re(2), ze(2)
     .         ,bre(2), bte(2), bze(2)
     .         ,y0(2), dydx0(2), y1(2), dydx1(2)
     .         ,y2(2), dydx2(2), y3(2), dydx3(2)
     .         ,yout(2)

      arcmax = 500.0

      arclen = 0.0
      torwnd = 0.0
      bdsint = 0.0
      ds = 0.0
      bds = 0.0

      iend = 1
      dth1 = 1.0e6
      dth2 = 1.0e6
      re(1) = rinit
      ze(1) = zinit
      bre(1) = brinit
      bte(1) = btinit
      bze(1) = bzinit
      do while ( iend .eq. 1 )
c-- Step field line along using a 4th order Runge-Kutta method.
c-- Define step size, dth
        if ( (bre(1) .eq. 0.0) .and. (bze(1) .eq. 0.0) ) then
```

```
 dth  = 10.0 * PI / 180.0
else
 if (bre(1) .ne. 0.0) dth1 = abs(dr*bte(1)/re(1)/bre(1))
 if (bze(1) .ne. 0.0) dth2 = abs(dz*bte(1)/re(1)/bze(1))
 if (dth1 .le. dth2) then
  dth = dth1
 else
  dth = dth2
 endif
endif
dth2 = dth/TWO
dth6 = dth/SIX

y0(1) = re(1)
y0(2) = ze(1)
dydx0(1) = y0(1)*bre(1)/bte(1)
dydx0(2) = y0(1)*bze(1)/bte(1)
do k=1,2
 y1(k) = y0(k) + dth2*dydx0(k)
enddo

call interpol(y1,bri,bti,bzi,iend)
if (iend .eq. 0) goto 10
dydx1(1) = y1(1)*bri/bti
dydx1(2) = y1(1)*bzi/bti
do k=1,2
 y2(k) = y0(k) + dth2*dydx1(k)
enddo

call interpol(y2,bri,bti,bzi,iend)
if (iend .eq. 0) goto 10
dydx2(1) = y2(1)*bri/bti
dydx2(2) = y2(1)*bzi/bti
do k=1,2
 y3(k) = y0(k) + dth*dydx2(k)
enddo

call interpol(y3,bri,bti,bzi,iend)
if (iend .eq. 0) goto 10
dydx3(1) = y3(1)*bri/bti
dydx3(2) = y3(1)*bzi/bti
do k=1,2
 yout(k) = y0(k) + dth6*( dydx0(k) + TWO*( dydx1(k) +
          dydx2(k) ) + dydx3(k) )
enddo
```

```
      re(2) = yout(1)
      ze(2) = yout(2)
      call interpol(yout,bri,bti,bzi,iend)
      if (iend .eq. 0) goto 10
      bre(2) = bri
      bte(2) = bti
      bze(2) = bzi
      delr = re(2) - re(1)
      delz = ze(2) - ze(1)
      delt = re(1)*dth
      brav = ( bre(2) + bre(1) )/TWO
      btav = ( bte(2) + bte(1) )/TWO
      bzav = ( bze(2) + bze(1) )/TWO
      ds = sqrt( delr*delr + delz*delz + delt*delt )
      bds = brav*delr + btav*delt + bzav*delz
10    continue
      if (iend .eq. 0) then
       ds = ZERO
       bds = ZERO
       dth = ZERO
      endif
      arclen = arclen + ds
      bdsint = bdsint + bds
      torwnd = torwnd + dth
      re(1) = re(2)
      ze(1) = ze(2)
      bre(1) = bre(2)
      bte(1) = bte(2)
      bze(1) = bze(2)
      if (arclen .gt. arcmax ) iend = 0
     enddo

     return
     end
```

C.9 Source code for interpol.for

```
      subroutine interpol(y,bri,bti,bzi,iend)
c*********************************************************************
c**
c**    ROLEQS2
c**
c**    MODULE: interpol.for
c**
```

```
c**    SUBPROGRAM DESCRIPTION:
c**          interpolate the B-field at a given rp, zp using
c**          the values of B on the r-z grid.  It returns
c**          iend = 0 if the point is outside the region of
c**          interest, and leaves iend unchanged otherwise
c**
c**    RECORD OF MODIFICATION:
c**       18/10/95.....first created
c**
c*********************************************************************

      include 'roleqs2.inc'

      dimension y(2)

      rp = y(1)
      zp = y(2)

      if (rp .le. r0) rp = r0 + dr / TWO
      if (zp .le. 0.0) zp = dz / TWO

c-- Find grid point closest to field-line point (rp,zp)
      j = 1
      do i=1,imax-1
       if ( (r(i) .lt. rp) .and.
     .      (r(i+1) .ge. rp) ) then
        i1 = i
        i2 = i + 1
       endif
      enddo
      i = 1
      do j=1,jmax-1
       if ( (z(j) .lt. zp) .and.
     .      (z(j+1) .ge. zp) ) then
        j1 = j
        j2 = j + 1
       endif
      enddo

c-- Test to determine if point (rp,zp) is within plasma volume

      if (zp .ge. h) iend = 0
      if ( (rp .ge. rlim(j1)) .or. (rp .ge. rlim(j2)) ) iend = 0
      if ( (ienable(i1,j1) .eq. 0) .and.
     .     (ienable(i2,j1) .eq. 0) .and.
     .     (ienable(i1,j2) .eq. 0) .and.
```

```
     .    (ienable(i2,j2) .eq. 0) ) iend = 0

c-- Find the interpolate field values as per the diagram below

c-- Find interpolated B-r and B-z at point p
c--
c--   i1,j2              i2,j2
c--
c--
c--            p
c--
c--
c--   i1,j1              i2,j1

      r11 = r(i1)
      r12 = r(i1)
      r21 = r(i2)
      r22 = r(i2)
      z1  = z(j1)
      z2  = z(j2)
      br11 = br(i1,j1)
      br12 = br(i1,j2)
      br21 = br(i2,j1)
      br22 = br(i2,j2)
      bt11 = bt(i1,j1)
      bt12 = bt(i1,j2)
      bt21 = bt(i2,j1)
      bt22 = bt(i2,j2)
      bz11 = bz(i1,j1)
      bz12 = bz(i1,j2)
      bz21 = bz(i2,j1)
      bz22 = bz(i2,j2)

c-- Interpolate
      wl1 = ( r21 - rp )/( r21 - r11 )
      wl2 = ( rp - r11 )/( r21 - r11 )
      wu1 = ( r22 - rp )/( r22 - r12 )
      wu2 = ( rp - r12 )/( r22 - r12 )
      brl = wl1*br11 + wl2*br21
      bru = wu1*br12 + wu2*br22
      btl = wl1*bt11 + wl2*bt21
      btu = wu1*bt12 + wu2*bt22
      bzl = wl1*bz11 + wl2*bz21
      bzu = wu1*bz12 + wu2*bz22
      wl = ( z2 - zp )/( z2 - z1 )
      wu = ( zp - z1 )/( z2 - z1 )
```

```
      bri = wl*brl + wu*bru
      bti = wl*btl + wu*btu
      bzi = wl*bzl + wu*bzu

c-- Test to determine if point (rp,zp) is within plasma volume

      if (zp .ge. h) iend = 0
      if ( (rp .ge. rlim(j1)) .or. (rp .ge. rlim(j2)) ) iend = 0
      if ( (ienable(i1,j1) .eq. 0) .and.
     .     (ienable(i2,j1) .eq. 0) .and.
     .     (ienable(i1,j2) .eq. 0) .and.
     .     (ienable(i2,j2) .eq. 0) ) iend = 0
      if ( (bri .eq. ZERO) .or.
     .     (bti .eq. ZERO) .or.
     .     (bzi .eq. ZERO) ) iend = 0
 10   return
      end
```

C.10 Source code for magaxfind.for

```
      subroutine magaxfind
c**********************************************************************
c**
c**    ROLEQS2
c**
c**    MODULE: magaxfind.for
c**
c**    SUBPROGRAM DESCRIPTION:
c**            Finds the value of psi at the magnetic axis
c**
c**    RECORD OF MODIFICATION:
c**        01/21/97.....first created
c**
c**********************************************************************
      include 'roleqs2.inc'

c-- Find magnetic axis
      do j=50,120
        i = 1
        ic = 1
        do while( ic .eq. 1 )
          if (psi(i,j) .le. psisep) then
           i = i + 1
          else
           ic = 0
          endif
```

```
        enddo
        psip = psi(i,j)
        i = i + 1
        do while (psi(i,j) .gt. psisep)
          if ( psi(i,j) .gt. psip ) psip = psi(i,j)
          i = i + 1
        enddo
        if (j .eq. 50) psi1 = psip
        if (j .eq. 51) psi2 = psip
        if (j .ge. 52) then
         psi3 = psip
         if ( (psi2 .gt. psi1) .and. (psi2 .gt. psi3) ) then
          psiax = psi2
         else
          psi1 = psi2
          psi2 = psi3
         endif
        endif
      enddo
      if (psiax .le. 0.0) psiax = 2.0 * psisep

c-- Define delpsi
      delpsi = psiax - psisep

      return
      end
```

C.11 Source code for sourcefind.for

```
      subroutine sourcefind(psip,sorp,alamp)
c*********************************************************************
c**
c**    ROLEQS2
c**
c**    MODULE: sourcefind.for
c**
c**    SUBPROGRAM DESCRIPTION:
c**           interpolates a value for the source function
c**           for a given value of psi
c**
c**    RECORD OF MODIFICATION:
c**        18/10/95.....first created
c**
c*********************************************************************
      include 'roleqs2.inc'
```

```
      i = 1
      j = 1
      jflag = 1
      do while ( jflag .eq. 1 )
       if (psi(i,j) .le. psip) then
        jflag = 0
       else
        j = j + 1
       endif
       if (j .eq. jmax) jflag = 0
      enddo
      if ( (j .ge. 2) .and. (j .lt. jmax) ) then
       j1 = j - 1
       j2 = j
       if ( (arc(j2) - arc(j1)) .gt. 5.0 ) then
        sorp = source(j2)
        alamp = alam(j2)
       else
        w1 = ( psi(i,j2) - psip )/( psi(i,j2) - psi(i,j1) )
        w2 = ( psip - psi(i,j1) )/( psi(i,j2) - psi(i,j1) )
        sorp  = w1*source(j1) +  w2*source(j2)
        alamp = w1*alam(j1)   +  w2*alam(j2)
       endif
      else
       sorp = source(j)
       alamp = alam(j)
      endif
      return
      end
```

C.12 Source code for jtor.for

```
      subroutine jtor
c**********************************************************************
c**
c**    ROLEQS2
c**
c**    MODULE: jtor.for
c**
c**    SUBPROGRAM DESCRIPTION:
c**            Calculates Toroidal Current Density at
c**            every point on the grid - also calculates
c**            I-plasma
c**
c**    MODULES USED: sourcefind.for
```

```
c**
c**    RECORD OF MODIFICATION:
c**         12/11/95.....first created
c**
c*******************************************************************************
      include 'roleqs2.inc'

c-- Calculate J-toroidal
      temp = ZERO
      do j = 1, jmax
      do i = 1, imax
        psip = psi(i,j)
        if (ienable(i,j) .eq. 1) then
         if ( (psip .ge. psisep) .and.
     .        (z(j) .ge. zsep) ) then
          if (iclose .eq. 1) then
           torj(i,j) = fvac * elam * ( ONE + alpha * ( psip -
     .               psisep ) / delpsi ) / r(i) / perm0
           if (expp0 .gt. 0.0) then
            torj(i,j) = torj(i,j) + r(i) * pres0 / delpsi
           endif
          else
           torj(i,j) = ZERO
          endif
         else
          call sourcefind(psip,sorp,alamp)
          torj(i,j) = sorp / r(i) / perm0
         endif
        else
         torj(i,j) = ZERO
        endif
c-- Calculate I-plasma
        if ( (z(j) .gt. zb) .and. (z(j) .lt. zt) ) then
         temp = temp + torj(i,j) * dela
        endif
      enddo              ! loop on j
      enddo              ! loop on i
c     calcip = temp

cakm+
cakm  Calculate calcip an alternate way
c     temp = ZERO
c     do k=1,nprobe
c       temp = temp + sprobe(k) * calcbp(k)
c     enddo
c     calcip = temp / perm0
```

```
cakm-
      return
      end
```

C.13 Source code for chi2calc.for

```
      subroutine chi2calc(chi2)
c**********************************************************************
c**
c**    ROLEQS2
c**
c**    MODULE: chi2calc.for
c**
c**    SUBPROGRAM DESCRIPTION:
c**            Calculates chi-squared given psi and alam
c**
c**    SUBROUTINES: bcalc.for
c**                 interpol.for
c**
c**    RECORD OF MODIFICATION:
c**        18/10/95.....first created
c**
c**********************************************************************
      include 'roleqs2.inc'

      dimension y(2)

c-- Calculate B field
      call bcalc
      chi2 = ZERO
      count = 0.0

c-- Contribution from B-poloidal probes
      do k=1,nprobe
       if (k .eq. 1) then
        y(1) = rprobe(k) - dr
        y(2) = zprobe(k)
       endif
       if ( (k .ge. 2) .and. (k .le. 8) ) then
        y(1) = rprobe(k) + dr
        y(2) = zprobe(k)
       endif
       if ( (k .ge. 9) .and. (k .le. 13) ) then
        y(1) = rprobe(k) - dr
        y(2) = zprobe(k) - dz
```

```
        endif
        if (k .ge. 14) then
         y(1) = rprobe(k) - dr
         y(2) = zprobe(k) + dz
        endif
        theta = aprobe(k)
        call interpol(y,bri,bti,bzi,iend)
        calcbp(k) = bri*cos(theta) + bzi*sin(theta)
        if ( sigbp(k) .ne. 0.0 ) then
         count = count + 1.0
         deviate = ( expbp(k) - calcbp(k) ) / sigbp(k)
         chi2 = chi2 + deviate * deviate
        endif
       enddo

c-- Contribution from injector current
c-- Calculate Injector current by calculating INT (lambda) dpsi
       calcig = ZERO
       count = count + 1.0
       i = 1
       jj = jmax
       do j=2,jmax
        jj = jmax - j + 1
        calcig = calcig + ( alam(jj) + alam(jj+1) ) *
     .           ( psi(i,jj) - psi(i,jj+1) ) / TWO
       enddo
       calcig = calcig / 2.0e-7
       deviate = ( calcig - expig ) / sigig
       chi2 = chi2 + deviate * deviate

c-- Contribution from bridge current
c-- Calculate bridge current by calculating INT (lambda) dpsi
c-- from the top of the grid to the limiting value at the upper
c-- corner, psicu
c      calcib = ZERO
c      count = count + 1.0
c      i = 1
c      j = jmax - 1
c      do while (psi(i,j) .le. psicu)
c       calcib = calcib + ( alam(j) + alam(j+1) ) *
c    .           ( psi(i,j) - psi(i,j+1) ) / TWO
c       j = j - 1
c      enddo
c      calcib = calcib / 2.0e-7
c      deviate = ( calcib - expib ) / sigib
c      chi2 = chi2 + deviate * deviate
```

```
c-- Contribution from plasma current
c-- Calculate current density on grid
      count = count + 1.0
      call jtor
c--  Calculate calcip an alternate way
      temp = ZERO
      do k=1,nprobe
        temp = temp + sprobe(k) * calcbp(k)
      enddo
      calcip = temp / perm0
      deviate = ( calcip - expip ) / sigip
      chi2 = chi2 + deviate * deviate

      chi2 = chi2 / count

      return
      end
```

C.14 Source code for output.for

```
      subroutine output(n)
c*********************************************************************
c**
c**    ROLEQS2
c**
c**    MODULE: output.for
c**
c**    SUBPROGRAM DESCRIPTION:
c**            Writes program output to a file
c**
c**    CALLING ARGUMENTS: none
c**
c**    RECORD OF MODIFICATION:
c**        18/10/95.....first created
c**
c*********************************************************************
      include 'roleqs2.inc'

      n = n - 1

      write(6,'( /1x, A, I6 )') '# iterations = ', n

c-- write data for input to IDL
      open(unit=10,status='new',file=outfile)
      write(10,'( 4(1X, I6) )') (nshot, ntime, n, itermax)
```

```
      write(10,'( 2(1X, I4) )') (nprobe, nparam)
      write(10,'( 2(1X, I4) )') (imax, jmax)
      write(10,'( 6(1X, E11.5) )') (r0,r1,r2,h1,h2,h3)
      write(10,'( 2(1X, E11.5) )') (omega,chimin)
      write(10,'( 6(1X, E11.5) )') (expitf,expvinj,expig,expib,expip
     .                             ,calcig,calcib,calcip,expp0)
      write(10,'( 6(1X, E11.5) )') (eta1,eta2,elam,alpha,psisep,psiax
     .                             ,psicu,psicm,pres0,rsep,zsep,chimin)
      write(10,'( 6(1X, E11.5) )') (expbp(k), k=1,nprobe)
      write(10,'( 6(1X, E11.5) )') (calcbp(k), k=1,nprobe)
      write(10,'( 6(1X, E11.5) )') ((psi(i,j), i=1,imax), j=1,jmax)
      write(10,'( 6(1X, E11.5) )') ((err(i,j), i=1,imax), j=1,jmax)
      write(10,'( 6(1X, E11.5) )') ((torj(i,j), i=1,imax), j=1,jmax)
      write(10,'( 6(1X, E11.5) )') (alam(j), j=1,jmax)
      write(10,'( 6(1X, E11.5) )') (angle(j), j=1,jmax)
      write(10,'( 6(1X, E11.5) )') (bint(j), j=1,jmax)
      write(10,'( 6(1X, E11.5) )') (arc(j), j=1,jmax)
      write(10,'( 6(1X, E11.5) )') (erriter(k), k=1,n)
      write(10,'( 6(1X, E11.5) )') ((reclam(j,k), j=1,jmax), k=1,n)
      close (unit=10,status='keep')

c-- if appropriate, write optimization data to the file optirec.dat
      if (iopti .eq. 1) then
       lll = nparam + 1
       open(unit=10,status='new',file='optirec.dat')
       write(10,'( 2(1X, I4) )') (nopti, nparam)
       write(10,'( 2(1X, I6) )') (nshot, ntime)
       write(10,'( 6(1X, I6) )') (noptirec(k), k=1,nopti)
       write(10,'( 6(1X, E11.5) )') ((optirec(k,l), k=1,nopti),
     .                              l=1,lll)
       close (unit=10, status='keep')
      endif
      return
      end
```

VITA

Adam Martin was born on August 23rd, 1964 in Santa Clara, California. He graduated from Sequoia High School in Redwood City, California in June of 1982. From June of 1982 until June of 1983 he attended the College of San Mateo in San Mateo, California. He attended the University of Arizona in Tucson, Arizona from August 1983 until May 1987. He studied physics at the Ludwig-Maximillians University in Munich, Germany from November 1985 until July 1986. Upon graduating from the University of Arizona in May of 1987 with a Bachelors of Science degree in physics he entered the Ph.D. program in physics at the University of Washington in September 1987. He was awarded the Master of Science degree in physics in December of 1989 and the Doctor of Philosophy in physics in March of 1997.